STEADY STATE MODELLING, SIMULATION AND OPTIMIZATION OF HYDROGEN PRODUCTION FROM CATALYTIC STEAM REFORMING OF ETHANOL

A thesis submitted to the
University of Petroleum and Energy Studies

For the Award of
Doctor of Philosophy
in
Chemical Engineering

By
Kumargaurao Dnyaneshwar Punase

October 2019

Supervisor(s)

Dr. Santosh Kumar Gupta
Dr. P. Vijay

UPES
UNIVERSITY WITH A PURPOSE

Department of Chemical Engineering
School of Engineering
University of Petroleum and Energy Studies
Dehradun – 248007: Uttarakhand

STEADY STATE MODELLING, SIMULATION AND OPTIMIZATION OF HYDROGEN PRODUCTION FROM CATALYTIC STEAM REFORMING OF ETHANOL

A thesis submitted to the
University of Petroleum and Energy Studies

For the Award of
Doctor of Philosophy
in
Chemical Engineering

By
Kumargaurao Dnyaneshwar Punase
(SAP ID: 500020799)

October 2019

Supervisor(s)

Dr. Santosh Kumar Gupta
Distinguished Professor

Co-Supervisor

Dr. P. Vijay
Senior Associate Professor
Department of Chemical Engineering
University of Petroleum and Energy Studies

UPES
UNIVERSITY WITH A PURPOSE

Department of Chemical Engineering
School of Engineering
University of Petroleum and Energy Studies
Dehradun – 248007: Uttarakhand

October 2019

DECLARATION

I declare that the thesis entitled "Steady State Modelling, Simulation and Optimization of Hydrogen Production from Catalytic Steam Reforming of Ethanol", has been prepared by me under the guidance of Dr. Santosh Kumar Gupta, Distinguished Professor and Dr. P. Vijay, Senior Associate Professor of Chemical Engineering Department, University of Petroleum & Energy Studies. No part of this thesis has formed the basis for the award of any degree or fellowship previously.
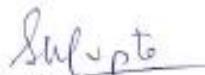
Kumargaurao Dnyaneshwar Punase
Department of Chemical Engineering,
School of Engineering,
University of Petroleum and Energy Studies,
Dehradun – 248007, Uttarakhand.

Date:_____

CERTIFICATE

UPES
UNIVERSITY WITH A PURPOSE

We certify that **Kumargaurao Dnyaneshwar Punase** has prepared his thesis entitled "**Steady State Modelling, Simulation and Optimization of Hydrogen Production from Catalytic Steam Reforming of Ethanol**", for the award of PhD degree of the University of Petroleum & Energy Studies, under our guidance. He has carried out the work at the Department of Chemical Engineering, University of Petroleum & Energy Studies.

Supervisor

Dr. Santosh Kumar Gupta
Distinguished Professor
Department of Chemical Engineering,
School of Engineering,
University of Petroleum and Energy Studies,
Dehradun – 248007, Uttarakhand.

Date: 18 Oct 2019

Co-Supervisor

Dr. P. Vijay
Sr. Associate Professor & Head
Department of Chemical Engineering,
School of Engineering,
University of Petroleum and Energy Studies,
Dehradun – 248007, Uttarakhand.

Date: 18/10/19

ENGINEERING | COMPUTER SCIENCE | DESIGN | BUSINESS | LAW | HEALTH SCIENCES

ABSTRACT

Hydrogen is considered to be the fuel of 21st century as it is theoretically the best fuel, environmentally friendly and its combustion emission is water only. The road map is being prepared by many developed countries to replace the fossil fuels by hydrogen energy for electricity generation and vehicular applications. There are several methods of hydrogen production like thermochemical, electrochemical, photochemical and photobiological. The thermochemical method is one of the proven technologies, which uses the fossil fuel resources for hydrogen production at present. There is an urgent need to replace the fossil fuels by renewable resources of energy to mitigate the climate changes. As ethanol is produced from biomass (renewable resource) fermentation, less toxic and easy to transport, it can be considered as an alternate resource for hydrogen production using the thermochemical conversion (steam reforming) method in the present industrial infrastructure. There is a considerable research going on to produce and increase the yield of ethanol from lignocellulosic biomass instead of using the substrates which are intended for food and feed purposes.

Several researchers have studied ethanol steam reforming (ESR) through the catalyst development, catalysis and reaction mechanism, using supported noble and non-noble metal catalysts. Methane steam reforming technology uses Ni-based catalyst for industrial scale hydrogen production. The modelling and simulation studies of ESR are limited in the literature that can develop and design the ESR process from lab scale study to large scale industrial application. This study can be further extended to the optimization problem to maximize the yield of hydrogen using optimum operating conditions.

In the present study, a mechanistic kinetic model based on Ni catalyst from the literature is used to develop a mathematical model of a fixed bed reactor for ESR process.

The ode23s module of MATLAB^{TM} (version 2010a) is used for simulation of ESR reactor using a mechanistic kinetic model (Langmuir-Hinshelwood approach) with proven reaction kinetics. The kinetic parameters of the reaction rate model based on Ni(II)-Al(III)-LDH catalyst are optimized using the evolutionary optimization technique, genetic algorithm (GA) to resolve a confusion regarding the values of the kinetic parameters even though earlier workers have used the *same* experimental data and the *same* model equations. Using this tuned model, multi-objective optimization (MOO) of an *isothermal* fixed bed ESR reactor has been carried out using NSGA-II to achieve the maximum hydrogen mole fraction in the product gas while simultaneously minimizing the mole fractions of the greenhouse gases, $CO + CO_2$. The more recent jumping gene adaptation of NSGA-II, namely, NSGA-II-JG, was also tried to check if it can give more rapid convergence to the Pareto set.

ACKNOWLEDGEMENT

Date: **(KUMARGAURAO D. PUNASE)**
Place: Dehradun

TABLE OF CONTENTS

LIST OF FIGURES

LIST OF TABLES

NOMENCLATURE

SYMBOLS

$E_{a,i}$ — Activation energy for rate constant of reaction i, [J/mol]

F — Total molar flow rate, [kmol/hr]

F_i — Molar flow rate of species i at any axial location, [kmol/hr]

F_T — Total molar flow rate at any axial location, [kmol/hr]

H_2O/E — Water to ethanol ratio

ΔH_{298}^0 — Standard heat of formation, [kJ/mol]

ΔH_i — Heat of adsorption for surface species [J/mol]

I_i — Objective function, i

k_i — Rate constant for reaction i, [mol/(min.gcat)]

$k_{i,0}$ — Rate constant for reaction i at a reference temperature, [mol/(min.gcat)]

K_3, K_4 — Equilibrium constants for reactions (3.3) and (3.4)

K_i — Adsorption coefficient for surface species i

$K_{i,0}$ — Adsorption coefficient for surface species i at reference temperature

L — Length of the reactor, [cm]

N_{gen} — Total number of generations

N_{pop} — Total number of members in the population

P — Total pressure [atm]

P_{cross}	Crossover probability
P_{jump}	Jumping gene probability
P_{mut}	Mutation probability
P_i	Partial pressure of component i, [atm]
r_i	Rate of reaction of component i, [mol/(min.gcat)]
R	Universal gas constant, [J/(mol.K)]
T	Temperature, [K]
u	Decision variables
w	Weight factor
W	Weight of the catalyst till axial location Z, [gm]
y_i	Mole fraction of component i
Z	Axial location
ϑ_{ij}	stoichiometric coefficient for reaction i for component j
θ	Space time, [(gcat.min)/mol]
Percent Relative Error	$\left\lvert \dfrac{y_{i,calc} - y_{i,exp}}{y_{i,exp}} \right\rvert \times 100$

ACRONYMS

ER	Eley-Rideal
ESR	Ethanol steam reforming
GA	Genetic algorithm
LHHW	Langmuir-Hinshelwood-Hougen-Watson

MOO	Multi-objective optimization
RDS	Rate determining step
SSE	Normalized sum of square errors
WGS	Water gas shift

SUBSCRIPTS

CO	Carbon monoxide
CO_2	Carbon dioxide
H_2	Hydrogen
H_2O	Water
E	Ethanol
M	Methane
$cross$	Crossover
gen	Generation
in	at reactor inlet
$jump$	Jumping gene
mut	Mutation
out	at reactor outlet
pop	Population

CHAPTER 1: INTRODUCTION

The energy production and consumption from the fossil fuels have led to several disadvantages like greenhouse gas emissions, environmental pollutions, ozone layer depletion, climate changes, etc. There has been a strong urge to replace the fossil fuels with the renewable and sustainable resources of energy. The world scientific community is looking for many alternative energy resources to meet the increasing demand for energy, which are clean, and energy efficient. These include solar energy, wind energy, hydel energy, ocean current energy, geothermal energy, nuclear energy, biomass energy, etc. The capital investment is very high for converting these energies into useful forms. At the same time, the availability and the storage of these energy forms have prompted to check their economic feasibility and reliability for major applications of energy consumption. The overnight capital cost (power generation, $/kW), which does not include the interest calculations during construction, is shown in Fig. 1.1 for different energy sources [1].

1.1 HYDROGEN AS A RENEWABLE SOURCE

The technologies based on fossil fuel conversion are well established, more efficient and offer the lower capital cost when compared to the capital costs of other energy resources. However, the fossil fuel resources are diminishing and causing the various environmental hazards. Of the various alternative energy resources, hydrogen is considered as the next generation energy source and will play a major role for the replacement of fossil fuels. It contains the highest amount of energy per unit weight (120 MJ/kg). It is the clean fuel as it produces

only water when burnt with oxygen and its conversion to heat or power is simple [2].
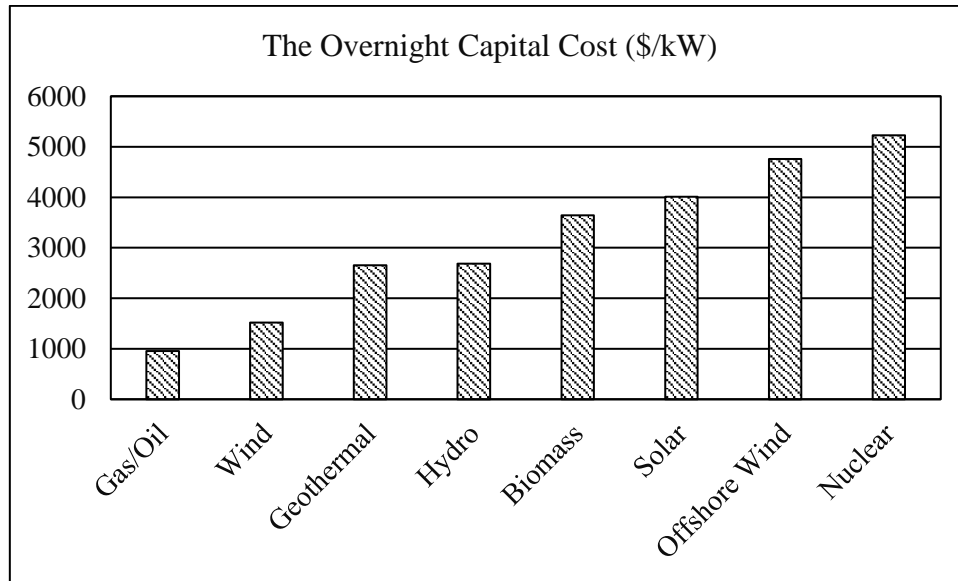
Fig. 1.1 The overnight capital cost for various energy sources [1]

However, hydrogen is separated from chemical compounds using thermochemical, electrochemical, photochemical and photobiological conversion methods, as it is not present in elemental form in the nature. Currently, the major hydrogen production is taking place from non-renewable energy sources and 85% of the total hydrogen is being produced using methane steam reforming (MSR) technology (thermochemical conversion method). The alternative resources like lower alcohols such as methanol and ethanol, biodiesel, glycerol, ethane, propane, butane, natural gas [3-7], etc. are studied widely to produce hydrogen from steam reforming. Methanol possesses high hydrogen to carbon ratio. When compared to other fuels, it is converted to hydrogen at low temperatures. But, it is relatively highly toxic. To mitigate the climate change, different studies have been proposed to replace the non-renewable energy resources for steam reforming process with the renewable energy resources. As a renewable resource for hydrogen production, much attention has been paid to ethanol for hydrogen production by many researchers as it is produced from biomass (renewable resource) fermentation, less toxic and easy to transport [4, 8].

1

1.2 ETHANOL AVAILABILITY

Hydrogen is produced from ethanol using the thermochemical conversion methods like steam reforming, autothermal reforming and partial oxidation. Sun et al. [9] reported that the steam reforming produces greater number of moles of hydrogen per mole of ethanol than autothermal reforming followed by partial oxidation. Ethanol steam reforming (ESR) would be a most suitable technology in the present industrial infrastructure of hydrogen production as methane can be easily replaced by ethanol as a renewable resource. Compared to methane, ethanol can be reformed at a significantly lower temperature and is a CO_2-neutral energy source.

Depending upon the feedstock, ethanol (or bioethanol) is produced as 1st generation and 2nd generation product. The 1st generation ethanol is produced from the edible, sugar and starch-rich agriculture crops and products such as sugarcane, corns, wheat and potatoes. However, there is a conflict of using these substrates, which are intended for food and feed purposes. Thus, the cost of 1st generation ethanol is quite high and the ethical issues are involved. The 2nd generation ethanol offers an alternative to 1st generation ethanol as it is produced from lignocellulosic biomass. This feedstock includes agriculture and forestry residues, waste generated from paper industry and wood processing. There is an active research being carried out to efficiently convert this lignocellulosic biomass into ethanol. Potentially, ethanol yield is found to increase from 270 liter/ton to 400 liter/ton of lignocellulosic biomass [8, 10]. Ethanol production has been increased manifolds in the agriculture-based countries like India, Brazil, America in the last 10 years. The ethanol production (million gallons) in major countries and regions is depicted in Fig. 1.2. There is an abundant amount of inexpensive cellulosic biomass available in India, which can be used for ethanol production to meet the energy demand in future. The biomass-derived ethanol production technology can be integrated with hydrogen fuel cell for electricity generation as shown in Fig. 1.3 along with its other applications.

2
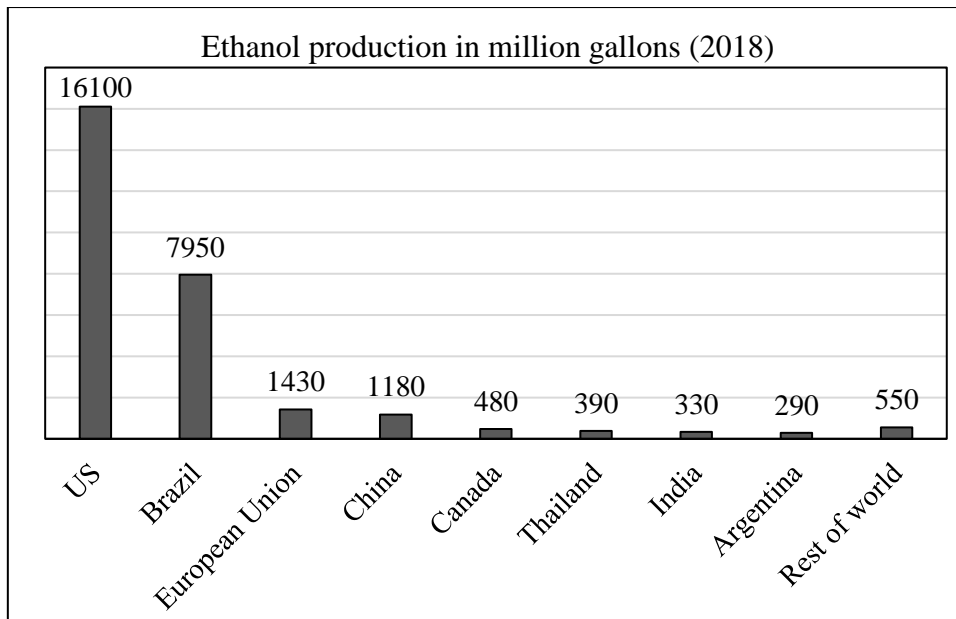
Fig. 1.2 Ethanol production in major countries and regions in 2018 [11]
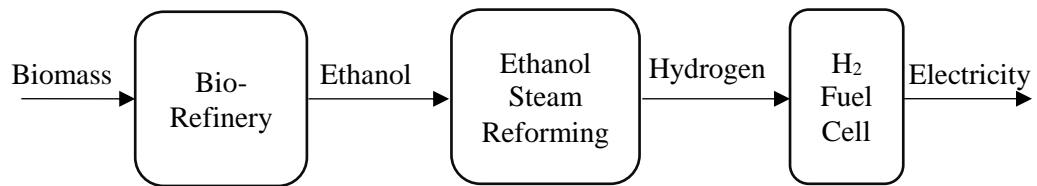
Fig. 1.3 Integration of biomass-derived ethanol with hydrogen fuel cell

1.3 ESR REACTION KINETICS, MECHANISMS AND CATALYSIS

ESR studies have been carried out based on the catalyst development, catalysis and reaction mechanism. The noble metal catalysts such as Pt, Rh, Ru, Ir, Pd, Au, etc. and non-noble metal catalysts such as Co, Cu, Fe, Ni, Al, Ce, etc. have been used for ESR along with the supporting materials like Al_2O_3, ZrO_2, SiO_2, La_2O_3, TiO_2, CeO_2, zeolites or a combination of all of these [12]. The aim is to develop an active catalyst that increases the hydrogen yield, inhibits coke formation and CO production. The kinetic rate models for ESR reactions are developed using power rate law based expressions and mechanistic kinetic mechanisms like Langmuir-Hinshelwood-Hougen-Watson (LHHW) mechanism and Eley-Rideal (ER) mechanism [13].

3

ESR follows the ideal stoichiometry shown in Eqn. (1.1) to produce hydrogen from ethanol.

$$C_2H_5OH + 3H_2O \rightarrow 6H_2 + 3CO_2 \qquad (1.1)$$
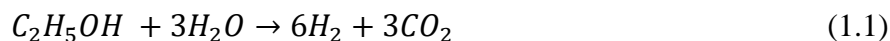
The standard heat of reaction (ΔH^0_{298}) is +173.4 kJ/mol for gas phase reactants and +347.4 kJ/mol for liquid phase reactants.

There are several side reactions occur during ESR depending upon water to ethanol molar ratio in the feed and the operating conditions of temperature and pressure as shown in Table 1.1. The products produced from these reactions include carbon monoxide, carbon dioxide, methane, hydrogen, acetaldehyde, acetone, ethylene, diethyl ether, acetic acid, and elemental carbon [14]. The type of catalyst, metal loading and its support along with the operating conditions govern the reaction mechanism and product formation of ESR.

Table 1.1 Side reactions during ESR [9, 13-14]

Sr. No.	Reaction	Equation	ΔH^0_{298} (kJ/mol)
1	Syngas formation	$C_2H_5OH + H_2O \rightarrow 2CO + 4H_2$	+256
2	Methane formation	$C_2H_5OH \rightarrow CH_4 + CO + H_2$	+49.7
		$C_2H_5OH + H_2O \rightarrow CH_4 + CO_2 + 2H_2$	+205
3	Acetaldehyde formation	$C_2H_5OH \rightarrow CH_3CHO + H_2$	+68.4
4	Acetone formation	$2C_2H_5OH \rightarrow CH_3COCH_3 + CO + 3H_2$	-93.8
5	Ethylene formation	$C_2H_5OH \rightarrow CH_2CH_2 + H_2O$	+45
6	Diethyl Ether formation	$2C_2H_5OH \rightarrow C_2H_5OC_2H_5 + H_2O$	+48
7	Acetic acid formation	$C_2H_5OH + H_2O \rightarrow CH_3COOH + 2H_2$	-26.7
8	Boudouard reaction	$2CO \rightarrow CO_2 + C$	-171.5
9	Coke formation	$nCH_2CH_2 \rightarrow coke + 2nH_2$	-171.5

The power rate law expressions are derived by fitting the kinetic data of ESR reaction as shown in Eqn. (1.2).

$$-r_{ESR} = k_0 exp\left(\frac{-E_a}{RT}\right) p_E^{\alpha} p_{H_2O}^{\beta} \qquad (1.2)$$

The mechanistic kinetic models give more insight into the ethanol steam reforming reactions. In the ER mechanism, ethanol is adsorbed on the surface or the active site of the catalyst. It is assumed that there is no pore diffusion resistance taking place on the surface of the catalyst. ER mechanism usually follows various steps; ethanol adsorption on the surface of the catalyst followed by dissociation of ethanol on the catalyst surface by the reaction of ethanol to the adjacent vacant site of the catalyst to form the oxygenated and hydrogenated carbon fraction. These react with the free water molecules present above the catalyst to form hydrogen, carbon dioxide and a vacant site as to have desorbed from the catalyst. LHHW mechanism is quite different from ER mechanism, in which all the reactant species are adsorbed on the catalyst surface. The next steps followed are as molecular rearrangement through surface reaction and desorption. ER and LHHW mechanisms are demonstrated for ESR in Fig. 1.4 and Fig. 1.5, respectively.
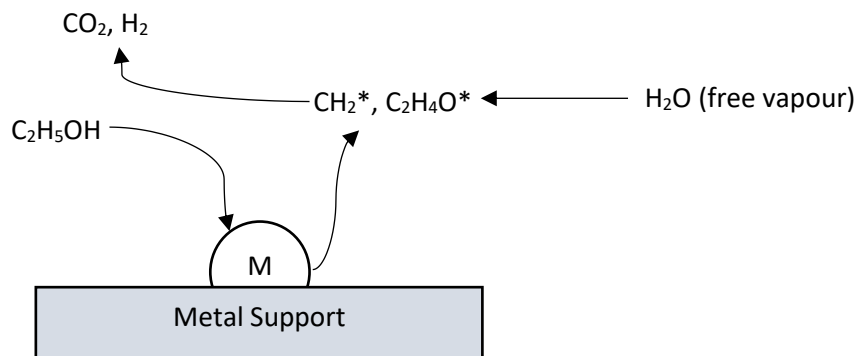
Fig. 1.4 Reaction routes for ESR using ER mechanism (M: Active Site)
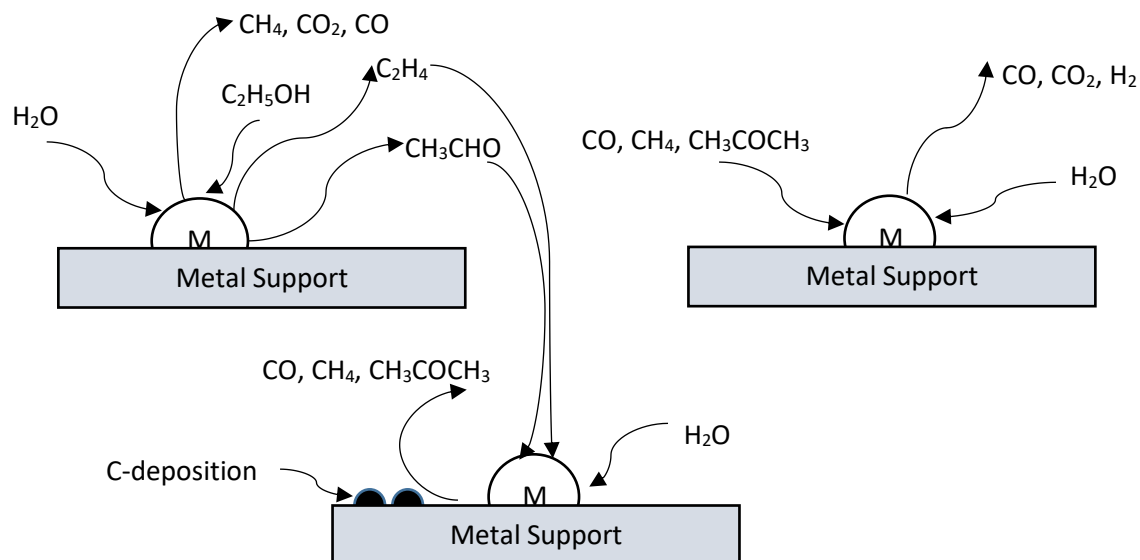
Fig. 1.5 Reaction routes for ESR using LHHW mechanism (M: Active Site)

The activation energies for the LHHW and the ER mechanisms are of the order of 10^3-10^5 and 10^3 (J/mol), respectively. This is because the ER mechanism does not account for the adsorption of gaseous species. This leads to the elimination of the formation of the oxygenated and hydrogenated radicals. The presence or absence of heat and mass transfer effects can affect the activation energies of these models. The LHHW mechanism is considered as reasonably complex and is a more reliable and accurate model as compared to the ER mechanism. There are very few mechanistic kinetic models available for ESR and its modelling and simulation studies are limited in the literature [13].

The ESR reaction is studied using fixed bed reactors, membrane reactors, fluidized bed reactors and wall-coated microchannel reactors [15-16]. MSR uses largely a fixed bed reactor to obtain the high purity of hydrogen with effective cost of its production.

1.4 OBJECTIVES OF THIS THESIS

Modeling and simulation is an important tool to design and scale up lab-scale studies of ESR based on catalyst development. This involves the estimation of kinetic parameters of the rate model to match the experimental results, develop

and validate the mathematical model for the ethanol steam reformer (a fixed bed reactor) using the proposed kinetic model and optimization studies to increase the yield of hydrogen based on the validated model. Surprisingly, only a few studies have been reported on the mathematical *modeling and simulation* of hydrogen production using ESR [16]. The ESR reactions are very complex in nature and identification of reliable reaction rate mechanisms is necessary to model the ESR process. In this thesis, a mathematical model is developed for a fixed bed reactor for ESR using the kinetic model proposed in the literature. The mathematical model is fitted with the experimental ESR reactor using the optimized kinetic parameters of ESR rate model obtained by a genetic algorithm (GA) technique. A multi-objective optimization (MOO) problem is solved for ESR reactor using these optimized parameters for maximizing the hydrogen mole fraction, simultaneously minimizing the mole fractions of carbon monoxide and carbon dioxide. The evolutionary algorithms like NSGA-II and a jumping gene adaptation of NSGA-II are used to solve a MOO problem.

The objectives of this study are as follows:

1) Estimation of kinetic parameters to tune the proposed kinetic model with experimental results

2) Development of a mathematical model for a 1-D, pseudo homogeneous fixed bed reactor to carry out ESR over Ni-based catalyst under operating conditions used in experimental study at steady state and isothermal conditions

3) Development of a MATLAB code to optimize the kinetic parameters and to solve the ODEs using the optimized values of these kinetic parameters

4) Validation of the model using experimental data

5) Multi-objective optimization of ESR reactor to maximize the yield of hydrogen whilst minimizing the amount of greenhouse gases, CO and CO_2, together using the solution techniques NSGA-II and a jumping gene adaptation of NSGA-II

1.5 STRUCTURE OF THESIS

This thesis is divided into five chapters.

Chapter 1 - Introduction - which elaborates about the need of renewable energy resources, hydrogen production using ESR process. The possible routes of hydrogen production from ESR are discussed using the catalytic reactions. It summarizes the work done in this subject area and setting up the objectives to meet the identified research gaps.

In Chapter 2, the literature survey is presented on the catalysts used and the mechanistic kinetic models developed for ESR process. A kinetic model based on Ni-catalyst is selected to mathematically model the ESR process through a comparative study. The differences in the results obtained by two different researchers using the same kinetic model and same data are identified. This is set as one of the objectives to re-establish the suitability and reliability of the proposed reaction kinetics of ESR by estimating the kinetic parameters using evolutionary algorithm like GA technique.

Chapter 3 covers the modelling and optimization aspects of ESR process including the tuning of kinetic parameters using GA technique. The mathematical model of a fixed bed reactor is developed for ESR using the kinetic model available in the literature. A multi-objective optimization of ESR reactor is formulated (first time in literature) to maximize the yield of hydrogen whilst minimizing the amount of greenhouse gases, CO and CO_2, together. The solution of a MOO problem is obtained by using the NSGA-II and a jumping gene adaptation of NSGA-II.

In Chapter 4, the results are discussed for the estimation of kinetic parameters for the proposed reaction rate model using GA technique in Section 4.1. The GA optimized kinetic parameters are used to fit the model predicted results with the experimental results. There was a conflict of the results obtained by two different researchers for the proposed kinetic model of ESR using the same reactor data and operating conditions. The comparative study of simulated results of earlier researchers and this study with the experimental results is

carried out to ascertain the reliability of the proposed kinetic model. In Section 4.2, the solution of a MOO problem is discussed using NSGA-II and NSGA-II-JG. The effect of decision variables on one of the objective functions, molar fraction of hydrogen, is discussed using NSGA – II. A jumping gene adaptation of NSGA-II is used to speed up the solution of a MOO problem.

The most relevant conclusions are summarized in Chapter 5 along with the future scope of this work.

CHAPTER 2: LITERATURE SURVEY

ESR is a surface reaction and the catalyst role is to: i) break the C-C bond rather than promoting the activation of C-O bond to produce CO and/or CO_2 and CH_4, ii) transform these carbon intermediates to produce H_2 and CO_2, and iii) inhibit coke formation by producing highly mobile oxygen through water activation. The metal supported catalysts facilitate the C-C bond cleavage over active metal surface and the diffusion of intermediates over the metal-support interface. The reaction selectivity and the occurrence of side reactions are dependent on alkalinity/acidity of the support and its redox property [17]. The supported noble metal and non-noble metal catalysts are used for ESR reactions. This is discussed in the sections 2.1, 2.2, and 2.3. Rh-based and Ni-based catalysts are widely investigated in ESR on different supports.

2.1 NOBLE METALS

Table 2.1 shows the details about the catalytic studies based on noble metals. The activity of the metals follows the order as Rh > Pd > Ni=Pt, whereas at higher temperature, it is followed as Pt > Rh > Pd. The order of the catalyst performance based on ethanol conversion is Rh >> Pt > Pd > Ru. Rh also shows the higher H_2 selectivity than Ru, Pt and Pd [18, 19].

Table 2.1 Noble catalysts used in ESR

Catalyst	Comments
Rh-supported catalyst	• $Rh/\gamma\text{-}Al_2O_3$ catalyst shows high activity, stability and H_2 selectivity. The coke formation decreases at high temperatures with increase in Rh loading and excess of water. The reaction conditions influence the performance of the Rh catalyst along with the nature of metal precursor salt and metal loading[19-22]. Aupreter et al. [23] observed C_1 products only in the exit stream at 973 K. • For $Rh/CeO_2\text{-}ZrO_2$ catalyst, ethylene is not produced at high temperatures. In presence of excess of water and a temperature range of 623-723 K, one mole of ethanol is found to produce around 5.7 mole H_2 [24]. • A very low coke formation is found for Rh/MgO catalyst. It also shows higher H_2 selectivity (> 95%) [25]. • The H_2 selectivity and stability are higher for Bimetallic Rh-[Ni, Co, Pd, Pt] catalysts used for ESR reaction [12].
Pt-supported catalyst	• Pt/Al_2O_3 catalyst shows low activity and selectivity towards CO_2. It is active at 873 K and gives 55% as H_2 selectivity [26]. • Pt/CeO_2 catalyst has strongest ability to break C-C bond. Methanation is observed which causes low H_2 yield [27].
Pd-supported catalyst	• Pd/Al_2O_3 catalyst shows high catalytic activity and stability for ESR reaction. Carbon formation is negligible. H_2 selectivity is 55% at 973 K [17].

	- 0.5%Rh-0.5%Pd/CeO$_2$ catalyst breaks the bond at lower temperature than 400 K and shows the maximum ethanol conversion and H$_2$ selectivity [28].
Ru-supported catalyst	- Ru/Al$_2$O$_3$ catalyst shows low activity and selectivity towards CO$_2$. The catalyst activity increases with increasing metal loading (5 wt%) at 1073 K [19].
Ir-based catalyst	- For Ir/CeO$_2$ catalyst, coke deposition is inhibited due to strong Ir-CeO$_2$ interactions [29]. - Ethanol conversion decreases from initial 100% to 80% and 62% after 60 h and 300 h, respectively. Hydrogen concentration changes from initial 61% to 55% in 60 h and remains unchanged thereafter [29].

2.2 NON-NOBLE METALS

Ni and Co based catalysts are extensively studied for ESR over different supports as shown in Table 2.2. Ni-based catalysts are largely used in the industries for hydrocarbon steam reforming and hydrogenation processes because of its high activity and low cost. Due to the higher hydrogenation activity of Ni, hydrogen molecule is produced from the reaction of adsorbed hydrogen atoms on the catalyst surface. In the comparative study of ESR over MgO supported Ni and Co catalysts, Freni et al. [30] observed that Ni-based catalyst shows higher activity and H$_2$ selectivity compared to Co-based catalyst as metallic Ni possesses a low tendency to oxidize during the reaction.

Table 2.2 Non-noble catalysts used in ESR

Catalyst	Comments
Ni-supported catalyst	• Ni/γ-Al_2O_3 catalyst shows no evidence of water gas shift reaction in the temperature range of 573-773 K. The intermediates acetaldehyde and ethylene produce CO, CO_2, CH_4 and H_2 [31]. • Ni/Y_2O_3 and Ni/La_2O_3 catalysts exhibit relatively high activity in ESR at 523 K. Ethanol conversion and H_2 selectivity increase with an increase in the reaction temperature to 593 K. Ni/Al_2O_3 exhibits comparatively lower activity in ESR and H_2 selectivity [32]. • Ni/MgO catalyst inhibits the coke formation [30]. • Ni/Al_2O_3/ZrO_2 catalyst promotes CH_4 reforming reaction and enhanced resistance toward coke deposition due to highest Ni surface area [33]. • CO, CO_2, CH_4 and H_2 are the main products for ESR reaction carried above 823 K [34].
Co-supported catalyst	• The order of H_2 formation: Co/Al_2O_3 > Co/ZrO_2 > Co/MgO > Co/SiO_2 > Co/C. The Co/Al_2O_3 catalyst suppresses CO methanation and ethanol decomposition. As a result, it shows the highest H_2 selectivity of 67% at 673 K [35]. • For Co/SiO_2 and Co/Al_2O_3 catalysts, the catalyst preparation method and its support influence the product distribution [36].
Cu-supported catalyst	• CuO/ZnO/Al_2O_3 catalyst shows good activity and the main products are CO, CO_2 and H_2 above 630 K [37].

	- For Cu/SiO$_2$ catalyst, a complete conversion of ethanol is observed at temperatures of 573–723 K to produce H$_2$ and acetaldehyde as the major reaction products and the traces of CO and CH$_4$ [38]. - Copper has high ability to maintain the C-C bond and is effective for ethanol dehydrogenation [39].

2.3 CATALYST SUPPORTS

The catalyst supports improve the performance of metal catalysts. Al$_2$O$_3$ is the commonly used support in ESR and is acidic in nature. Coke deposition takes place over catalyst surface through the polymerization of ethylene produced from dehydration of ethanol. MgO is basic in nature and offers more stability and selectivity in case of less active metal catalysts when compared to Al$_2$O$_3$. It also inhibits the coke formation and promotes the interaction of Ni atoms with electron acceptor intermediates [30]. ZnO and CeO$_2$ are basic and exhibit the redox properties. Ethanol dehydrogenates to acetaldehyde in case of MgO and ZnO supported catalysts. CeO$_2$ also promotes the WGS reaction. La$_2$O$_3$ supported Ni catalysts show the improved performance and stability compared to Al$_2$O$_3$. ZrO$_2$ is thermally stable and possesses both acidic and basic properties [18].

2.4 KINETIC MODELS

The fundamental understanding of ESR reactions taking place at molecular level is required to design the highly efficient ESR process. This involves the analysis of the reaction mechanism and kinetics. In this section, the reaction kinetics are discussed for the low cost and efficient non-noble metal catalysts as noble metals are scarce and very expensive. Co exhibits higher activity but sintering takes place at higher temperatures [25]. Ni is an effective catalyst to

break C-C, CH_2, CH_3 and O-H bonds along with its ability to produce molecular hydrogen [20]. The mechanistic kinetic models, which consider the actual ESR reaction mechanism, are developed based on ER mechanism and LHHW mechanism. There are six kinetic models analysed having the hydrogen yield of 4 or more per mole of ethanol in feed (Stoichiometric yield: 6 moles of hydrogen per mole of ethanol).

2.4.1 MODEL FOR COMMERCIAL Ni CATALYST BASED ON ER MECHANISM

Akande et al. [40] proposed the kinetic model of ESR using commercial Ni catalysts based on ER mechanism. The steps followed in ER mechanism are:

(1) Adsorption of crude ethanol on the active site of the catalyst

$$C_2H_5OH + (a) \xrightleftharpoons{k_{1,-1}} C_2H_5OH(a) \qquad (2.1)$$
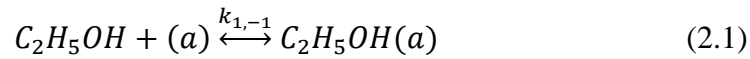
(2) Dissociation of adsorbed crude ethanol to form the oxygenated hydrocarbon and hydrocarbon fractions

$$C_2H_5OH(a) + (a) \xrightleftharpoons{k_{2,-2}} CH_4O^*(a) + CH_2^*(a) \qquad (2.2)$$
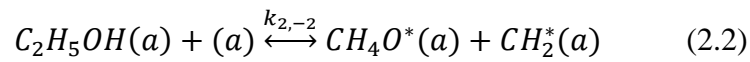
(3) Surface reaction of adsorbed oxygenated hydrocarbon with the molecules of unadsorbed water vapour

$$CH_4O^*(a) + H_2O \xrightleftharpoons{k_{3,-3}} CO_2 + 3H_2 + (a) \qquad (2.3)$$
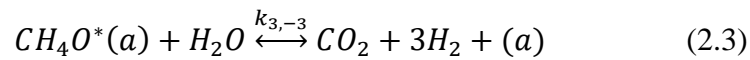
(4) Surface reaction of hydrocarbon with the molecules of unadsorbed water vapour

$$CH_2^*(a) + 2H_2O \xrightleftharpoons{k_{4,-4}} CO_2 + 3H_2 + (a) \qquad (2.4)$$
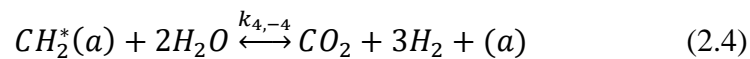
Where (a) is an active site of the catalyst, * represents the adsorbed species present, k_i represents the rate of forward reaction and k_{-i} represents the rate of backward reaction. Rate Determining Step (RDS) depends on the type of catalyst used in ESR. The elementary steps are considered as RDS, to develop four different rate models. However, this is not applicable to every catalyst.

Some of the catalysts employ dissociation of adsorbed ethanol to form oxygenated hydrocarbon and hydrocarbon as the main RDS in which kinetic parameters have been associated. The Average Absolute Deviation (AAD) between predicted and experimental results for the determined RDS were obtained to fit the rate model for ESR. CH_2 formed as an intermediate at a very low quantity, is dissolved during the reaction. This kind of kinetic model does not consider the mass-transfer resistance and the intraparticle resistance. These resistances were not considered for acetaldehyde and acetic acid in the product analysis. The kinetic rate models and their parameters are shown in Tables 2.3 and 2.4, respectively.

Another mechanism proposed is the LHHW mechanism, in which ethanol and steam get adsorbed on the surface of a catalyst and reacted with the adjacent vacant side of catalyst. The products formed, are desorbed after the reaction on the surface of the catalyst. The adsorbed water vapour dissociates to form the hydrogen and oxygen.

Table 2.3 Kinetic model for commercial Ni catalyst based on ER mechanism [40]

Rate model	Reaction	Rate equation
1	Adsorption of ethanol on the surface of catalyst (RDS)	$$r_a = \frac{k_0 e^{-\frac{E_a}{RT}}\left[C_A - \frac{C_C^2 C_D^6}{K_p C_B^3}\right]}{\left[1 + \frac{K_F C_C C_D^3}{C_B} + \frac{K_G C_C C_D^3}{C_B^2} + \frac{K_E C_C^2 C_D^6}{C_B^3}\right]}$$
2	Dissociation of adsorbed ethanol into CH_4O and CH_2 (RDS)	$$r_a = \frac{k_o e^{-\frac{E_a}{RT}}\left[C_A - \left(\frac{C_C^2 C_D^6}{K_p C_B^3}\right)\right]}{\left[1 + K_A C_A + K_F \frac{C_C C_D^3}{C_B} + \frac{K_G C_C^2 C_D^3}{C_B^2}\right]^2}$$
3	Surface reaction of CH_4O and steam (RDS)	$$r_a = \frac{k_0 e^{-\frac{E_a}{RT}}\left[\frac{C_A C_B^3}{C_C C_D^3} - \frac{C_C C_D^3}{K_p}\right]}{\left[1 + K_A C_A + \frac{K_Q C_A C_B^2}{C_C C_D^3} + \frac{K_G C_C C_D^3}{C_B^2}\right]}$$
4	Surface reaction of CH_2 and steam (RDS)	$$r_a = \frac{k_o e^{-\frac{E_a}{RT}}\left[\frac{C_A C_B^3}{C_C C_D^3} - \frac{C_C C_D^3}{K_p}\right]}{\left[1 + K_A C_A + \frac{K_F C_C C_D^3}{C_B} + \frac{K_H C_A C_B}{C_C C_D^3}\right]}$$

$A = C_2H_5OH, B = H_2O, C = CO_2$, and $D = H_2$

Table 2.4 Kinetic Parameters for commercial Ni catalyst [40]

Parameter	Model 1	Model 2	Model 3	Model 4
k_0 [kgcat.s]$^{-1}$	8.91E+02	2.08E+03	1.31E+14	2.75E-02
E_a [kJ/kmol]	4.03E+03	4.43E+03	3.55E+03	7.56E+03
K_A [-]	-	3.83E+07	1.00E+20	2.27E+14
K_E [-]	0	-	-	-
K_F [-]	0	0	-	1.00E+20
K_G [-]	0	0	0	-
K_H [-]	-	-	-	0
K_Q [-]	-	-	3.66E+12	-

2.4.2 MODELS USING COMMERCIAL Ni CATALYST BASED ON LHHW MECHANISM

Akpan et al. [41] proposed the kinetic model of ESR using commercial Ni catalysts based on LHHW mechanism. The steps followed in the LHHW mechanism are:

(1) Adsorption of crude ethanol on the active site of catalyst

$$C_2H_5OH + (a) \xrightleftharpoons{k_{1,-1}} C_2H_5OH^*(a) \qquad (2.5)$$
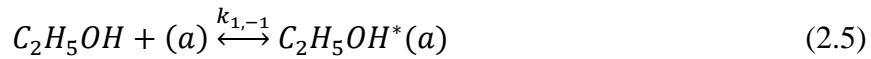
(2) Interaction of the adsorbed crude ethanol with an adjacent vacant site

$$C_2H_5OH^*(a) + (a) \xrightleftharpoons{k_{2,-2}} CH_3O^*(a) + CH_3^*(a) \qquad (2.6)$$
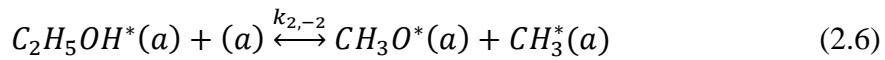
(3) Adsorption of water on the active site of catalyst

$$3H_2O + 3(a) \xrightleftharpoons{k_{3,-3}} 3H_2O^*(a) \qquad (2.7)$$

(4) Surface reaction of water to form the surface oxygen and molecular hydrogen vapour

$$3H_2O^*(a) \xrightleftharpoons{k_{4,-4}} 3O^*(a) + 3H_2 \qquad (2.8)$$

18

(5) Surface reaction between the oxygenated hydrocarbon and oxygen

$$CH_3O^*(a) + O^*(a) + 2(a) \overset{k_{5,-5}}{\longleftrightarrow} CO_2^*(a) + 3H^*(a) \qquad (2.9)$$
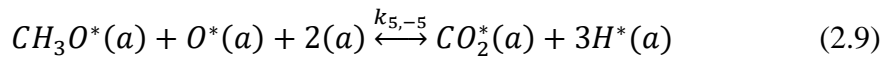
(6) Surface reaction between hydrocarbon and oxygen

$$CH_3^*(a) + 2O^*(a) + (a) \overset{k_{6,-6}}{\longleftrightarrow} CO_2^*(a) + 3H^*(a) \qquad (2.10)$$
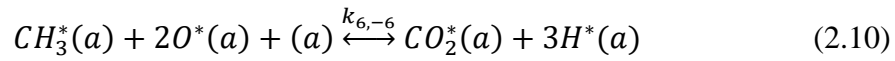
(7) Desorption of hydrogen

$$3H_2^*(a) \overset{k_{7,-7}}{\longleftrightarrow} 3H_2 + 3(a) \qquad (2.11)$$

Eqns. (2.5) to (2.10) are considered as RDS. The kinetic rate models and parametric values are given in Tables 2.5 and 2.6, respectively.

Table 2.5 Kinetic model for commercial Nickel catalyst based on LHHW mechanism [41]

Rate Model	Reaction	Rate Equation
1	Molecular adsorption of ethanol (RDS)	$$r_a = \frac{k_o e^{-\frac{E_a}{RT}}\left[C_A - \frac{C_C^2 C_D^6}{K_p C_B^3}\right]}{\left[1 + \frac{K_1 C_C^2 C_D^6}{C_B^3} + K_2 C_B + K_3 C_C + K_4 C_D + \frac{K_5 C_C C_D^{2.5}}{C_B} + \frac{K_6 C_B}{C_D} + \frac{K_7 C_C C_D^{3.5}}{C_B^2} + K_8 C_D^{0.5}\right]^2}$$
2	Dissociation of adsorbed ethanol to form chemisorbed radicles such as CH_3O and CH_3 (RDS)	$$r_a = \frac{k_o e^{-\frac{E_a}{RT}}\left[C_A - \frac{C_C^2 C_D^6}{K_p C_B^3}\right]}{\left[1 + K_1 C_A + K_2 C_B + K_3 C_C + K_4 C_D + \frac{K_5 C_C C_D^{0.5}}{C_B} + \frac{K_6 C_B}{C_D} + \frac{K_7 C_C C_D^{1.5}}{C_B^2} + K_8 C_D^{0.5}\right]^2}$$
3	Molecular adsorption of water (RDS)	$$r_a = \frac{k_0 e^{-\frac{E_a}{RT}}\left[C_B^3 - \frac{C_C^2 C_D^6}{K_p C_A}\right]}{\left[1 + K_1 C_A + \frac{K_2 C_C^{\frac{2}{3}} C_D^2}{C_D^{\frac{1}{3}}} + K_3 C_C + K_4 C_D + K_5 C_C^{\frac{1}{3}} C_D^{0.5} + \frac{K_6 C_C^{\frac{2}{3}} C_D}{C_A^{\frac{2}{3}}} + \frac{K_7 C_A^{\frac{2}{3}}}{C_C^{\frac{1}{3}} C_D^{0.5}} + K_8 C_D^{0.5}\right]^3}$$

4	Surface reaction of water to form free hydrogen vapour and oxygen radical (RDS)	$$r_a = \frac{k_o e^{-\frac{E_a}{RT}}\left[C_B^3 - \dfrac{C_C^2 C_D^6}{K_p C_A}\right]}{\left[1 + K_1 C_A + K_2 C_B + K_3 C_C + K_4 C_D + K_5 C_C^{\frac{1}{3}} C_D^{0.5} + \dfrac{K_6 C_C^{\frac{2}{3}} C_D}{C_A^{\frac{2}{3}}} + \dfrac{K_7 C_A^{\frac{2}{3}}}{C_C^{\frac{1}{3}} C_D^{0.5}} + K_8 C_D^{0.8}\right]^3}$$
5	Surface reaction between oxygenated radical and CH_3O (RDS)	$$r_a = \frac{k_o e^{-\frac{E_a}{RT}}\left[\dfrac{C_A C_B^3}{C_D^{4.5} C_C} - \dfrac{C_C C_D^{1.5}}{K_p}\right]}{\left[1 + K_1 C_A + K_2 C_B + K_3 C_C + K_4 C_D + \dfrac{K_5 C_A C_B^2}{C_C C_D^{3.5}} + \dfrac{K_6 C_B}{C_D} + \dfrac{K_7 C_C C_D^{3.5}}{C_B^2} + K_8 C_D^{0.5}\right]^4}$$
6	Chemical reaction between oxygenated radical and CH_4	$$r_a = \frac{k_0 e^{-\frac{E_A}{RT}}\left[\dfrac{C_A C_B^3}{C_D^{4.5} C_C} - \dfrac{C_C C_D^{1.5}}{K_p}\right]}{\left[1 + K_1 C_A + K_2 C_B + K_3 C_C + K_4 C_D + \dfrac{K_5 C_C C_D^{2.5}}{C_B} + \dfrac{K_6 C_B}{C_D} + \dfrac{K_7 C_A C_B}{C_C C_D^{2.5}} + K_8 C_D^{0.5}\right]^4}$$

Table 2.6 Kinetic Parameters for commercial Ni catalyst [41]

Parameter	Model 1	Model 2	Model 3
k_0 [-]	5.08E+08	3.26E+13	3.90E+34
E_a [J/mol]	3.52E+04	5.54E+04	5.78E+04
K_1 [-]	-	-	-
K_2 [-]	-	-	-
K_3 [-]	7.84E+10	4.48E+10	-
K_4 [-]	-	-	-
K_5 [-]	-	7.28E+06	2.27E+10
K_6 [-]	-	-	-
K_7 [-]	-	-	-
K_8 [-]	-	-	6.42E+07

The Average Absolute Deviation (AAD) between predicted and experimental results for the determined RDS were obtained to fit the rate model for ESR. Model 4, 5 and 6 were not included due to the non-convergence while solving the regression model.

2.4.3 MODEL FOR Ni/Al/LDH CATALYST BASED ON LHHW MECHANISM

Mas et al. [42] presented two models experimented on Ni based catalyst which have two different sets of feed. Model A (Table 2.7) feed consists of ethanol, steam and inert. Model B (Table 2.8) feed consists of ethanol, methane, steam and inert. The Model A assumes the negligible CO and CO_2 adsorptions, single active site (Ni^0) and negligible dissociation of the adsorbed ethanol and water. The assumptions of Model B are similar to Model A. The LHHW mechanisms proposed for Model A and Model B are shown as below.

Model A

(1) Ethanol adsorption

$$C_2H_5OH + (a) \leftrightarrow C_2H_5OH^* \qquad (2.12)$$

(2) Water adsorption

$$H_2O + (a) \leftrightarrow H_2O^* \tag{2.13}$$

(3) Surface reactions take place between ethanol and water

$$C_2H_5OH^* + H_2O^* \leftrightarrow 2CO + 4H_2 + 2(a) \tag{2.14}$$

$$C_2H_5OH^* + 2H_2O^* \leftrightarrow 2CO_2 + 6H_2 + 3(a) \tag{2.15}$$
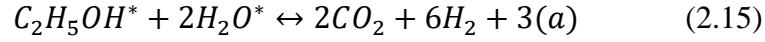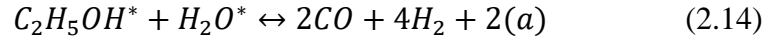
The surface reactions, Eqns. (2.14) and (2.15), between ethanol and water are considered as RDS for developing the kinetic equations.

Table 2.7 Kinetic model for Model A based on LHHW mechanism [42]

Rate Model	Reaction	Rate equation
1	Surface reaction between ethanol and water (RDS)	$r_a = \dfrac{k_5 k_E k_W P_E P_W C_T^2}{(1 + P_E K_E + P_W K_W)^2}$
2	Surface reaction between ethanol and water (RDS)	$r_a = \dfrac{(k_6 K_E K_W^3 P_E P_W^3) C_T^2}{(1 + P_E K_E + P_W K_W)^4}$

Model B

The active sites of Ni/Al/LDH catalyst facilitate the competitive adsorption of ethanol and methane.

(1) Ethanol adsorption

$$C_2 H_5OH + (a) \rightarrow C_2H_5OH^* \tag{2.16}$$

(2) Water adsorption

$$H_2O + (a) \rightarrow H_2O^{*`} \tag{2.17}$$

(3) Surface reaction which causes dissociation of ethanol

$$C_2H_5OH^* \rightarrow CO + CH_4^* + H_2 \tag{2.18}$$

(4) Surface reaction between ethanol and water

$$C_2H_5OH^* + H_2O^* \rightarrow CO_2 + CH_4^* + 2H_2 + (a) \tag{2.19}$$
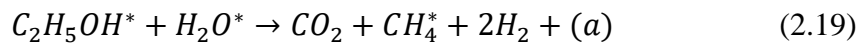
(5) Methane desorption

$$CH_4^* \leftrightarrow CH_4 + (a) \tag{2.20}$$

(6) Surface reaction between methane and water

$$CH_4^* + H_2O^* \rightarrow CO + 3H_2 + 2(a) \tag{2.21}$$

$$CH_4^* + 2H_2O^* \rightarrow CO_2 + 4H_2 + 3(a) \tag{2.22}$$
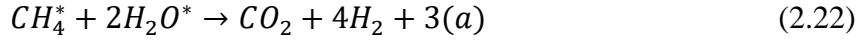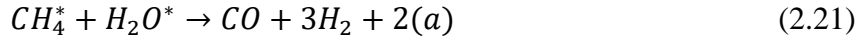
Ethanol decomposition, ethanol steam reforming and methane steam reforming reactions are determined as RDS.

Table 2.8 Kinetic model for Model B based on LHHW mechanism [42]

Rate Model	Reaction	Rate equation
1	Ethanol decomposition (RDS)	$r_a = \dfrac{k_1 K_E P_E}{1 + P_E K_E + P_W K_W + P_M K_M}$ $k_1 = k_1^* C_T$
2	Ethanol steam reforming (RDS)	$r_a = \dfrac{k_2 K_E K_W P_E P_W}{(1 + P_E K_E + P_W K_W + P_M K_M)^2}$ $k_2 = k_2^* C_T^2$
3	Methane steam reforming - I (RDS)	$r_a = \dfrac{k_3 K_M K_W \left(P_M P_W - \dfrac{P_{CO} P_{H_2}^3}{K_3} \right)}{(1 + P_E K_E + P_W K_W + P_M K_M)^2}$ $k_3 = k_3^* C_T^2; \; K_3 = K_3^* K_M K_w$
4	Methane steam reforming – II (RDS)	$r_a = \dfrac{k_4 K_M K_W \left(K_W P_M P_W^2 - \dfrac{P_{CO_2} P_{H_2}^4}{K_4} \right)}{(1 + P_E K_E + P_W K_W + P_M K_M)^3}$ $k_4 = k_4^* * C_T^3; \; K_4 = K_4^* K_M K_W$

The kinetic parameters for Model A (Table 2.9) and Model B (Table 2.10) are calculated by regression model. The constrained optimization problem was formulated and solved using General Algebraic Model System (GAMS) in

Conopt solver that implement Generalized Reduced Gradient (GRG) algorithm. The algorithm can be used to find the values of the mole fractions, kinetic and adsorption parameters in order to minimize the error between experimental and theoretical values.

Table 2.9 Kinetic parameters for Model A using Ni/Al/LDH catalyst [42]

Parameter	Values
k_5 [mol/min.gcat] at 873 K	1.365E-04
k_6 [mol/min.gcat] at 873 K	4.226E-05
$E_{a,5}$ [kJ/mol]	145.8
$E_{a,6}$ [kJ/mol]	112.9
K_W [-] at 873 K	1.279E+03
K_E [-] at 873 K	4.667E+02
ΔH_W [kJ/mol]	-1.878E+02
ΔH_E [kJ/mol]	-1.673E+02

Table 2.10 Kinetic parameters for Model B using Ni/Al/LDH catalyst [42]

Parameter	Values
k_1 [mol/min.gcat] at 873 K	2.9E-05
k_2 [mol/min.gcat] at 873 K	3.1E-04
k_3 [mol/min.gcat] at 873 K	1E-04
k_4 [mol/min.gcat] at 873 K	2.4E-04
$E_{a,1}$[kJ/mol]	278.74
$E_{a,2}$ [kJ/mol]	235.06
$E_{a,3}$ [kJ/mol]	123.50
$E_{a,4}$ [kJ/mol]	213.90
K_W [-] at 873 K	37.4
K_E [-] at 873 K	61.7
K_M [-] at 873 K	1135
ΔH_W [kJ/mol]	-92.40
ΔH_E [kJ/mol]	-199.70
ΔH_M [kJ/mol]	-124.70

2.4.4 MODEL FOR Co/Al$_2$O$_3$ CATALYST BASED ON LHHW MECHANISM

Sahoo et al. [43] developed a mechanism for Co/Al$_2$O$_3$ catalyst that include ethanol steam reforming (ESR), water gas shift (WGS) and ethanol decomposition (ED) reactions as below.

$$C_2H_5OH + 2(a) \leftrightarrow CH_3CH_2O^* + H^* \tag{2.23}$$

$$CH_3CH_2O^* + (a) + \leftrightarrow CH_3CHO^* + H^* \tag{2.24}$$

$$H_2O + 2(a) \leftrightarrow OH^* + H^* \tag{2.25}$$

$$CH_3CHO^* + H^* \leftrightarrow CH_3^* + HCHO^* \tag{2.26}$$

$$CH_3^* + OH^* \leftrightarrow CH_3OH^* + (a) \tag{2.27}$$

$$CH_3OH^* \leftrightarrow CH_3O^* + OH^* \tag{2.28}$$

$$CH_3O^* + (a) \leftrightarrow HCHO^* + H^* \qquad\qquad (2.29)$$

$$HCHO^* + OH^* \leftrightarrow +H^* \qquad\qquad (2.30)$$

$$HCOOH^* + 2(a) \leftrightarrow CO_2^* + H^* \qquad\qquad (2.31)$$

$$CO_2^* \leftrightarrow CO_2 + (a) \qquad\qquad (2.32)$$

$$2H^* \leftrightarrow H_2 + 2(a) \qquad\qquad (2.33)$$
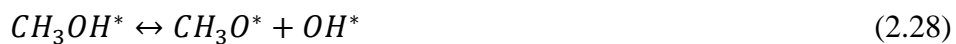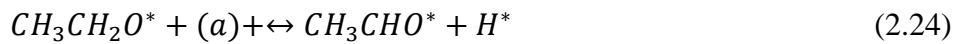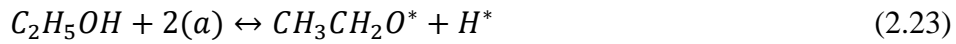
According to Sahoo et al. [43], RDS for ESR, WGS and ED are taken as dehydrogenation of adsorbed ethoxy, decomposition of formate species and decomposition of acetaldehyde, respectively. The rate models are given in Table 2.11 for ESR, WGS and ED. The kinetic parameters of the rate models estimated by Rossetti et al. [44] using the total sum of squares (TSS) are shown in Table 2.12.

Table 2.11 Kinetic model for Co/Al$_2$O$_3$ catalyst based on LHHW mechanism [43]

Rate Model	Reaction	Rate equation
1	Ethanol steam reforming (RDS)	$$r_a = \frac{k_r K_{CH_3CH_2O^*}\left[\dfrac{p_{C_2H_5OH}}{p_{H_2}^{0.5}} - \dfrac{\left(\dfrac{1}{K_{SRE}}\right)p_{CO_2}^2 p_{H_2}^{5.5}}{p_{H_2O}^3}\right][C_T]^2}{DEN^2}$$
2	Water-gas shift (RDS)	$$r_a = \frac{k_w K_{HCOO^*}\left[p_{CO}p_{H_2}^{0.5} - \dfrac{\left(\dfrac{1}{K_{WGS}}\right)p_{H_2O}p_{CO}}{p_{H_2}^{0.5}}\right][C_T]^2}{DEN^2}$$
3	Ethanol decomposition (RDS)	$$r_a = \frac{k_d K_{CH_3CHO^*}\left[\dfrac{p_{CO_2}^2 p_{H_2}^5}{p_{H_2O}^3} - \left(\dfrac{1}{K_{ED}}\right)p_{CH_4}p_{CO}\right][C_T]^2}{DEN^2}$$

$$DEN = 1 + K_{CO_2^*}p_{CO_2} + K_{CO^*}p_{CO} + K_{CH_4^*}p_{CH_4} + K_{HCOO^*}p_{CO_2}p_{H_2}^{0.5} + K_{H^*}p_{H_2}^{0.5} + K_{CH_3CHO^*}\frac{p_{CO_2}^2 p_{H_2}^5}{p_{H_2O}^3} + K_{CH_3CH_2O^*}\frac{p_{C_2H_5OH}}{p_{H_2}^{0.5}} + K_{OH^*}\frac{p_{H_2O}}{p_{H_2}^{0.5}}$$

Table 2.12 Kinetic Parameters for Co/Al$_2$O$_3$ catalyst [44]

Parameter	$\ln(K_0)$	$-\Delta H/R$	Parameter	Value [mol/s.g]	E_a [J/mol]	Species	K_0 [-]	ΔH [J/mol]
K_{SRE}	50.1	-23458.9	$k_{0,r}$	4.332E+00	38150	CO_2^*	1.115E-03	-10543
K_{WGS}	-4.3	4626.3	$k_{0,w}$	2.393E+04	64247	CO^*	1.147E-02	-47295
K_{ED}	-20.8	17076.2	$k_{0,d}$	1.048E+07	122649	$HCOO^*$	7.003E-07	-160270
						CH_3CHO^*	1.553E-02	-35371
						$CH_3CH_2O^*$	9.707E-04	-87143
						OH^*	3.868E-02	-38250
						CH_4^*	6.53E-08	-126795
						H^*	1.37E-01	-32808

2.4.5 MODEL USING Rh(1%) MgAl$_2$O$_4$/Al$_2$O$_3$ BASED ON LHHW MECHANISM

Graschinsky et al. [45] developed a model based on Rh(1%) MgAl$_2$O$_4$/Al$_2$O$_3$ catalyst which is similar to the spinel structure where four reaction schemes were proposed: ethanol steam reforming, ethanol decomposition, water-gas shift reaction and methane steam reforming. The steps that involve two active sites are considered as RDS which include dissociative adsorption of ethanol, dehydrogenation of ethoxide, scission of C–C bonds and surface reactions of two adsorbed species. The regression model was applied to compare all five mechanisms with the experimental data the catalytic conversion of ethanol as well as the yield of H$_2$, as a function of the space–time and the yields of CH$_4$, CO and CO$_2$.

The reaction mechanisms proposed are as follow:

$$C_2H_5OH + (a) \rightarrow C_2H_5OH^* \tag{2.34}$$

$$C_2H_5OH^* + (a) \rightarrow CH_3CH_2O^* + H^* \tag{2.35}$$

$$CH_3CH_2O^* + (a) \rightarrow CH_3CHO^* + H^* \tag{2.36}$$

$$CH_3CHO^* + (a) \rightarrow CH_3^* + CHO^* \tag{2.37}$$

$$CHO^* + (a) \rightarrow CO^* + H^* \tag{2.38}$$

$$CH_3^* + H^* \rightarrow CH_4^* + (a) \tag{2.39}$$

$$CHO^* + OH^* \rightarrow CO_2^* + H_2 + (a) \tag{2.40}$$

$$H_2O + 2(a) \rightarrow OH^* + H^* \tag{2.41}$$

$$CH_4^* \rightarrow CH_4 + (a) \tag{2.42}$$

$$CO^* \rightarrow CO + (a) \tag{2.43}$$

$$CO_2^* \rightarrow CO_2 + (a) \tag{2.44}$$

$$2H^* \rightarrow H_2 + (a) \tag{2.45}$$

$$CH_3^* + OH^* \rightarrow CO^* + 2H_2 + (a) \tag{2.46}$$

$$CO^* + OH^* \rightarrow CO_2^* + H^* \tag{2.47}$$
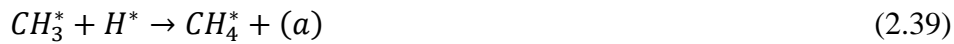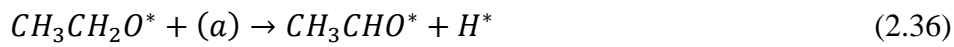
Graschinsky et al. [45] proposed the five reaction mechanisms. The reaction mechanism V of the five reaction mechanisms (I-V) fits the model predicted values more closely with the experimental data and its kinetic expressions are shown in Table 2.13. The rate model V is selected for activation energy calculations as it predicts the experimental values much better than other models. The various terms of denominators in the rate expression are enlisted in Table 2.14 for the Rh $MgAl_2O_4/Al_2O_3$ catalyst. The kinetic parameters for the above kinetic model are estimated by Rossetti et al. [44] using the total sum of squares (TSS) as shown in Table 2.15.

Table 2.13 Kinetic model for Rh/Al$_2$O$_3$ catalyst based on LHHW mechanism [45]

Rate Model	Reaction	Rate equation	DEN
I	Dissociative adsorption of ethanol Reaction (2.35)	$r = kK_1 y_{et}/DEN^2$	$1 + Ay_{et} + By_{CO}y_{H_2}^{\frac{1}{2}} + Cy_{CH_4}y_{CO}$ $+ Ey_{CH_4}y_{CO}Y_{H_2}^{\frac{1}{2}}$ $+ \dfrac{Fy_{H_2O}}{y_{H_2}^{\frac{1}{2}}} + Gy_{CH_4}$ $+ Hy_{CO} + Iy_{CO_2}$ $+ Jy_{H_2}^{\frac{1}{2}}$

II	Dehydrogenation of ethoxide Reaction (2.36)	$r = \dfrac{kK_1K_2y_{et}}{\sqrt{K_{12}y_{H_2}}} \times \left(\dfrac{1}{DEN^2}\right)$	$1 + Ay_{et} + By_{CO}y_{H_2}^{\frac{1}{2}} + C\dfrac{y_{CH_4}}{y_{H_2}^{\frac{1}{2}}}$ $+ Dy_{CH_4}y_{CO}$ $+ F\dfrac{y_{H_2O}}{y_{H_2}^2} + Gy_{CH_4}$ $+ Hy_{CO} + Iy_{CO_2}$ $+ Jy_{H_2} + L\left(\dfrac{y_{et}}{y_{H_2}^{\frac{1}{2}}}\right)$
III	Scission of C-C bonds Reaction (2.37)	$r = \dfrac{kK_1K_2y_{et}}{\sqrt{K_{12}y_{H_2}}} \times \left(\dfrac{1}{DEN^2}\right)$	$1 + Ay_{et} + By_{CO}y_{H2}^{\frac{1}{2}}$ $+ C\left(\dfrac{y_{CH_4}}{y_{H2}^{\frac{1}{2}}}\right)$ $+ Dy_{CH_4}y_{CO}$ $+ F(y_{H2O}/y_{H2}^{\frac{1}{2}})$ $+ Gy_{CH_4} + Hy_{CO}$ $+ Iy_{CO_2} + Jy_{H2}^{\frac{1}{2}}$ $+ L(y_{et}/y_{H2}^{\frac{1}{2}})$

| IV | Surface reaction: Scheme A

Reaction (2.38), Reaction (2.46), Reaction (2.47) | $r_{ED} = \dfrac{k_5 K_1 K_2 K_3 K_4 K_6}{K_9 K_{12}^{\frac{1}{2}}} \left(\dfrac{y_{et}}{y_{CH_4}} \times y_{H_2}^{\frac{1}{2}}\right) \times \left(\dfrac{1}{DEN^2}\right)$

$r_{ER} = \dfrac{k_7 K_1 K_2 K_3 K_4 K_6 K_8}{K_9 K_{12}} \times \left(\dfrac{y_{et} y_{H_2O}}{y_{CH_4} y_{H_2}}\right) \times \left(\dfrac{1}{DEN^2}\right)$

$r_{SRM} = \left[\left(\dfrac{k_{13} K_8 K_9}{K_{12}^{\frac{1}{2}}}\right)\left(\dfrac{y_{CH_4} y_{H_2O}}{y_{H_2}}\right) - k_{-13} K_{11} K_{12}^{\frac{1}{2}} y_{CO_2} y_{H_2}^{\frac{1}{2}}\right]$
$\times \left(\dfrac{1}{DEN^2}\right)$

$r_{WGS} = \left[k_{14}\left(\dfrac{K_8 K_9}{K_6 K_{12}}\right)\left(\dfrac{y_{CH_4} y_{H_2O}}{y_{H_2}}\right) - k_{-14} K_{10} y_{CO} y_{H_2}^{\frac{1}{2}}\right] \times \left(\dfrac{1}{DEN^2}\right)$ | $1 + A y_{et} + B y_{CO} y_{H_2}^{\frac{1}{2}}$

$+ C \left(\dfrac{y_{CH_4}}{y_{H2}^{\frac{1}{2}}}\right)$

$+ F \left(\dfrac{y_{H_2O}}{y_{H2}^{\frac{1}{2}}}\right)$

$+ G y_{CH_4} + H y_{CO}$

$+ I y_{CO_2} + J y_{H2}^{\frac{1}{2}}$

$+ L \left(\dfrac{y_{et}}{y_{H2}^{\frac{1}{2}}}\right)$

$+ M \left(\dfrac{y_{et}}{y_{H2}}\right)$ |

V	Surface reaction: Scheme B Reaction (2.38), Reaction (2.40), Reaction (2.46), Reaction (2.47)	$r_{ED} = k_5 \left(\dfrac{K_1 K_2 K_3 K_4 K_6}{K_9 K_{12}^{\frac{1}{2}}} \right) \left(\dfrac{y_{et}}{y_{CH_4} y_{H_2}^{\frac{1}{2}}} \right) \left(\dfrac{1}{DEN^2} \right)$ $r_{ER} = k_7 \left(\dfrac{K_1 K_2 K_3 K_4 K_6 K_8}{K_9 K_{12}} \right) \times \left(\dfrac{y_{et} y_{H_2O}}{y_{CH_4} y_{H_2}} \right) \times \left(\dfrac{1}{DEN^2} \right)$ $r_{SRM} = \left[k_{13} \left(\dfrac{K_8 K_{10}}{K_{12}^{\frac{1}{2}}} \right) \left(\dfrac{y_{CO} y_{H_2O}}{y_{H_2}^{\frac{1}{2}}} \right) - k_{-13} K_{11} K_{12}^{\frac{1}{2}} y_{CO_2} y_{H_2}^{\frac{1}{2}} \right]$ $\times \left(\dfrac{1}{DEN^2} \right)$ $r_{WGS} = \left[k_{14} \left(\dfrac{K_8 K_9}{K_6 K_{12}} \right) \left(\dfrac{y_{CH_4} y_{H_2O}}{y_{H_2}} \right) - k_{-14} K_{10} y_{CO} y_{H_2}^2 \right]$ $\times \left(\dfrac{1}{DEN^2} \right)$	$1 + A y_{et} + B y_{CO} y_{H_2}^{\frac{1}{2}}$ $+ C \left(\dfrac{y_{CH_4}}{y_{H_2}^{\frac{1}{2}}} \right)$ $+ F \left(\dfrac{y_{H_2O}}{y_{H_2}} \right)$ $+ G y_{CH_4} + H y_{CO}$ $+ I y_{CO_2} + J y_{H_2}^{\frac{1}{2}}$ $+ L \left(\dfrac{y_{et}}{y_{H_2}^{\frac{1}{2}}} \right)$ $+ M \left(\dfrac{y_{et}}{y_{H_2}} \right)$

Table 2.14 The denominator terms of the rate model developed for Rh $MgAl_2O_4/Al_2O_3$ catalyst [45]

Denominator Terms	Adsorbed species	Denominator Terms	Adsorbed species
1	Empty site	$G = K_9$	CH_4
$A = K_1$	CH_3CH_2OH	$H = K_{10}$	CO
$B = \dfrac{K_{10} K_{12}^{\frac{1}{2}}}{K_5}$	CHO	$I = K_{11}$	CO_2
$C = \dfrac{K_{10} K_{12}^{\frac{1}{2}}}{K_5}$	CH_3	$J = K_{12}^{\frac{1}{2}}$	H
$D = \dfrac{K_9 K_{10}}{K_4 K_5 K_6}$	CH_3CHO	$L = \dfrac{K_1 K_2}{K_{12}^{\frac{1}{2}}}$	CH_3CH_2O
$E = \dfrac{K_9 K_{10} K_{12}^{\frac{1}{2}}}{K_4 K_5 K_6}$	CH_3CH_2O	$M = \dfrac{K_1 K_2 K_3}{K_{12}}$	CH_3CHO
$F = \dfrac{K_8}{K_{12}^{\frac{1}{2}}}$	OH	$N = \dfrac{K_1 K_2 K_3 K_5 K_6}{K_9 K_{12}^{\frac{1}{2}}}$	CHO

Table 2.15 Kinetic parameters for Rh $MgAl_2O_4/Al_2O_3$ catalyst [44]

Parameter	Value [mol/s.g]	E_a [J/mol]	Parameter	K_0 [-]	ΔH [J/mol]
$k_{0,5}$	1.554E+20	302980	C_0	2.926E-02	-55199
$k_{0,7}$	1.920E+05	41605	F_0	2.412E-04	-76661
$k_{0,13}$	7.756E+09	187783	G_0	9.940E+01	-13965
$k_{0,14}$	5.044E+05	56252	H_0	2.322E+00	27945
			I_0	4.907E-02	-67738
			M_0	1.369E-01	-32808
			N_0	1.660E-05	16489

2.4.6 MODEL FOR Ni-BASED CATALYST BASED ON LHHW MECHANISM

Llera et al. [46] developed a model (Table 2.16) based on the Ni/Al/LDH which uses Lamellar Double Hydroxide (LDH) and involves four reactions: ethanol steam reforming, ethanol decomposition, water gas shift and methane steam reforming. These elementary steps are considered as RDS. The reaction mechanism assumes neither coke formation on the catalyst nor acetaldehyde formation, due to selective operating conditions. The kinetic parameters are estimated using the regression analysis based on validating the calculated data with the experimental data (Table 2.17).

The reaction mechanisms are shown below.

$$C_2H_5OH + (a) \leftrightarrow C_2H_5OH^* \tag{2.48}$$

$$C_2H_5OH^* + (a) \leftrightarrow C_2H_5O^* + H^* \tag{2.49}$$

$$C_2H_5O^* + (a) \leftrightarrow C_2H_4O^* + H^* \tag{2.50}$$

$$C_2H_4O^* + (a) \leftrightarrow CH_3{}^* + CHO^* \tag{2.51}$$

$$CH_3{}^* + (a) \leftrightarrow CH_2{}^* + H^* \tag{2.52}$$

$$CH_2{}^* + (a) \leftrightarrow CH^* + H^* \tag{2.56}$$

$$CHO^* + (a) \leftrightarrow CO^* + H^* \tag{2.57}$$

$$CH_3{}^* + H^* \leftrightarrow CH_4{}^* \tag{2.58}$$

$$CHO^* + OH^* \leftrightarrow CO_2^* + H_2^* \tag{2.59}$$

$$CH^* + 2OH^* \leftrightarrow CO_2^* + H_2^* + H^* \tag{2.60}$$

$$CO_2^* + H^* \leftrightarrow CO^* + OH^* \tag{2.61}$$

$$H_2O + (a) \leftrightarrow H_2O^* \tag{2.62}$$

$$H_2O^* + (a) \leftrightarrow H^* + OH^* \tag{2.63}$$

$$CH_4{}^* \leftrightarrow CH_4 + (a) \tag{2.64}$$

$$CO^* \leftrightarrow CO + (a) \tag{2.65}$$

$$2H^* \leftrightarrow H_2^* + (a) \tag{2.66}$$

$$CO_2^* \leftrightarrow CO_2 + (a) \tag{2.67}$$

$$H_2^* \leftrightarrow H_2 + (a) \tag{2.68}$$
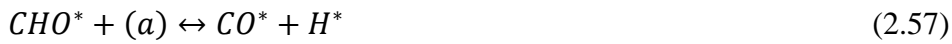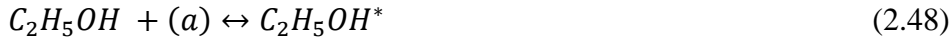
Table 2.16 Kinetic model for nickel-based catalyst based on LHHW mechanism [46]

Rate Model	Reaction	Rate Equation
1	Ethanol decomposition	$r_{E1} = \dfrac{k_{E1} y_E y_{CH_4}^{-1} y_{H_2}^{-\frac{1}{2}}}{DEN}$
2	Ethanol steam reforming	$r_{E2} = \dfrac{k_{E2} y_E y_{H_2O} y_{CH_4}^{-1} y_{H_2}^{-1}}{DEN}$
3	Methane Steam reforming	$r_{R1} = \dfrac{k_{R1} y_{H_2O}^2 y_{CH_4} y_{H_2}^{-\frac{5}{2}}(1 - \beta_{R1})}{DEN}$
4	Water -Gas shift reaction	$r_{R2} = \dfrac{k_{R2} y_{CO_2} y_{H_2}^{\frac{1}{2}}(1 - \beta_{R2})}{DEN}$

$$DEN = 1 + K_{Et} y_{Et} + K_{Etx} y_{Et} y_{H_2}^{-\frac{1}{2}} + K_{Ac} y_{Et} y_{H_2}^{-1} + K_{CHO} y_{Et} y_{CH_4}^{-1} y_{H_2}^{-\frac{1}{2}}$$

$$+ K_{CH_3} y_{CH_4} y_{H_2}^{-\frac{1}{2}} + \cdots + K_{CH_2} y_{CH_4} y_{H_2}^{-1} + K_{CH} y_{CH} y_{H_2}^{-\frac{3}{2}}$$

$$+ K_{H_2O} y_{H_2O} + K_{OH} y_{H_2O} y_{H_2}^{-\frac{1}{2}} + K_{CH_4} y_{CH_4} + \cdots + K_{CO} y_{CO}$$

$$+ K_{CO_2} y_{CO_2} + K_H y_{H_2}^{\frac{1}{2}} + K_{H_2} y_{H_2}$$

Table 2.17 Kinetic parameters for nickel-based catalyst [46]

Kinetic parameters	Value	Activation energy and Enthalpy (kJ/mol)	Value
k_{E1}[mol/min.mg]	1.13E-07	Ea_{E1}	122.9
k_{E2}[mol/min.mg]	3.06E-07	Ea_{E2}	195.5
k_{R1}[mol/min.mg]	2.48E-03	Ea_{R1}	174.0
k_{R2}[mol/min.mg]	9.12E-04	Ea_{R2}	166.3
K_{Et}[-]	8.76E-27	ΔH_{Et}	-601.4
K_{Etx}[-]	1.93E-22	ΔH_{Etx}	-207.9
K_{CHO}[-]	2.10E-01	ΔH_{CHO}	-410.4
K_{Ac}[-]	8.76E-27	ΔH_{Ac}	-83.1
K_{CH_2}[-]	1.93E-22	ΔH_{CH_2}	-118.4
K_{CH}[-]	1.93E-22	ΔH_{CH}	-360.7
K_{CH_3}[-]	1.93E-22	ΔH_{CH_3}	-126.8
K_{H_2O}[-]	6.34E-18	ΔH_{H_2O}	-83.1
K_{OH}[-]	1.93E-22	ΔH_{OH}	-145.5
K_{CH_4}[-]	6.34E-18	ΔH_{CH_4}	-86.1
K_{CO}[-]	1.93E-22	ΔH_{CO}	-83.1
K_{H}[-]	8.76E-27	ΔH_{H}	-247.4
K_{CO_2}[-]	1.93E-22	ΔH_{CO_2}	-83.4
K_{H_2}[-]	1.93E-22	ΔH_{H_2}	-931.2

The value for the β* for WGS and MSR$_{CO2}$ are 1.32 and 0.25 respectively.

The set of differential equations is solved to obtain the outlet component molar flow rates and respective mole fractions. The kinetic parameters are estimated by fitting the model predicted values with the experimental data using different mathematical functions like AAD, sum of squared errors, sum of squares residual as shown in Table 2.18.

Table 2.18 Data fitting method for different models

Ref.	Rate Model	Data fitting method	Value
Akande et al. [40]	ER/Rate Model 1	Average Absolute Deviation (AAD)	20.6%
	ER/Rate Model 2		6.0%
	ER/Rate Model 3		10.6%
	ER/Rate Model 4		58.5%
Akpan et al. [41]	LHHW/Rate Model 1	Average Absolute Deviation (AAD)	15.2%
	LHHW/Rate Model 2		3.63%
	LHHW/Rate Model 3		4.32%
	LHHW/Rate Model 4		3.71%
	LHHW/Rate Model 5		9.16%
	LHHW/Rate Model 6		17.28%
Mas et al. [42]	Ethanol decomposition	Sum of squares residual	0.99 (Correlation Coefficient)
	Ethanol steam reforming		
	Methane steam reforming (1)		
	Methane steam reforming (2)		
Sahoo et al. [43]	SRE	Sum of squared errors	0.95 (Correlation Coefficient)
	ED		
	WGS		
Graschinsky et al. [45]	Ethanol decomposition	Sum of squares residual	1.7×10^{-2}
	Ethanol steam reforming		
	Water-Gas shift		
	Methane steam reforming		
Llera et al. [46]	Ethanol decomposition	Normalized sum of squared errors	0.95 (Correlation Coefficient)
	Ethanol steam reforming		
	Methane Steam reforming		
	Water-gas shift		

The various mechanistic models based on ER and LHHW approaches are compared in Table 2.19 with respect to activation energy, ethanol conversion and hydrogen yield. The activation energy reported for ER mechanism is in the order of the 10^3 and LHHW mechanism is in the order of the 10^3-10^5.

The maximum ethanol conversion (Fig. 2.1) is obtained by Sahoo et al. [43] for 15% Co/Al_2O_3 catalyst at 973 K and Mas et al. [42] and Llera et al. [46] for Ni(II)-Al(III)-LDH catalyst at 923 K for higher values of space-time. Llera et al. [46] has observed that the ethanol conversion reaches to 90% for smaller values of space-time at 923 K.
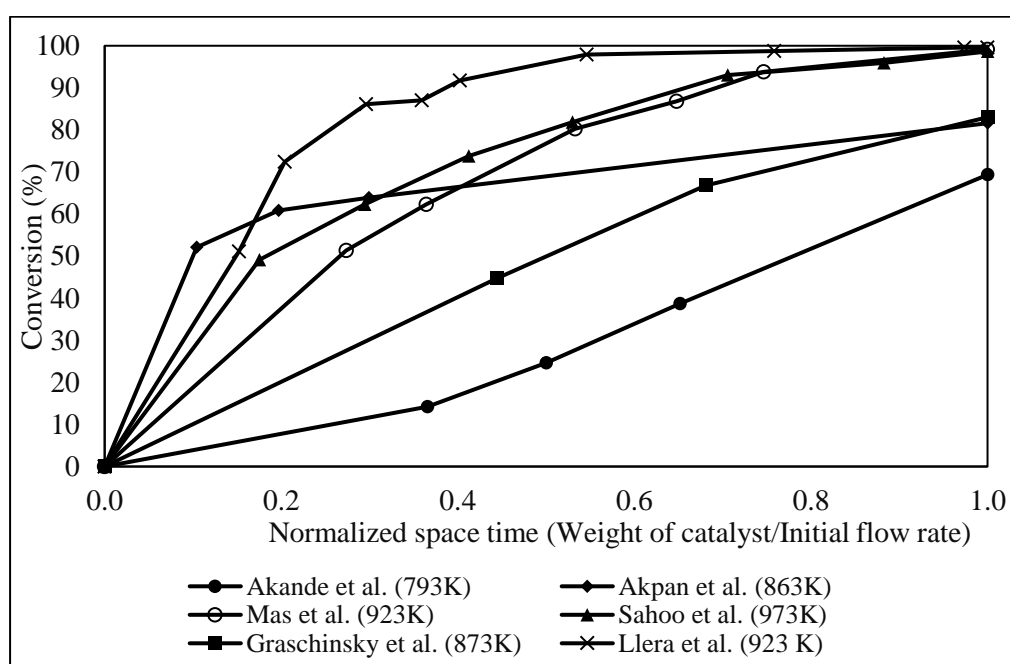

Fig. 2.1 Ethanol conversion as a function of normalized space-time [40-43, 45, 46]

Mas et al. [42] and Sahoo et al. [43] obtained the yield of hydrogen more than 5 per mole of ethanol in the feed (Fig. 2.2).
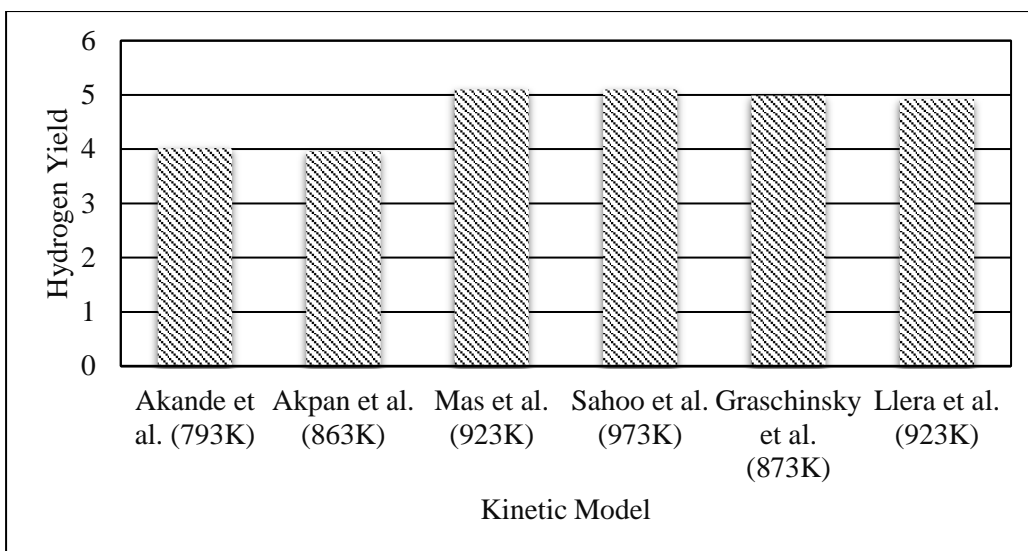
Fig. 2.2 Hydrogen yield for different kinetic models [40-43, 45, 46]

It is observed from the literature that Ni-based catalysts show the higher activity and H_2 selectivity when compared to Co-based catalysts. Thus, the kinetic model proposed by Mas et al. [42] using Ni-based catalyst can be used to model a fixed bed reactor for ESR. The other reactors like a wall-coated microchannel reactor [16, 47], a membrane reactor [48-50] and a fluidized reactor [51, 52] were not able to achieve the complete conversion of ethanol.

Dehkordi et al. [53] used the three different (conical, cylindrical and inversed conical) configurations of a fixed bed reactor and reported the best performance by conical reactor as the overall contact time is higher as compared to other two reactor configurations. Arteaga et al. [54] simulated a fixed bed ESR reactor using FEMLAB and found that the isothermal condition is achieved above 773 K. Peela et al. [16] developed the kinetics of ESR over 2% $Rh/20\%$ CeO_2/Al_2O_3 catalyst in a microchannel reactor for a temperature range of 450-550 ^{0}C at atmospheric pressure. The complete conversion of ethanol was obtained at the maximum reactor temperature of 922.7 K. Gorke at al. [47] showed that the mass and heat transport limitations do not affect the kinetic parameters obtained experimentally using microchannel reactor coated with Rh/CeO_2 catalyst. The assumption of isothermal behaviour of the microchannel reactor closely fitted

the model predicted data with the experimental data. Galluci et al. [48] used a dense Pd-Ag membrane reactor for ESR using Co-based catalyst. The production of hydrogen was found to increase due to the highly selective palladium-based membrane as compared to a traditional packed bed reactor. The maximum ethanol conversion was reported to be 94% at 673 K, water to ethanol molar feed ratio of 3 and a pressure of 8 bar. Montero et al. [52] studied ESR in a fluidized bed reactor using $Ni/La_2O_3-\alpha Al_2O_3$ catalyst and observed that the ethanol conversion and hydrogen yield increase with increase in temperature from 500-650 ^0C. But, the attenuation of hydrogen yield was observed above 600^0C as WGS reaction shifts towards the left at higher temperature.

In addition to the conventional methods of hydrogen production using different configurations of steam reforming reactor, some novel methods like sorption-enhanced steam reforming (SESR) and chemical looping steam reforming (CLSR) are being developed for low cost and energy-efficient hydrogen production [55].

Table 2.19 Ethanol conversion and hydrogen yield for different models

Reactor Type	Catalyst	Operating Conditions	Reaction Mechanism	Maximum Ethanol Conversion and H_2Yield	Ref.
Packed Bed Tubular Reactor	15%-Ni/Al$_2$O$_3$	Temperature: 593-793 K Pressure: 1 atm Space time: 779-2143 kgcat.s/kg crude ethanol	ER	72% (at 793K) 4.01 (H_2 yield)	Akande et al. [40]
Packed Bed Tubular Micro-reactor	Ni-based	Temperature: 673-863 K Pressure: 1 atm Space time: 3472-34722 kgcat.s/kmol crude ethanol	LHHW and ER	81% (at 863K) 3.96 (H_2 yield)	Akpan et al. [41]

Quartz Reactor	Ni(II)-Al(III)-LDH	Temperature: 823-923 K Pressure: 1 atm Space time: 5.5×10^{-6}-2.7×10^{-5} g.min/mL	LHHW	99.7% (at 923K) 5.1 (H_2 yield)	Mas et al. [42]
Fixed Bed Tubular Reactor	Co/Al_2O_3	Temperature: 673-973 K Pressure: 1 atm Space time: 3-17 kgcat.s/mol	LHHW	99.9% (at 973K) 5.1 (H_2 yield)	Sahoo et al. [43]
Quartz Reactor	Rh(1%) $MgAl_2O_4$ $/Al_2O_3$	Temperature: 773-873 K Pressure: 1 atm Space time: 0.56-1.82 mgcat.min/mL	LHHW	83% (at 873K) 4.99 (H_2 yield)	Graschi-nsky et al. [45]
Quartz Reactor	Ni (II)-Al (III)-LDH	Temperature: 873-923 K Pressure: 1 atm Space time: 0-3 mgcat.min /mL *100	LHHW	99.6% (at 923K) 4.92 (H_2 yield)	Llera et al. [46]

2.5 OPTIMIZATION TECHNIQUES

The GA technique is based on the biological evolution process followed by the nature [56]. It is used for the constrained and unconstrained optimization problems. Fatemi et al. [57] used the GA technique for kinetic parameter optimization of the kinetic model corresponding to hydrogenolysis of dibenzothiophene. GA technique is found to be effective and robust for the limited information of the reaction mechanism, unlike gradient based methods. It needs appropriate selection of the genetic operators and their parameters. GA technique is useful for estimating the optimum kinetic model corresponding to a complex reaction mechanism [57, 58]. Tutkun [59] showed that the real code genetic algorithm can be efficiently used the obtain the unknown parameters of the mathematical model. It was found that the improvement of the estimated parameters mainly depends upon the population size, crossover and mutation rates with a little influence of number of generation.

Multi-objective optimization methods provide a Pareto set of candidate solutions, which are equally good. NSGA-II uses the concept of elitism and has the several advantages over other multi-objective optimization methods [60, 61]. Rajesh et al. [62] used the NSGA-II technique to optimize the performance of methane steam reformer. The results gave more insight into the process to decide on the operating conditions of the industrial reformer. The elitism criteria decreases the diversity in the population using NSGA-II. The jumping gene adaptations of NSGA-II counteracts this problem by increasing the genetic diversity in the population. Kasat et al. [63] observed that the jumping gene operator adapted in NSGA-II reduced the computation time for obtaining the solution of a complex FCCU problem as compared to when NSGA-II is used.

The mathematical modelling of a fixed bed reactor involves the identification of a reliable and an accurate kinetic model. Earlier workers, Mas et al. [42] and Rossetti et al. [44] have obtained the different values of kinetic parameters for the *same* rate model and the *same* experimental data as proposed by Mas et al. [42]. The values of the model parameters obtained using two different curve-

fitting techniques, the Generalized Reduced Gradient (GRG) algorithm [42] and a derivative-free approach based on the simplex method [44], were different. This leads to differences in the agreement between model predictions and experimental results. A more powerful and recent technique, genetic algorithm (GA), has been used to resolve this problem by minimizing a sum-of-square errors (SSE). The multi-objective optimization is formulated for the first time in literature for ESR to increase the hydrogen mole fraction by reducing the mole fraction of carbon monoxide and carbon dioxide. The evolutionary algorithms of NSGA-II and a jumping gene adaptation of NSGA-II are used for its solution.

CHAPTER 3: MODELLING AND OPTIMIZATION OF AN ISOTHERMAL TUBULAR REACTOR

In the present study, a simple yet accurate model is developed to simulate, adequately, a fixed bed reactor for ESR using the kinetic model proposed by Mas et al. [42]. The reaction mechanism proposed by Mas et al. [42] (their Model B, used in the *present* study) involves ethanol adsorption, water adsorption, surface reaction involving the dissociation of ethanol, surface reaction between the adsorbed water and ethanol, methane desorption and surface reactions between methane and water.

3.1 KINETIC MODEL

Taking into account the thermodynamic analysis of ESR, the experimental conditions and the catalysts were selected in order to avoid the formation of acetaldehyde and ethylene. Eqns. (3.1)-(3.4), give the four major reactions that properly represent the ESR production of hydrogen (and side products) over nickel-based catalysts in wide range of water to ethanol ratio.

Ethanol decomposition: $\quad C_2H_5OH \quad \overset{k_1}{\rightarrow} \quad CH_4 + CO + H_2 \quad$ (3.1)

Ethanol steam reforming: $\quad C_2H_5OH + H_2O \overset{k_2}{\rightarrow} CH_4 + CO_2 + 2H_2 \quad$ (3.2)

Methane steam reforming-I: $CH_4 + H_2O \quad \leftrightarrow \quad CO + 3H_2 (k_3; K_3) \quad$ (3.3)

Methane steam reforming-II: $CH_4 + 2H_2O \quad \leftrightarrow \quad CO_2 + 4H_2 \ (k_4; K_4) \ $ (3.4)
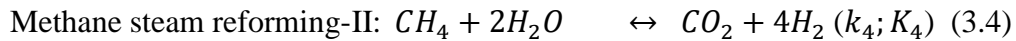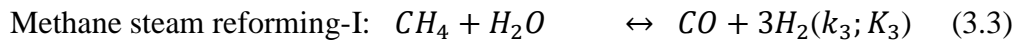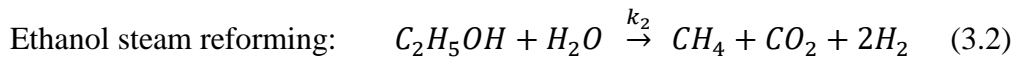
Table 3.1 gives the final rate expressions as well as the standard heats of formations.

Table 3.1 Rate equations (Model B) and standard heats of formation [42]

No.	Reaction	Rate equation	ΔH_{298}^0, kJ/mol
1	Ethanol decomposition	$r_1 = \dfrac{k_1 K_E P_E}{1 + P_E K_E + P_{H_2O} K_{H_2O} + P_M K_M}$	49.7
2	Ethanol steam reforming	$r_2 = \dfrac{k_2 K_E K_{H_2O} P_E P_{H_2O}}{1 + P_E K_E + P_{H_2O} K_{H_2O} + P_M K_M}$	205
3	Methane steam reforming-I	$r_3 = \dfrac{k_3 K_M K_{H_2O} \left(P_M P_{H_2O} - \dfrac{P_{CO} P_{H_2}^3}{K_3} \right)}{\left(1 + P_E K_E + P_{H_2O} K_{H_2O} + P_M K_M \right)^2}$	206.1
4	Methane steam reforming-II	$r_4 = \dfrac{k_4 K_M K_{H_2O} \left(K_{H_2O} P_M P_{H_2O}^2 - \dfrac{P_{CO_2} P_{H_2}^4}{K_4} \right)}{\left(1 + P_E K_E + P_{H_2O} K_{H_2O} + P_M K_M \right)^3}$	165

Here, P_i is the partial pressure of component, i (= $y_i P$; P being the total pressure), with i: ethanol (E, $i = 1$), water (H_2O, $i = 2$), carbon monoxide (CO, $i = 3$), carbon dioxide (CO_2, $i = 4$), methane (M, $i = 5$) and hydrogen (H_2, $i = 6$), while K_i is the equilibrium constant for the adsorption of ethanol (E, $i = 1$), water (H_2O, $i = 2$) and methane (M, $i = 5$).

The rate constants, k_i, in reactions (3.1)-(3.4) are given by the Arrhenius equations

$$k_i = k_{i,0} exp \left(\frac{-E_{a,i}}{RT} \right) \qquad (3.5)$$

while the equilibrium constants for adsorption are given by

$$K_i = K_{i,0} exp \left(\frac{-\Delta H_i}{RT} \right) \qquad (3.6)$$

T is the absolute temperature (isothermal in this case) and R is the universal gas constant.

The equilibrium constants for reactions (3.3) and (3.4) are given by Eqns. (3.7) and (3.8), respectively [44].

$$K_3 = 5.30 \times 10^{12} exp\left(\frac{-26211.7}{T}\right) \qquad (3.7)$$

$$K_4 = 7.20 \times 10^{10} exp\left(\frac{-21585.3}{T}\right) \qquad (3.8)$$

Table 3.2 gives the values of the several parameters as obtained by Mas et al. [42] for their Model B.

Table 3.2 Kinetic parameters for Model B using the Ni/Al/LDH catalyst [42]

Parameter	Value	Unit
k_1 at T = 873 K	2.9E-05	[mol/(min.gcat)]
k_2 at T = 873 K	3.1E-04	[mol/(min.gcat)]
k_3 at T = 873 K	1.0E-04	[mol/(min.gcat)]
k_4 at T = 873 K	2.4E-04	[mol/(min.gcat)]
$E_{a,1}$	278.74E+03	[J/mol]
$E_{a,2}$	235.06E+03	[J/mol]
$E_{a,3}$	123.50E+03	[J/mol]
$E_{a,4}$	213.90E+03	[J/mol]
K_E at T = 873 K	61.7	[-]
K_{H_2O} at T = 873 K	37.4	[-]
K_M at T = 873 K	1135	[-]
ΔH_E	-199.70E+03	[J/mol]
ΔH_{H_2O}	-92.40E+03	[J/mol]
ΔH_M	-124.70E+03	[J/mol]

3.2 MATHEMATICAL MODEL OF THE FIXED BED REACTOR

The fixed bed reactor is shown in Fig. 3.1, along with the reactants and products. Argon is the inert gas in this case. The one-dimensional, pseudo-homogeneous reactor model is simulated to obtain the solution of all the mass balance equations under steady state and isothermal conditions.
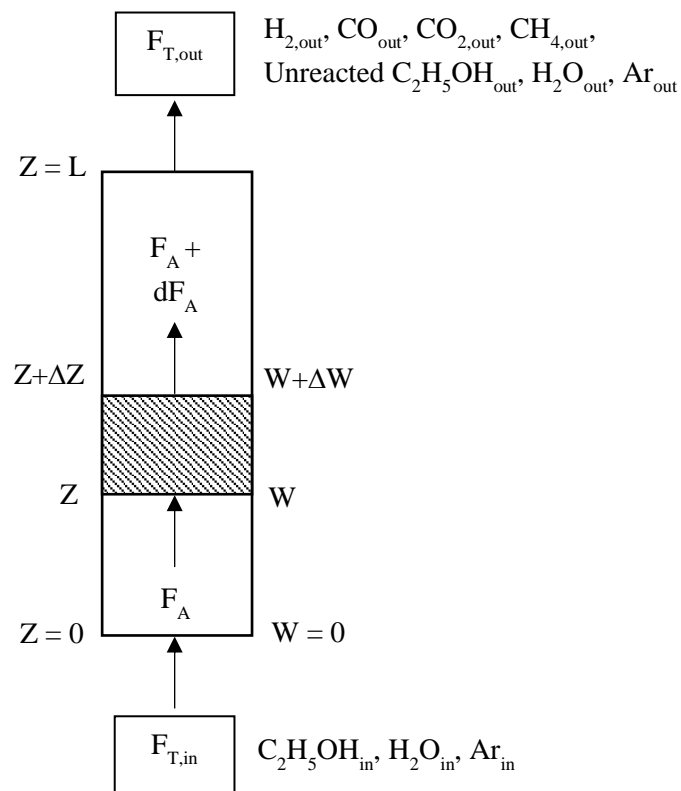

Fig. 3.1 Fixed bed reactor model for ESR. F is the total kmol/hr while F_A is the kmol/hr of species, A, at location, Z

3.2.1 MASS BALANCE

We can easily write the mole balance equation [64] for any species, A, at steady state as

$$F_A\big|_W \quad - \quad F_A\big|_{W+\Delta W} \quad + \quad r_A\Delta W \quad = 0 \quad (3.9)$$

or

51

$$\frac{dF_A}{dW} = r_A \qquad (3.10)$$

and

$$F_A \equiv y_A F_T \qquad (3.11)$$

Here, F_T = total molar flow rate at any Z ($\approx F_{T,0}$ due to the presence of the inert).
Hence

$$\frac{d(y_A F_T)}{dW} = r_A \qquad (3.12)$$

or,

$$\frac{dy_A}{d\left(\frac{W}{F_T}\right)} = r_A \qquad (3.13)$$

Defining the space time as

$$\theta \equiv \frac{W}{F_{T,0}} \qquad (3.14)$$

we get

$$\frac{dy_A}{d\theta} = r_A \qquad (3.15)$$

As the system is dilute, the mole balance can be written in terms of the mole fractions for the j components as

$$\frac{dy_j}{d\theta} = \sum_i \vartheta_{ij} r_i \qquad (3.16)$$

Where,

j = 1: Ethanol, 2: Water, 3: Carbon monoxide, 4: Carbon dioxide, 5: Methane and 6: Hydrogen

Here

$\vartheta_{ij} \equiv$ stoichiometric coefficient for reaction, i, for component, j. These may be expanded to give

$$\frac{dy_1}{d\theta} = -r_1 - r_2 \tag{3.17}$$

$$\frac{dy_2}{d\theta} = -r_2 - r_3 - 2r_4 \tag{3.18}$$

$$\frac{dy_3}{d\theta} = r_1 + r_3 \tag{3.19}$$

$$\frac{dy_4}{d\theta} = r_2 + r_4 \tag{3.20}$$

$$\frac{dy_5}{d\theta} = r_1 + r_2 - r_3 - r_4 \tag{3.21}$$

$$\frac{dy_6}{d\theta} = r_1 + 2r_2 + 3r_3 + 4r_4 \tag{3.22}$$

The above set of differential equations describing the mole balances in terms of the mole fractions for all the reaction species as a function of the space time, θ, have been solved using the ode23s solver of MATLAB™. Ode23s solver is used to solve the set of stiff differential equations and additionally finds where event functions are zero.

3.2.2 ESTIMATION OF KINETIC PARAMETERS

Mas et al. [42] originally fitted the model predicted values with their experimental data using GAMS package with the Conopt (GRG) technique. Rossetti et al. [44] estimated the kinetic parameters using the *same* experimental data under the *same* operating conditions through a derivative-free approach based on the simplex technique. The values of the model parameters obtained using two different curve-fitting techniques were different. This leads to differences in the agreement of model predictions *vs.* experimental results. A more powerful and recent technique, genetic algorithm (GA), has been used to

resolve this problem by minimizing a sum-of-square errors (SSE) function for the products; CO, CO_2, CH_4 and H_2. It is also helpful to assess the validity and establishing the reliability of the kinetic model.

Eqn. (3.23) gives the SSE function.

$$SSE = \sum_{j=1}^{n} \sum_{i=1}^{4} w_i \left(\frac{y_{i,exp} - y_{i,calc}}{y_{i,calc}} \right)_j^2 \tag{3.23}$$

Here i represents the number of the component (from among CO, CO_2, CH_4 and H_2) and j represents the experimental data-set, out of a total of n ($= 9$) sets. The *entire* set (for all values of θ, including the values at the outlet) of experimental data [42] is used to evaluate the SSE.

Genetic algorithms are computer search that follow the optimization algorithms based on the theory of natural evolution. The process of natural selection involves reproduction, crossover and mutation. In the present study, the variables (genes) are first coded in binary (1's and 0's) into the string structures (chromosomes) in a simple genetic algorithm. The process starts with the initial population (a set of solutions/chromosomes) which is tested using the fitness function. The fittest parents are selected to produce the offspring of the next generation, which will be better than their parents do. This process will keep on repeating to find out a generation of fittest individuals at the end. GA follows the algorithm as represented in Fig. 3.2.
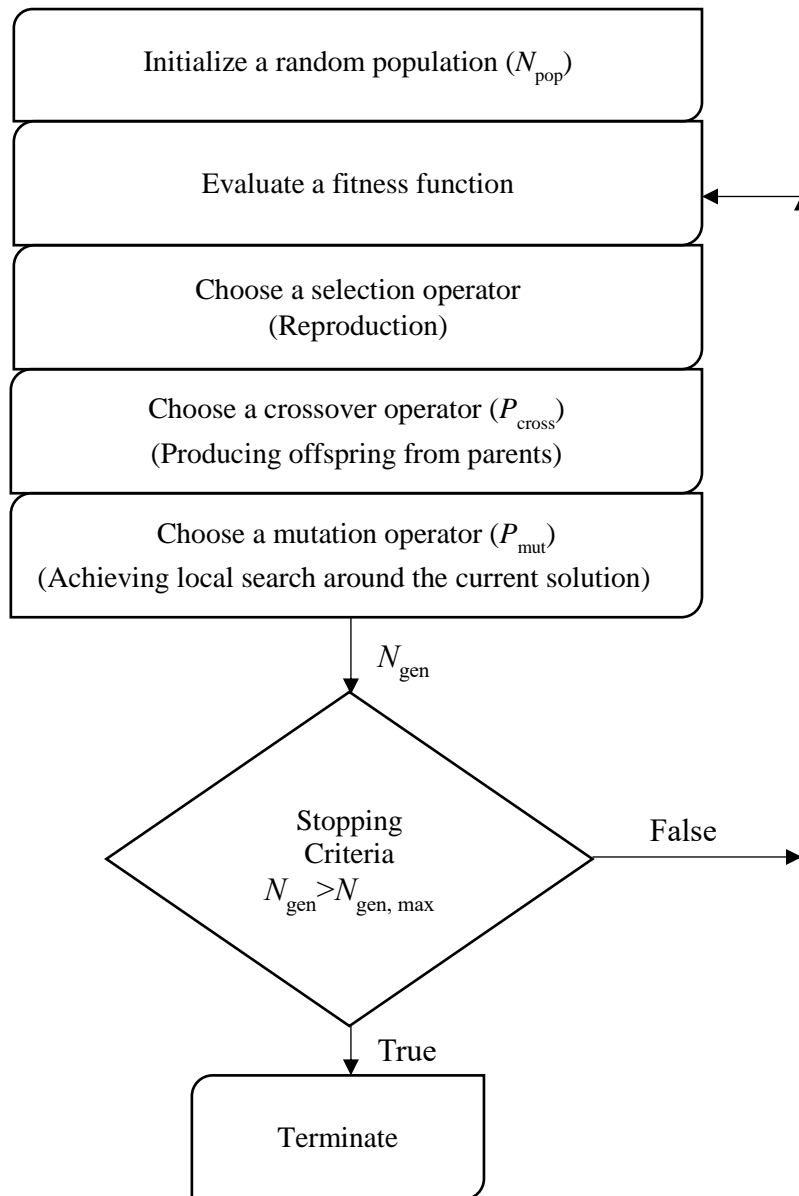
Fig. 3.2 A systematic GA algorithm [56]

3.3 MULTI-OBJECTIVE OPTIMIZATION OF AN ISOTHERMAL TUBULAR REACTOR

ESR produces H_2 and CH_4 along with CO and CO_2 as the final products in the reactor outlet according to the proposed kinetic rate model [42]. Though CO is only a very weak direct greenhouse gas, unlike CO_2, it has a potential effect on global warming and can lead to the formation of the tropospheric ozone. Owing to the environmental hazards associated with CO and CO_2, a multi-objective optimization (MOO) problem is formulated for an isothermal tubular reactor to minimize their amounts in the product outlet by maximizing the amount of hydrogen. To the best of our knowledge, a MOO problem has been formulated and solved for the first time in the literature using a validated model of ESR and Non-Dominated Sorting Genetic Algorithm – II (NSGA-II) [60, 62]. The effect of varying the process parameters like (isothermal) temperature, pressure and water/ethanol molar ratio in the feed around their optimal values are then studied. In addition, a recent improved technique, jumping genes adaptations of NSGA – II (NSGA-II-JG) [61, 63], has been used to obtain the optimal Pareto solution to see if the computational time is significantly reduced (as was the case for an industrial fluidized bed catalyst cracker [63], FCCU).

3.3.1 MOO PROBLEM FORMULATION

The following MOO problem is now solved for an actual reactor (using the best-fit values of the model parameters). The three decision variables are, the (isothermal) temperature, T, the (constant) pressure, P, and the water to ethanol (mole fraction) ratio in the feed, $(H_2O/E)_{in}$. The Objective functions are as follows:

Maximize the mole fraction of hydrogen *at the outlet*, and   (3.24)

Minimize the mole fractions of CO + CO_2, together, *at the outlet*   (3.25)

This will help increase the yield of hydrogen using the ESR process that will meet its increased demand in the future for various applications and at the same time, the greenhouse gas emissions will be reduced. This MOO optimization problem is represented mathematically by

$$Max \ I_1 = y_{H_2,out} \tag{3.26}$$

$$Min \ I_2 = \left(y_{CO,out} + y_{CO_2,out}\right) \tag{3.27}$$

Here, I_i are the two objective functions. The above optimization problem is solved using an adapted version of GA, namely, NSGA-II [60]. As the available codes of NSGA-II minimize all the objective functions, the first objective function is transformed into one involving minimization. Thus, the optimization problem studied is

$$Min \ I_1(\boldsymbol{u}) = \frac{1}{1 + y_{H_2,out}} \tag{3.28}$$

$$Min \ I_2(\boldsymbol{u}) = \left(y_{CO,out} + y_{CO_2,out}\right) \tag{3.29}$$

where

$$\boldsymbol{u} = [T, P, (H_2O/E)_{in}] \tag{3.30}$$

The lower and upper bounds of the reaction temperature, T, pressure, P, and water to ethanol ratio in the feed, $(H_2O/E)_{in}$, are taken [42] as

$$823 \leq T \leq 923 \ K \tag{3.31}$$

$$101.325 \leq P \leq 151.988 \ kPa \tag{3.32}$$

$$3.5 \leq (H_2O/E)_{in} \leq 10 \tag{3.33}$$

3.3.2 SOLUTION TECHNIQUE

The optimization toolbox of MATLAB™ is used to obtain the Pareto optimal (non-dominated) solutions using NSGA-II (two points on the two-objective Pareto front that are non-dominated refers to one objective function improving while the other becomes worse as one goes from one point to another).

NSGA-II uses an elite-preservation strategy as well as an explicit diversity-preserving mechanism [60].

NSGA-II, as discussed below, selects the next generation using two specialized multi-objective operators and mechanisms in addition to the genetic operators; selection, crossover and mutation [60].

Non-dominated Sorting: The initial parent chromosomes are sorted according to nondomination. Elitism is ensured by combining the best nondominated solutions from the current population and previous population. These are partitioned into non-dominated fronts (F_1, F_2, etc.), where F_1 (set of best solutions) indicates the best non-dominated Pareto front.

Crowding Distance: It measures the density of solutions surrounding a particular solution in the population. It is a mechanism of nondomination ranking among members of a front, which are dominating or dominated by each other (i.e. same ranking). Better solution is selected as having a smaller value of a Rank no. (I_{rank}) or, if I_{rank} are identical, having a larger value of a crowding distance (I_{dist}).

The population of next generation is created using these ranking mechanisms with genetic selection operators (popularly Tournament Selection Operator).

NSGA–II–JG utilizes a modified mutation operator in its algorithm, which adopts the concept of jumping genes (JG) in natural genetics [61, 63]. The jumping genes operator is utilized after crossover and normal mutation in NSGA-II. It modifies a randomly selected fraction (P_{jump}) of chromosomes in the population. The adaptations are referred as replacement (Fig. 3.3) and reversion (Fig. 3.4), which mimic natural genetics largely. In the replacement process, a new and randomly generated binary string replaces a part (same length) of the binary string in the offspring population. It uses the same procedure for the jumping string generation as used for initial population generation. In the reversion process, the binaries between two sites are selected using random numbers in a chromosome and are reversed in the offspring

population. Amongst the various transposon possibilities, a single transposon is assumed to simplify the algorithm. The replacement provides higher genetic diversity as it involves the macro-macro-mutation whereas the reversion involves macro-mutation.

This adaptation reduces the computation time, thus speed up the solution of an optimization problem when compared to NSGA-II. The algorithms followed by NSGA-II and NSGA-II-JG are shown in Fig. 3.5.
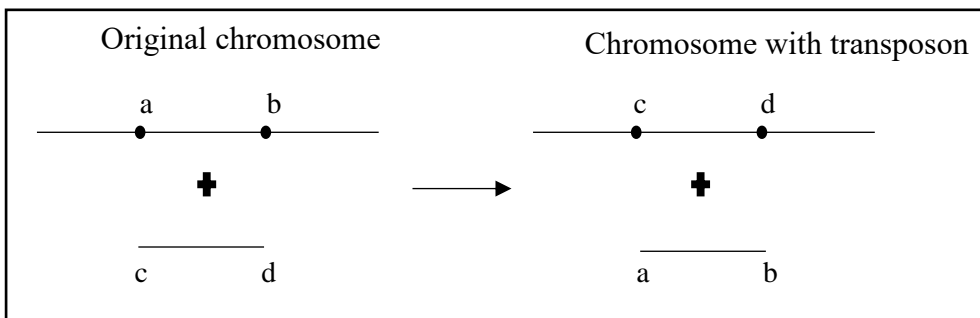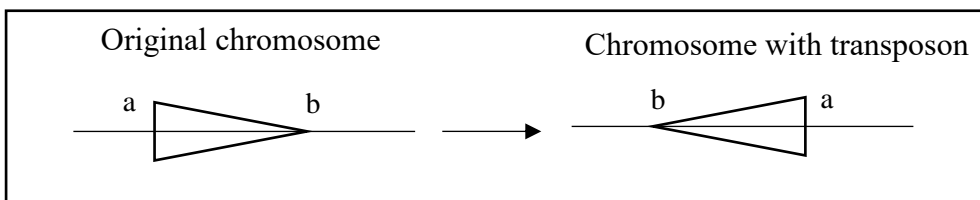

Fig. 3.3 Replacement adaptation of jumping gene in GA

Fig. 3.4 Reversion adaptation of jumping gene in GA
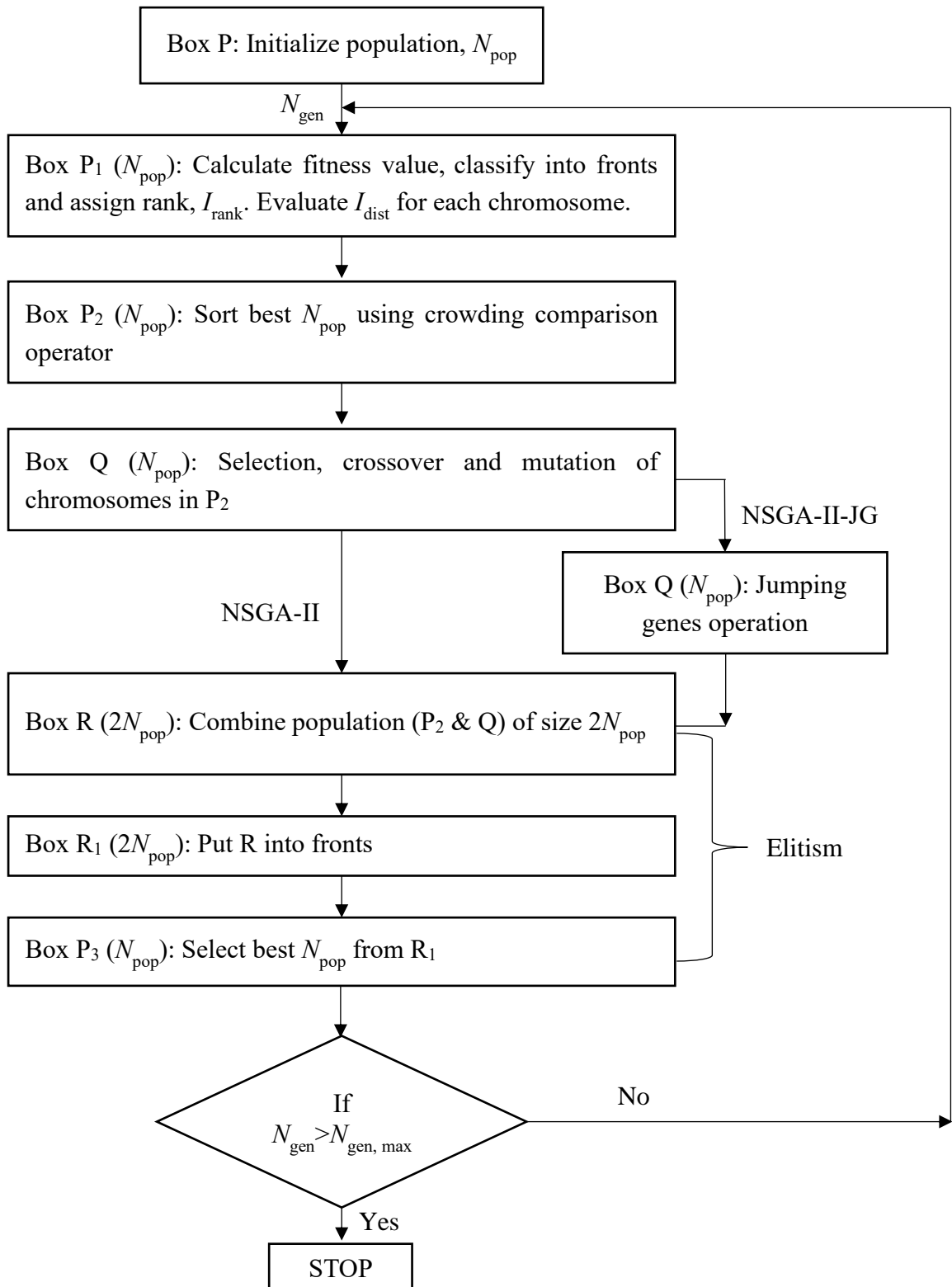
Fig. 3.5 Algorithms of NSGA-II and NSGA-II-JG

CHAPTER 4: RESULTS AND DISCUSSIONS

In this chapter, the results are discussed for the estimation of kinetic parameters for the reaction rate model proposed by Mas et al. [42]. Section 4.1 discusses kinetic parameter estimation using GA technique. The computational parameters for GA are obtained through the parametric study to improve the value of the fitness function. The kinetic parameters optimized using GA are used to fit the model against the experimental results of Mas et al. [42]. Inconsistency in the results obtained by Mas et al. [42] and Rossetti et al. [44] for the proposed kinetic model of ESR using the same reactor data and operating conditions were observed. The comparative study of simulated results of Mas et al. [42], Rossetti et al. [44] and this study with the experimental results [42] is carried out to ascertain the reliability of the kinetic model proposed by Mas et al. [42].

In Section 4.2, the solution of a MOO problem is discussed using NSGA-II and NSGA-II-JG. The computation parameters for NSGA-II and NSGA-II-JG are obtained through the parametric study to improve the *Pareto* set. The effect of decision variables on one of the objective functions, molar fraction of hydrogen, is discussed using NSGA – II and the results are validated with the experimental observations [42]. This study also shows the betterment in the spread of Pareto front using NSGA-II-JG as compared to when NSGA-II is used. The solution of a MOO problem converges faster using NSGA-II-JG and thus reduces the computation time.

4.1 PARAMETER ESTIMATION AND MODEL VALIDATION

The fixed bed reactor is simulated using Eqns. (3.17) – (3.22) using the GA-optimized model parameters to obtain the mole fractions of C_2H_5OH, H_2O, CO, CO_2, CH_4 and H_2, respectively, at different locations (including the outlet). The data [42] for the reactor is given in Table 4.1.

Table 4.1 Details of the *isothermal* ESR system of Mas et al. [42]

No.	Item	Description
1	Catalyst	Nickel based with Ni(II)-Al(III) lamellar double hydroxide (LDH) as catalyst precursor
2	Catalyst particle diameter (spherical)	44 - 88 µm
3	Quartz reactor	4 mm ID
4	Liquid Flow	1.32-6.80 $\times$ 10^{-2} mL/min
5	$\left(F_{H_2O}/F_E\right)_{in}$	3.5-10
6	Temperature	823-923 K
7	Pressure	Atmospheric pressure
8	Residence time	$5.5 \times 10^{-6} – 2.7 \times 10^{-5}$ g.min/ml
9	$y_{E,in}$	0.016
10	$y_{H_2O,in}$	0.09
11	Reactor type	Plug flow; $L/D_p \geq 50$ and $D/D_p \geq 30$
12	Carbon balance	95%, no carbon deposition

The optimized kinetic (and a few other) parameters are obtained by minimizing the sum-of-square errors, Eqn. (3.23), between model predictions and experimental data of Mas et al. [42] using GA. The parametric sensitivity of GA is first studied by varying the *computational* parameters one by one, e.g., the generation number (N_{gen}), population size (N_{pop}), crossover probability (P_{cross}) and the mutation probability (P_{mut}) as given in Table 4.2.

Table 4.2 Computational parameters for GA

Sr. No.	Parameter	Value
1	Generation number (N_{gen})	30
2	Population size (N_{pop})	50
3	Crossover probability (P_{cross})	0.995
4	Mutation probability (P_{mut})	0.01
5	Function tolerance	1.00E-06

The effect of generation number (N_{gen}) on the fitness function value is shown in Fig. 4.1. It is noted that the algorithm stalls at approximately generation number 23. Thus, the generation number, 30, is selected for improving the results and reducing the computation time, as there is no further improvement in the fitness function.
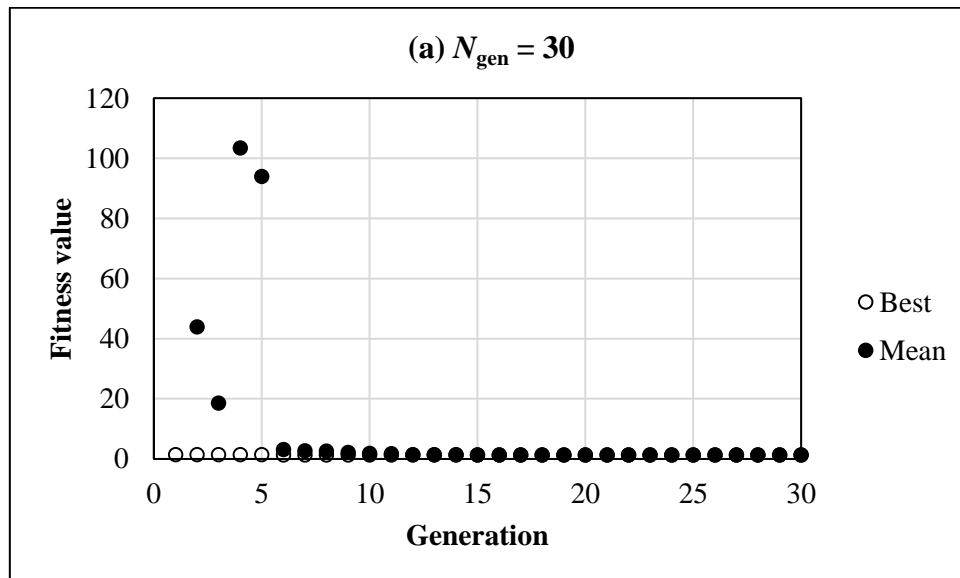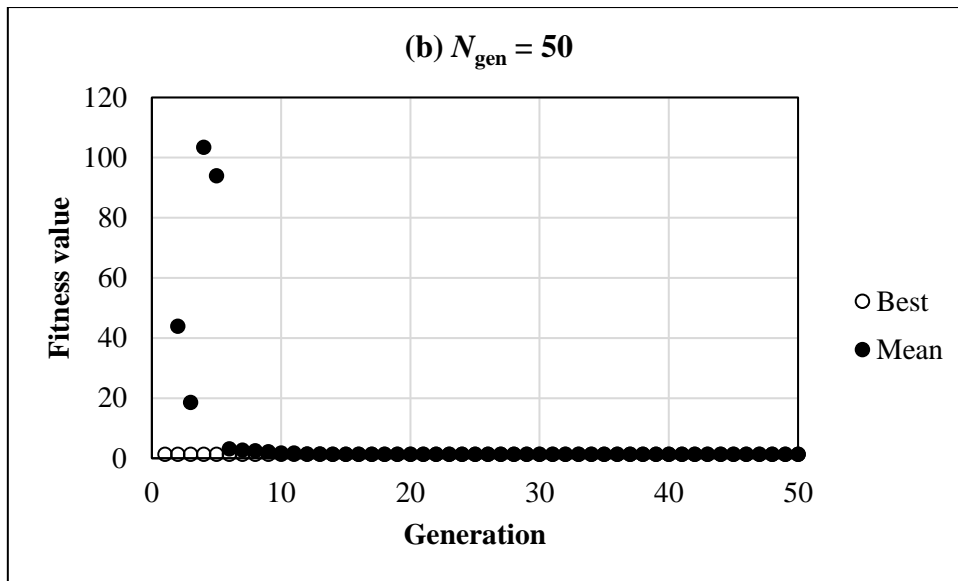

Fig. 4.1 (contd.)
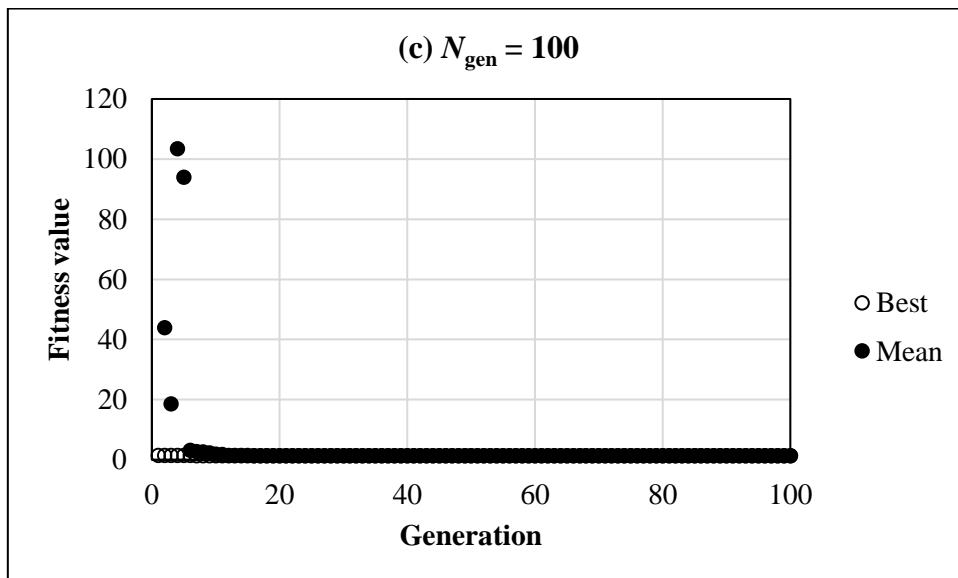
Fig. 4.1 Effect of generation number on the fitness function value for (a) N_{gen} = 30, (b) N_{gen} = 50 and (c) N_{gen} = 100 [Ref: N_{pop} = 50, P_{cross} = 0.8 and P_{mut} = 0.02]

Population size represents the set of solution of GA model. The results get better with increase in population size as it enables GA to search more points. However, it takes longer computation time for each generation with increase in population size as shown in Fig. 4.2.
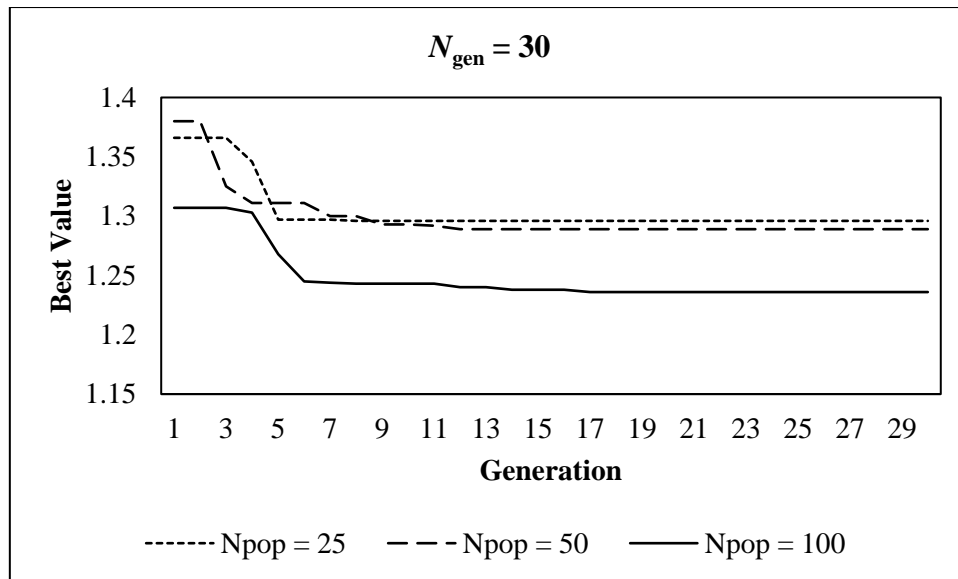
Fig. 4.2 Best value per population size

The new strings are produced by a crossover function through the information exchange among strings of the mating pool. Mutation is needed to achieve a local search around the current solution by creating a point near to the current point. The parametric effects of crossover probability and the mutation probability are studied through the comparison between experimental values and model predicted values of the mole fractions y_1, y_2, y_3, y_4, y_5, and y_6 of C_2H_5OH, H_2O, CO, CO_2, CH_4, and H_2, respectively. The results obtained for CO, CO_2, CH_4 and H_2 mole fractions are shown in Fig. 4.3 for the crossover probabilities of 0.8 and 0.995. The crossover probability of 0.995 shows the close proximity of model predicted mole fractions with the experimental data [42] as shown in Fig 4.3. In case of a mutation probability, the model predicted mole fraction values were same for C_2H_5OH, H_2O, CO, CO_2, CH_4 and H_2 for the different values of mutation probability. In a view to brevity, the model predicted values of hydrogen mole fraction are shown in Fig. 4.4 for the mutation probabilities of 0.01 and 0.02.

Finally, the best values of these are taken as $N_{gen} = 30$, $N_{pop} = 50$, $P_{cross} = 0.995$, $P_{mut} = 0.01$.
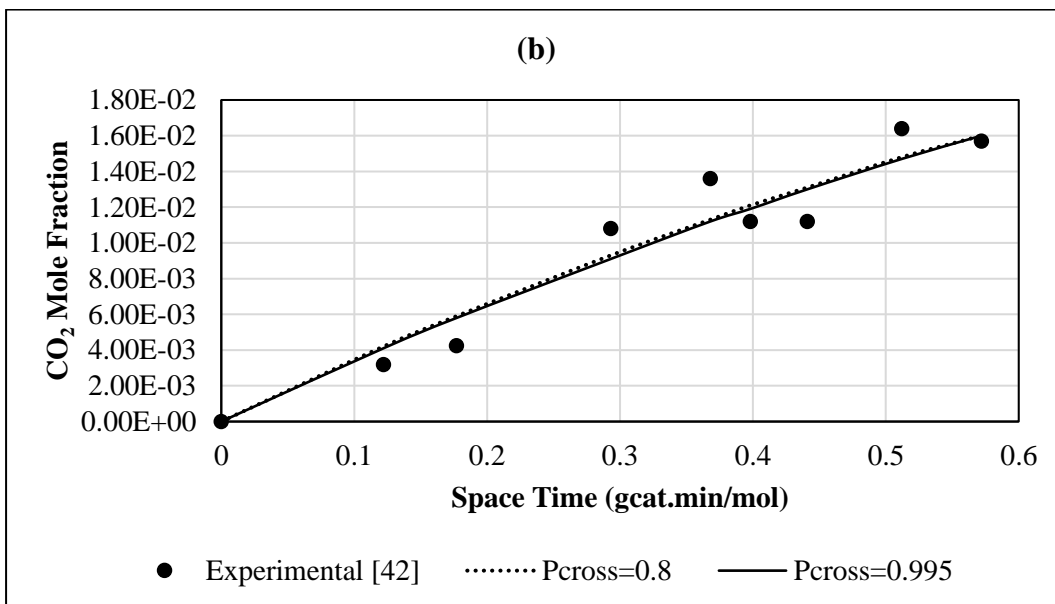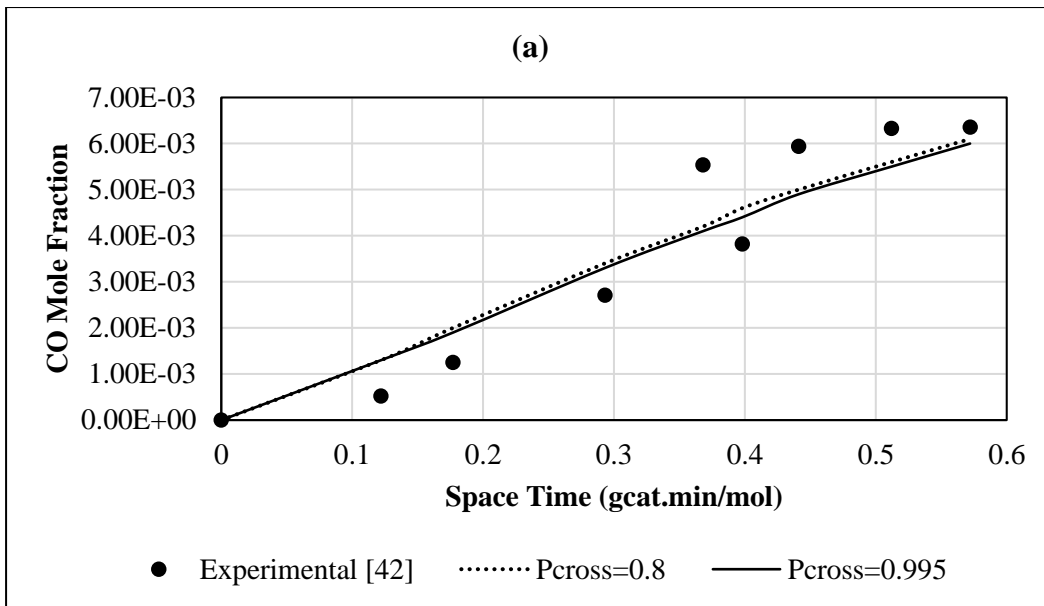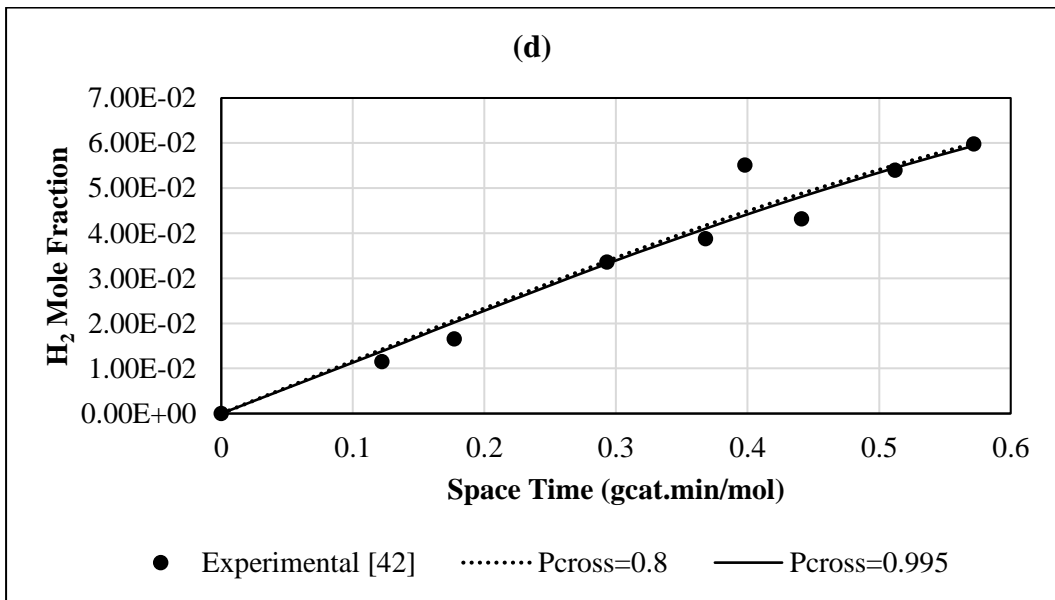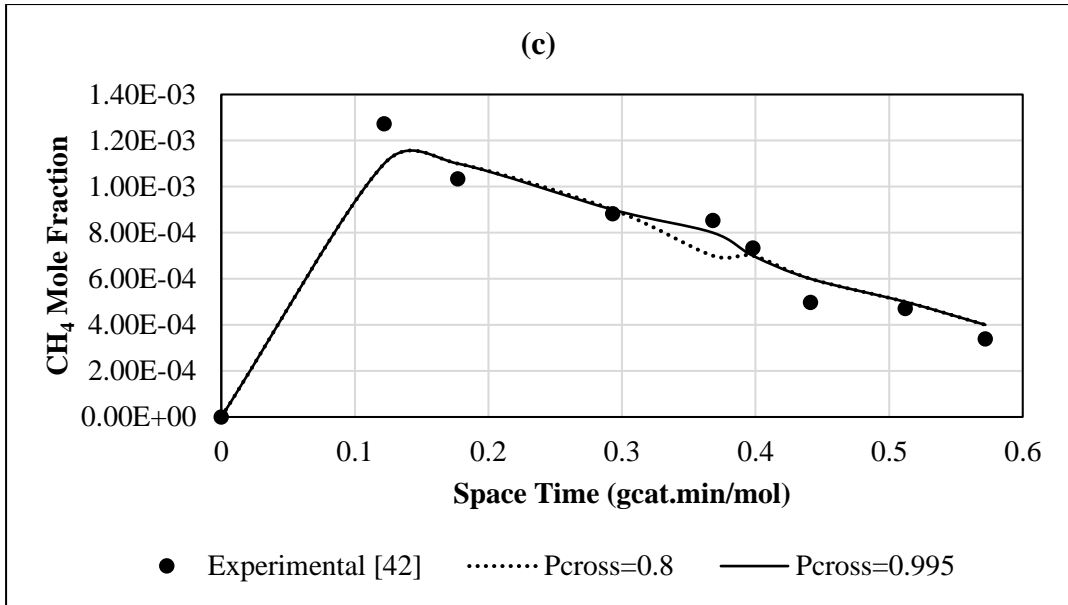
(a)

(b)

Fig. 4.3 (Contd.)

Fig. 4.3 Effect of crossover probability on theoretical mole fraction of (a) carbon monoxide, (b) carbon dioxide, (c) methane and (d) hydrogen
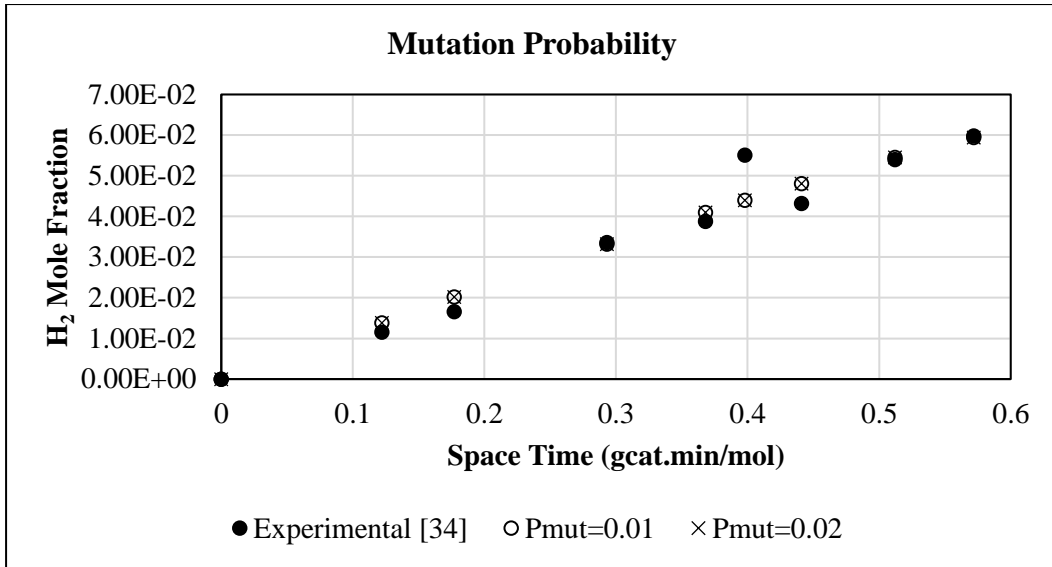
Fig. 4.4 Effect of mutation probability on hydrogen mole fraction

The (fourteen) model parameters obtained by Mas et al. [42], Rossetti et al. [44] and the present study (GA) are given in Table 4.3.

Table 4.3 Parameters reported in [42, 44] and obtained (this study) for kinetic Model B

Parameter	Mas et al. [42]	Rossetti et al. [44]	This Study (GA)	Units
$k_{1,0}$	1.38E+12	1.79E+16	3.27E+11	[mol/(min.gcat)]
$k_{2,0}$	3.60E+10	5.30E+12	1.39E+10	[mol/(min.gcat)]
$k_{3,0}$	2.45E+03	2.76E+12	2.21E+03	[mol/(min.gcat)]
$k_{4,0}$	1.51E+09	2.68E+30	1.26E+09	[mol/(min.gcat)]
$E_{a,1}$	278740	304529	271902	[J/mol]
$E_{a,2}$	235060	210596	226768	[J/mol]
$E_{a,3}$	123500	166619	123279	[J/mol]
$E_{a,4}$	213900	428652	213936	[J/mol]
$K_{E,0}$	6.94E-11	3.78E-02	6.98E-11	[-]
$K_{H_2O,0}$	1.11E-04	4.79E-12	1.14E-04	[-]
$K_{M,0}$	3.92E-05	6.53E-08	3.96E-05	[-]
ΔH_E	-199700	-60978	-197964	[J/mol]
ΔH_{H_2O}	-92400	-187349	-91708	[J/mol]
ΔH_M	-124700	-126795	-124789	[J/mol]

The mole fractions as a function of the space-time are plotted in Fig. 4.5 using the kinetic parameters of Mas et al. [42], Rossetti et al. [44] and this study (GA). The reactor model shows good validation with the experimental [42] results for the kinetic parameters in case of Mas et al. [42] and this study. In fact, simulation carried out using the GA-optimized model parameters shows a slightly better fit of the experimental data. Simulation using the kinetic parameters of Rossetti et al. [44] shows deviation from the experimental results in the case of CO, CO_2, CH_4 and H_2. They also minimized the sum-of-square errors using *all* the experimental values of Mas et al. [42] (for different values of θ) and got reasonable converged values for their parameters. However, the variation of the mole fractions of several components with θ are not appreciable. This is shown in Fig. 4.5. The values for the SSE and the percent relative error for different mole fractions are reported in Table 4.4. The error analysis shows that the simulated results obtained using the kinetic parameters from GA match closely with the experimental data [42].

Table 4.4 Error analysis

Reference	SSE	Relative error (%)					
		y_1	y_2	y_3	y_4	y_5	y_6
Mas et al. [42]	1.57E-02	9.29	2.81	5.35	4.46	17.99	4.01
Rossetti et al.[44]	3.69E-02	48.16	9.92	129.56	28.66	283.47	3.18
This Study	5.10E-04	3.67	4.63	5.66	1.91	17.99	0.67

(a) Ethanol

(b) Water

(c) Carbon monoxide

Fig. 4.5 (Contd.)
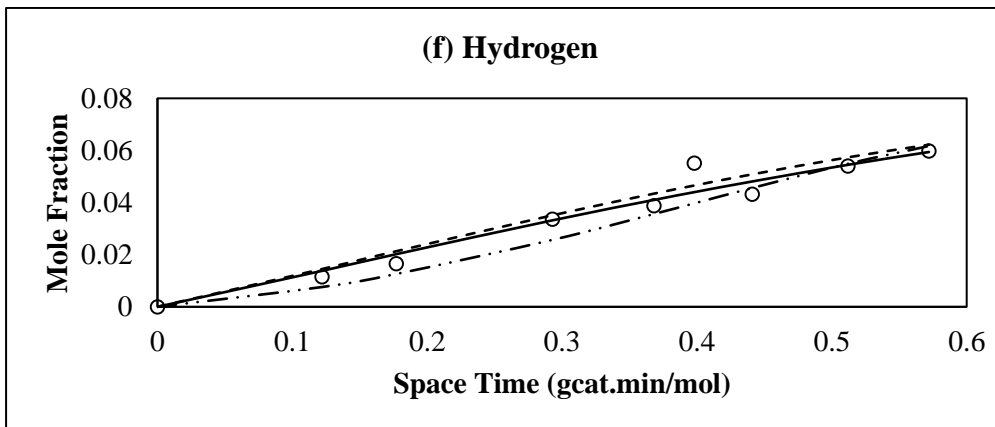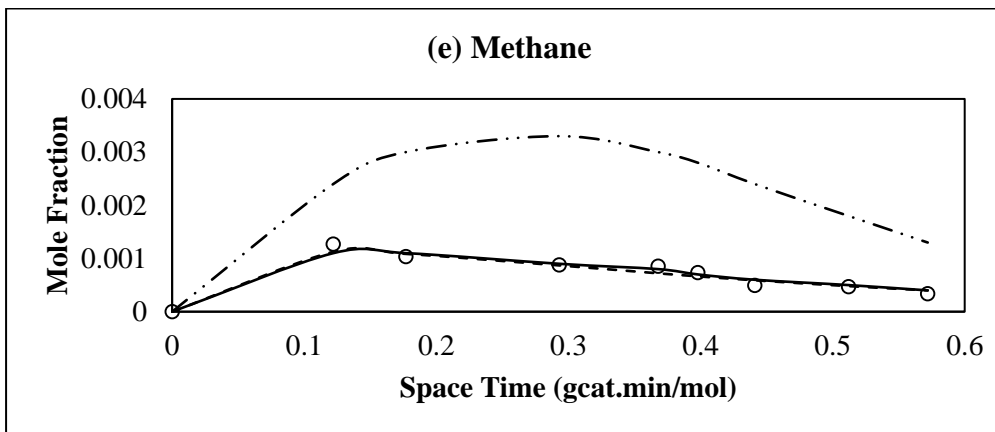
(d) Carbon dioxide
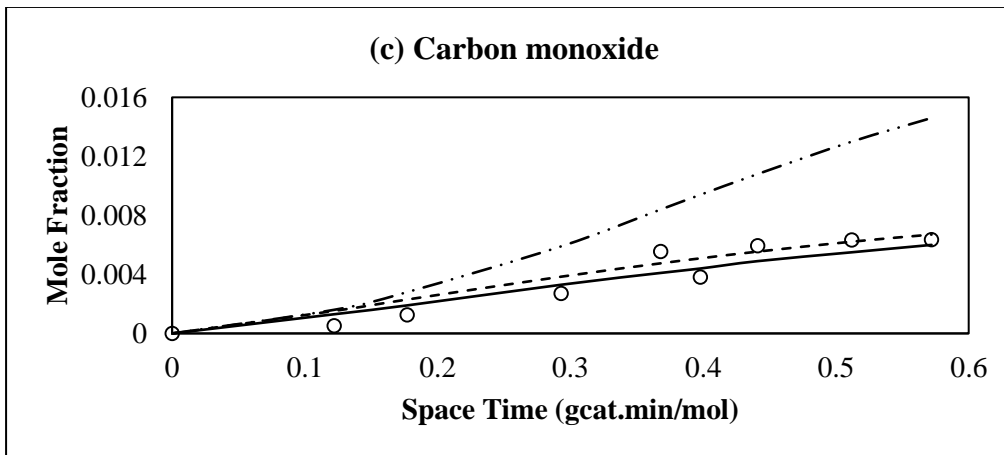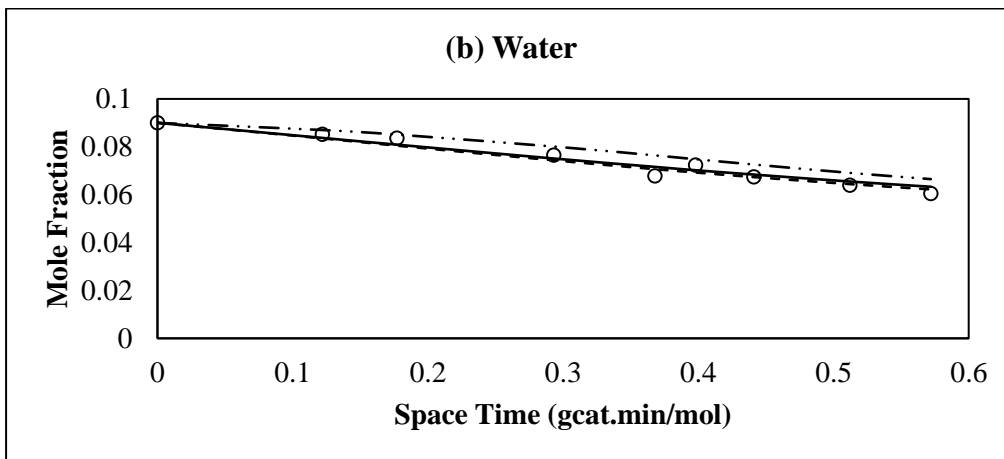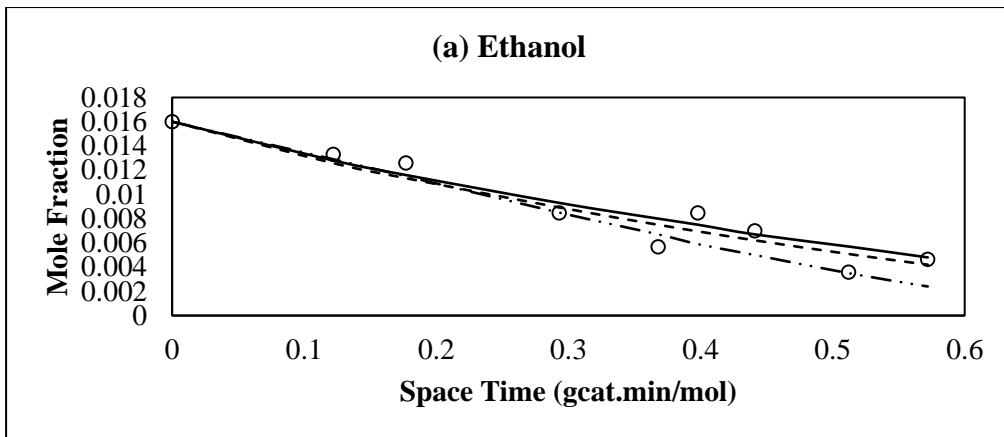
(e) Methane

(f) Hydrogen

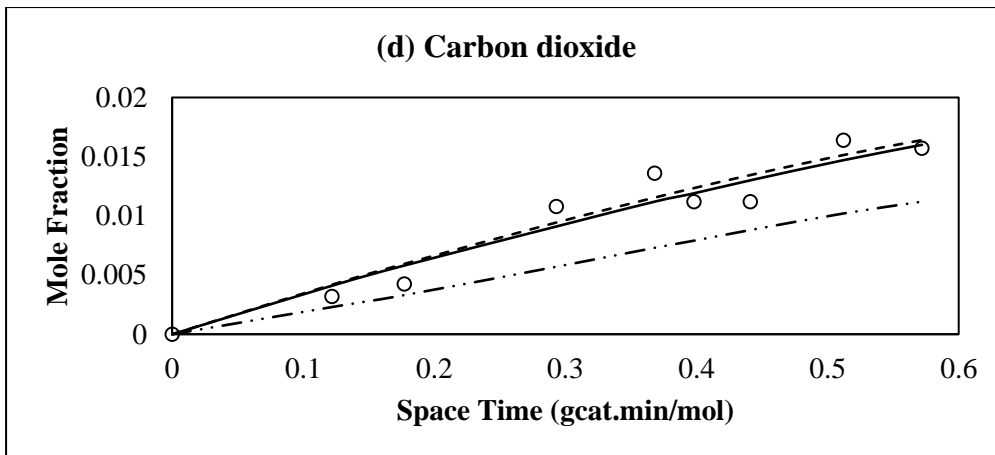——— This Study ○ Experimental [42] ------- Mas et al. [42] –··–··– Rossetti et al. [44]

Fig. 4.5 Comparison of mole fractions for (a) ethanol (b) water (c) carbon monoxide (d) carbon dioxide (e) methane and (f) hydrogen using the kinetic parameters of Mas et al. [42], Rossetti et al.[44] and this study (GA) with experimental data [42]

4.2 SOLUTION OF A MOO PROBLEM

A MOO problem, Eqns. (3.28) – (3.33), is solved using NSGA-II and NSGA-II-JG in Sections 4.2.1 and 4.2.2, respectively.

4.2.1 NSGA-II

The optimization toolbox of MATLAB^{TM} is used to obtain the Pareto optimal (non-dominated) solutions using NSGA-II (two points on the two-objective Pareto front that are non-dominated refers to one objective function improving while the other becomes worse as one goes from one point to another). NSGA-II uses an elite-preservation strategy as well as an explicit diversity-preserving mechanism [60-61].

Fig. 4.6 shows the improvement in the Pareto set over generations. The scatter of the Pareto reduces with higher generation number. The parametric effects of crossover probability and mutation probability on the Pareto set are shown in Fig. 4.7 and Fig. 4.8, respectively. The computational parameters used to obtain the solutions are given in Table 4.5.

Table 4.5 Computational parameters for NSGA-II

Parameter	Value
Maximum number of generation, N_{gen}	100
Population size, N_{pop}	50
Crossover probability, P_{cross}	0.8
Mutation probability, P_{mut}	0.02
Seed for random number generator	0.5434
No. of decision variables	3

(a) $N_{gen} = 5$

(b) $N_{gen} = 10$

(c) $N_{gen} = 20$
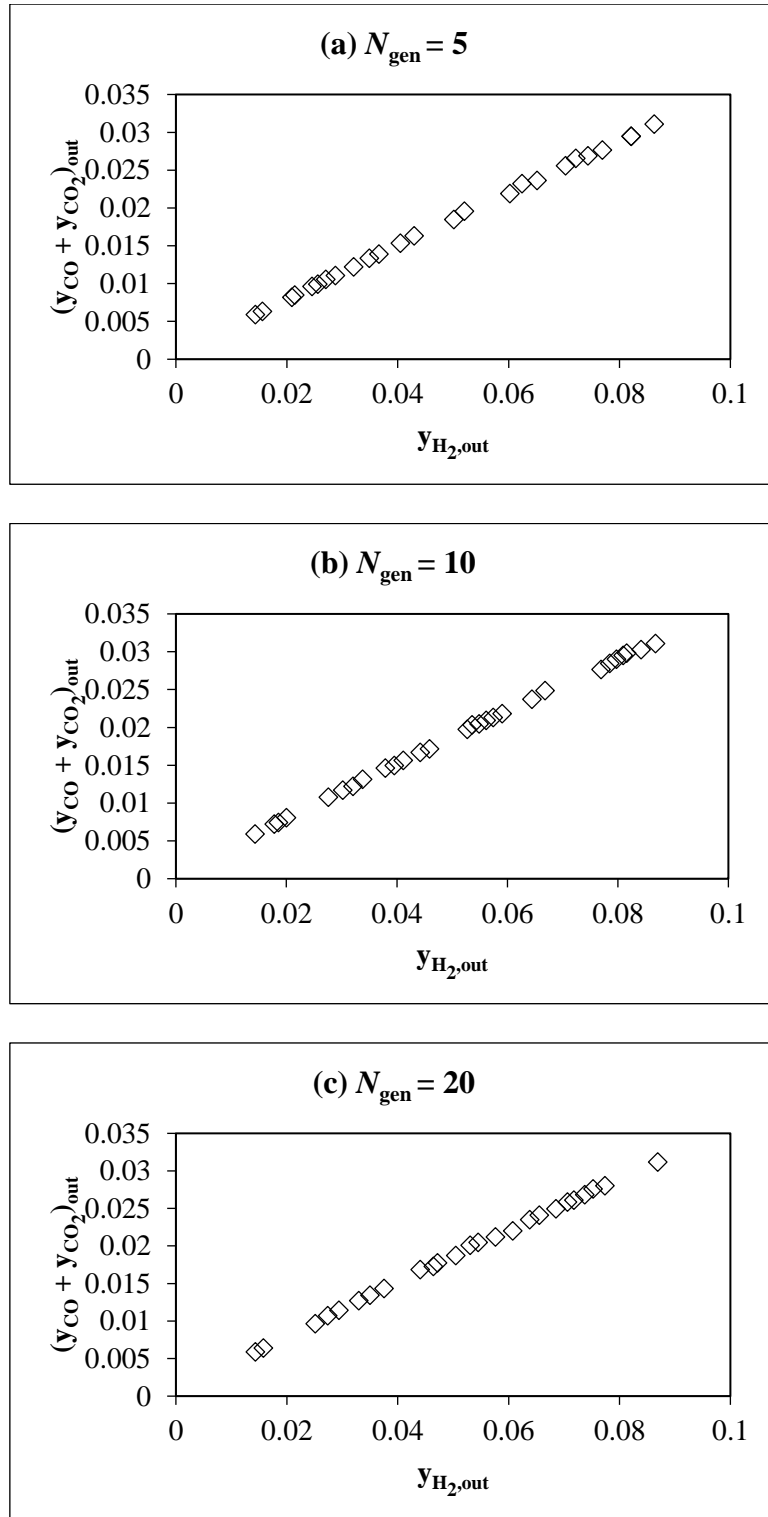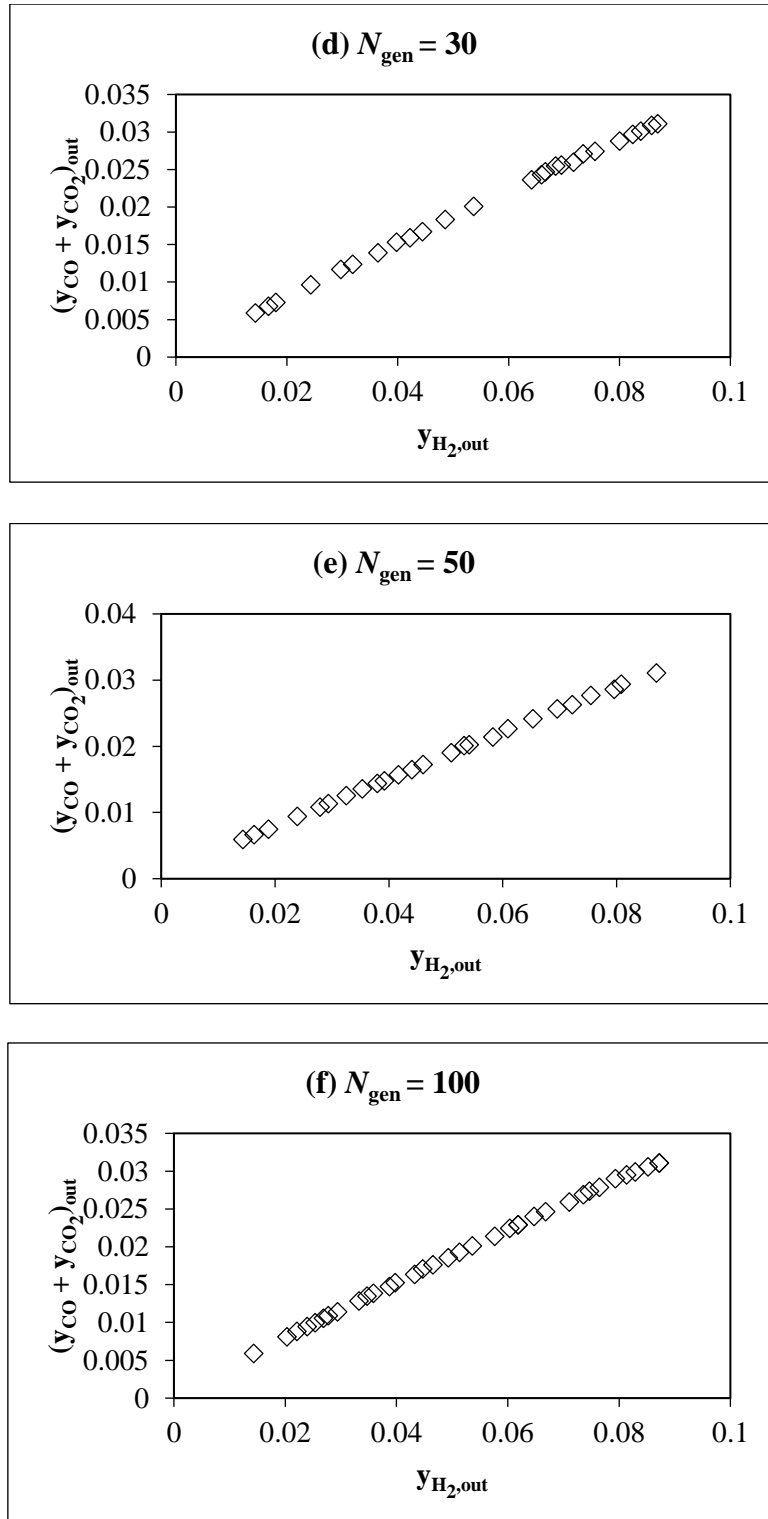
Fig. 4.6 (Contd.)

Fig. 4.6 Evolution of the Pareto set using NSGA-II with generation number (a) $N_{gen} = 5$, (b) $N_{gen} = 10$, (c) $N_{gen} = 20$, (d) $N_{gen} = 30$, (e) $N_{gen} = 50$ and (f) $N_{gen} = 100$

Crossover Probability
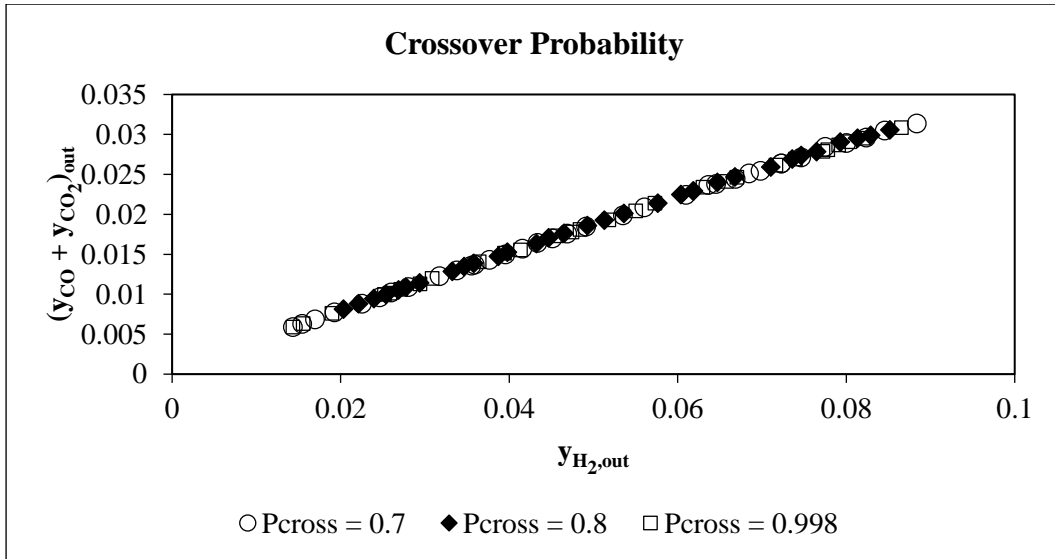
Fig. 4.7 Effect of crossover probability on the Pareto

Mutation Probability
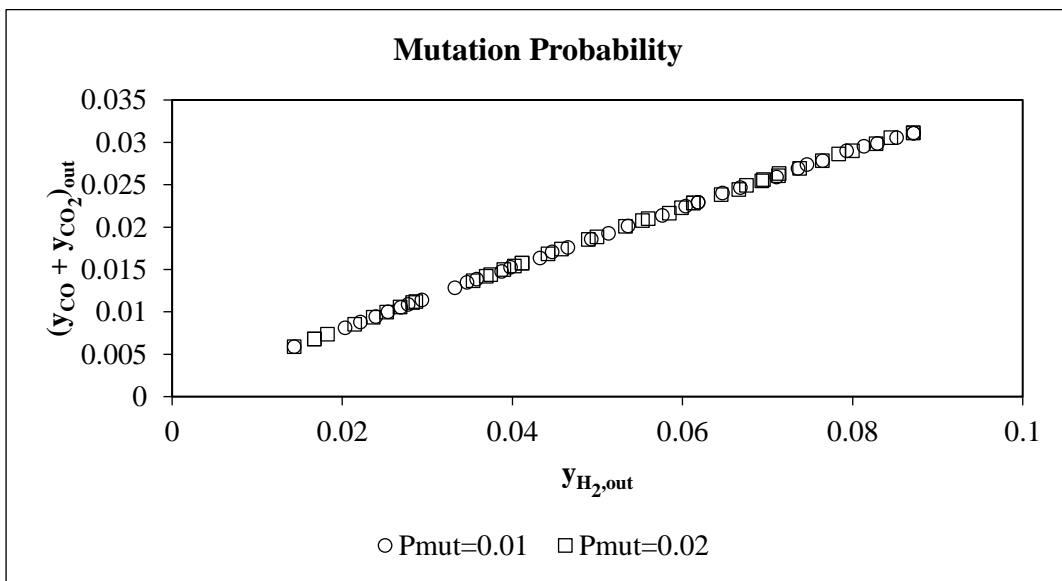
Fig. 4.8 Effect of mutation probability on the Pareto

The non-dominated Pareto optimal solution after 100 generations is shown in Fig. 4.9. Each point (referred to as a chromosome) in the Pareto set is associated with a (different) set of decision variables. Three points, A, B and C, are taken on the Pareto set as shown in Fig. 4.9. These span the entire Pareto set. It is seen that the mole fraction of H_2 at the outlet increases as we go from point, A, to point, C, (desirable) while the mole fractions of CO and CO_2 at the

outlet increases as we go from A to B (undesirable). Table 4.6 shows the decision and process variables corresponding to three chromosomes A, B and C, on the Pareto set of Fig. 4.9. The decision variables corresponding to these three points are shown in Fig. 4.10.

The maximum mole fraction of hydrogen is found to be approximately 0.088 at a temperature of 911.86 K, as shown in Fig. 4.9 against a maximum 0.080 at 923 K reported in experiments by Mas et al. [42].

The preferred solution refers to a single point on the Pareto. An engineer with the operating experience and other information like plant economics does the selection of any one of the Pareto points. The weighted average of Pareto point choices given by several plant personnel is taken to arrive at the operating conditions of the reformer corresponding to a single point.
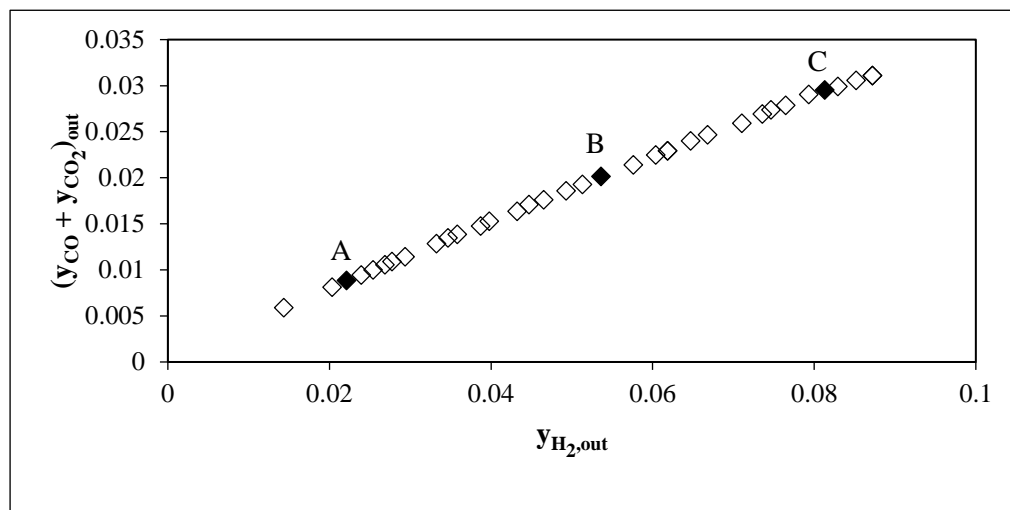

Fig. 4.9 Pareto optimal front after 100 generations

Table 4.6 Decision and Process variables for Chromosomes A, B and C of the Pareto set in Fig. 4.9

Parameters	Chr. A	Chr. B	Chr. C
Decision Variables			
T (K)	835.76	865.295	902.316
P (kPa)	107.842	132.689	122.961
$(H_2O/E)_{in}$	365	423	472
Process Variables			
$y_{H_2,out}$	0.02212	0.05362	0.08134
$\left(y_{CO} + y_{CO_2}\right)_{out}$	0.00882	0.02012	0.02953

As observed experimentally [42], it is theoretically proven that the hydrogen mole fraction increases with increase in the reaction temperature and the water/ethanol molar ratio in the feed as shown in Fig. 4.10. As the reaction temperature and/or the water/ethanol molar ratio increase, methane steam reforming reactions occur significantly, though some traces of methane are obtained in the effluent stream. The operating pressure of a fixed bed reactor also affects the desired values of hydrogen mole fraction due to the reversible reactions. The increase in mole fractions of CO and CO_2 supports the proven reaction mechanism that the WGS reaction is not taking place over this Ni-based catalyst.

It is meaningful to achieve more favorable objectives through optimization since the kinetic model has been validated mathematically to match experimental data.
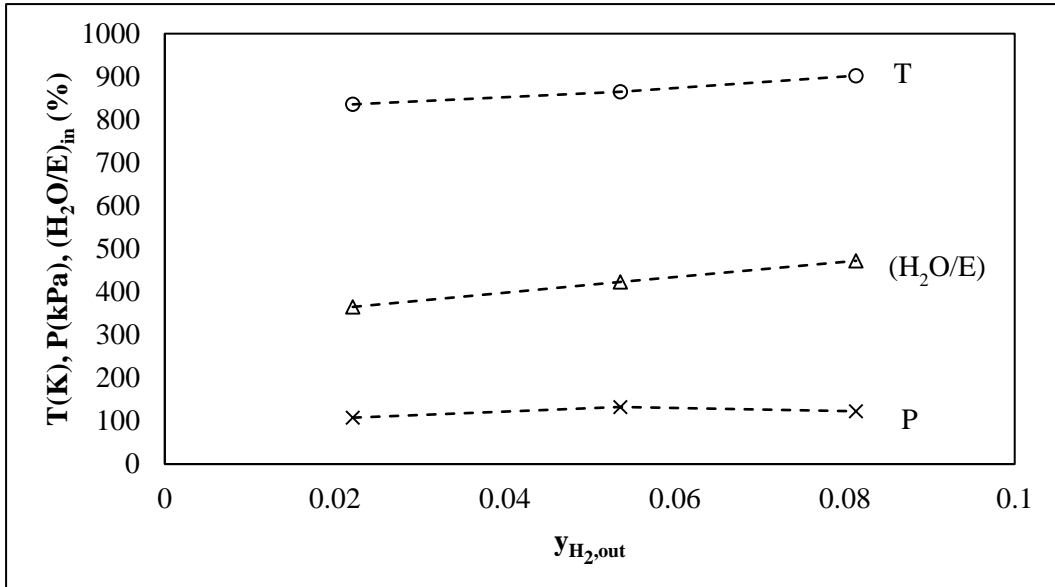
Fig. 4.10 Decision variables corresponding to points A, B and C on the
Pareto set of Fig. 4.9

Fig. 4.11 shows the profiles of the several mole fractions as a function of the
space-time for the three cases, A, B and C (of Fig. 4.9). Interestingly, Case B
seems to be quite close to the experimental data of Mas et al. [42] The
computational time taken for NSGA-II for $N_{gen} = 50$ on a Core-i5-6400 CPU
clocked at 2.70 GHz is 292 s.

(a) Ethanol

(b) Water

(c) Carbon monoxide

Fig. 4.11 (Contd.)

(d) Carbon dioxide

(e) Methane

(f) Hydrogen

— ·· — ·· — A   – – – – – B   ——— C   ○ Experimental [42]

Fig. 4.11 Mole fraction profiles of (a) ethanol (b) water (c) carbon monoxide (d) carbon dioxide (e) methane and (f) hydrogen for points A, B and C of Figure 4.9. Experimental points of Mas et al. [42] also shown by circles.
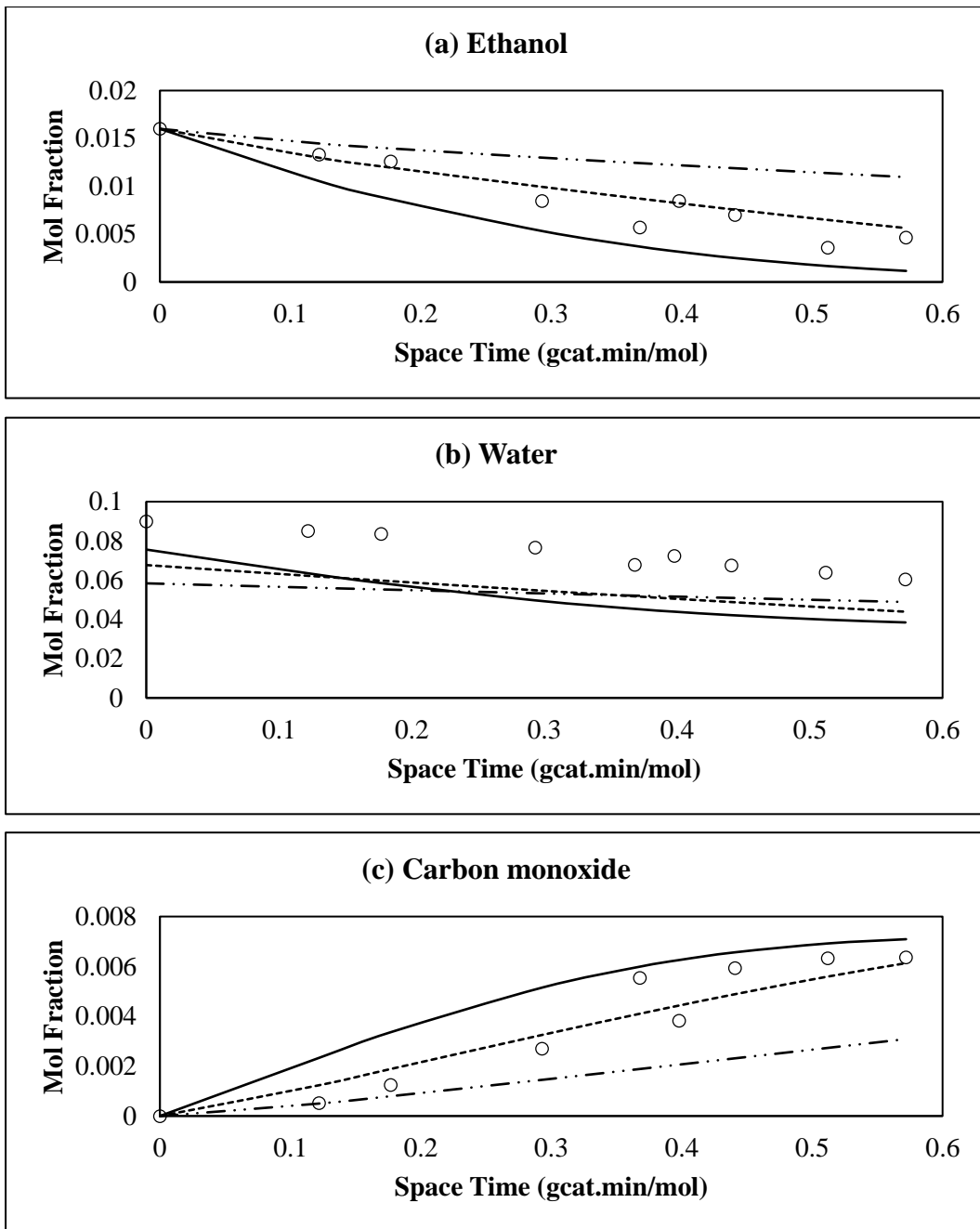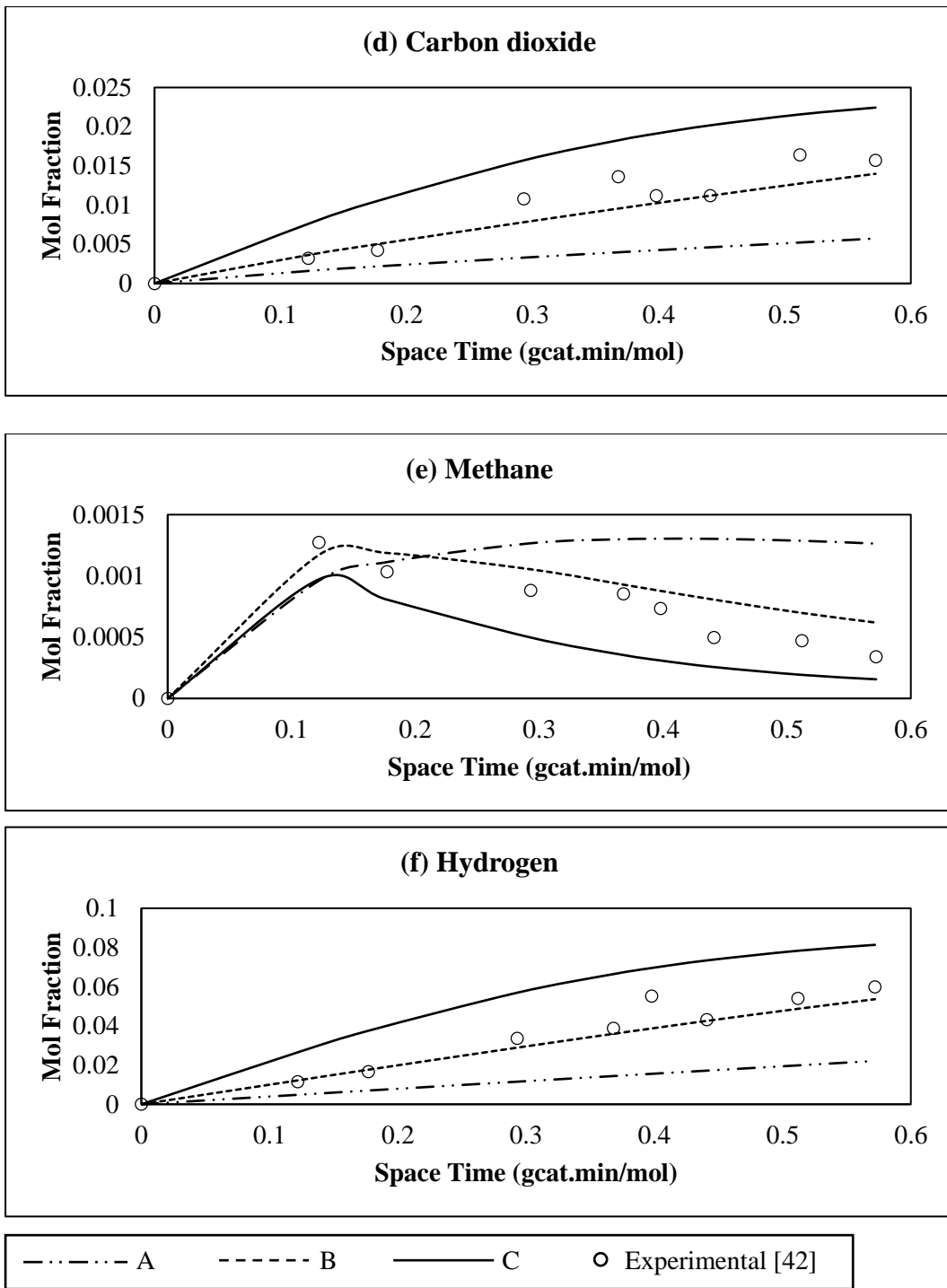
4.2.2 NSGA-II-JG

It is interesting to see how the jumping gene adaptation, NSGA-II-JG, of NSGA-II works for this MOO problem (Eqns. (3.28) - (3.33)). The MATLAB code is developed to modify a default mutation function to adapt the jumping gene operator based on the *replacement* approach using NSGA-II. This adaptation is used to solve and speed up the optimization problem. The optimization toolbox of MATLAB$^{\text{TM}}$ is used to obtain the Pareto optimal (non-dominated) solutions using the modified code of mutation operator in NSGA-II.

Fig. 4.12 shows the improvement in the Pareto set over the generations using P_{jump} = 0.5 in NSGA-II-JG. The scatter of the Pareto reduces with higher generation number. The parametric effect of jumping gene probability is shown in Fig. 4.13 for P_{jump} values of 0.2, 0.5 and 0.8.

The computational parameters used to obtain the solutions using the jumping gene adaptations of NSGA-II (NSGA-II-JG) are given in Table 4.7.

Table 4.7 Computational parameters for NSGA-II-JG

Parameter	Value
Maximum number of generation, N_{gen}	100
Population size, N_{pop}	50
Crossover probability, P_{cross}	0.8
Mutation probability, P_{mut}	0.02
Seed for random number generator	0.5434
Jumping gene probability, P_{jump}	0.5
No. of decision variables	3

(a) $N_{gen} = 5$

(b) $N_{gen} = 10$

(c) $N_{gen} = 20$
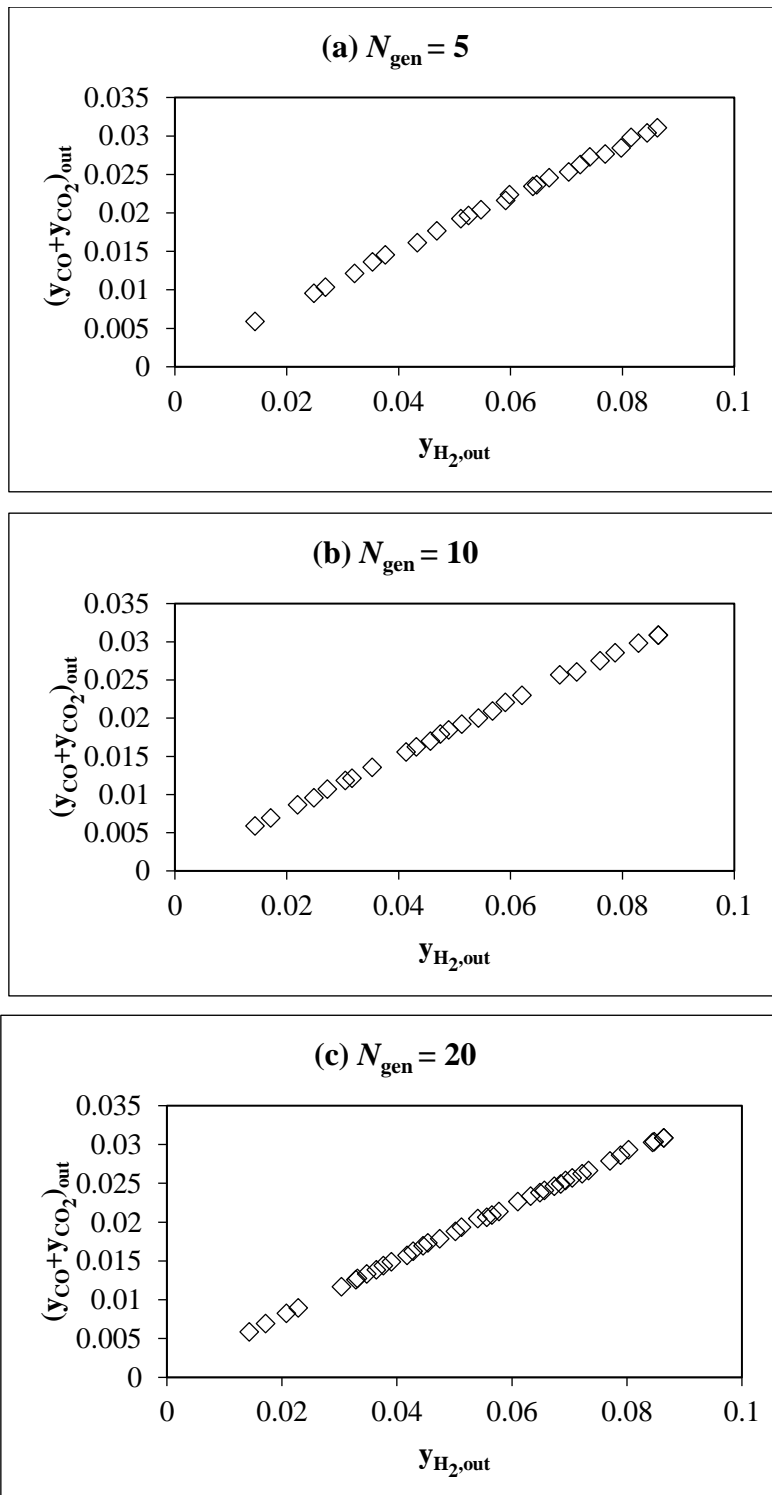
Fig. 4.12 (Contd.)
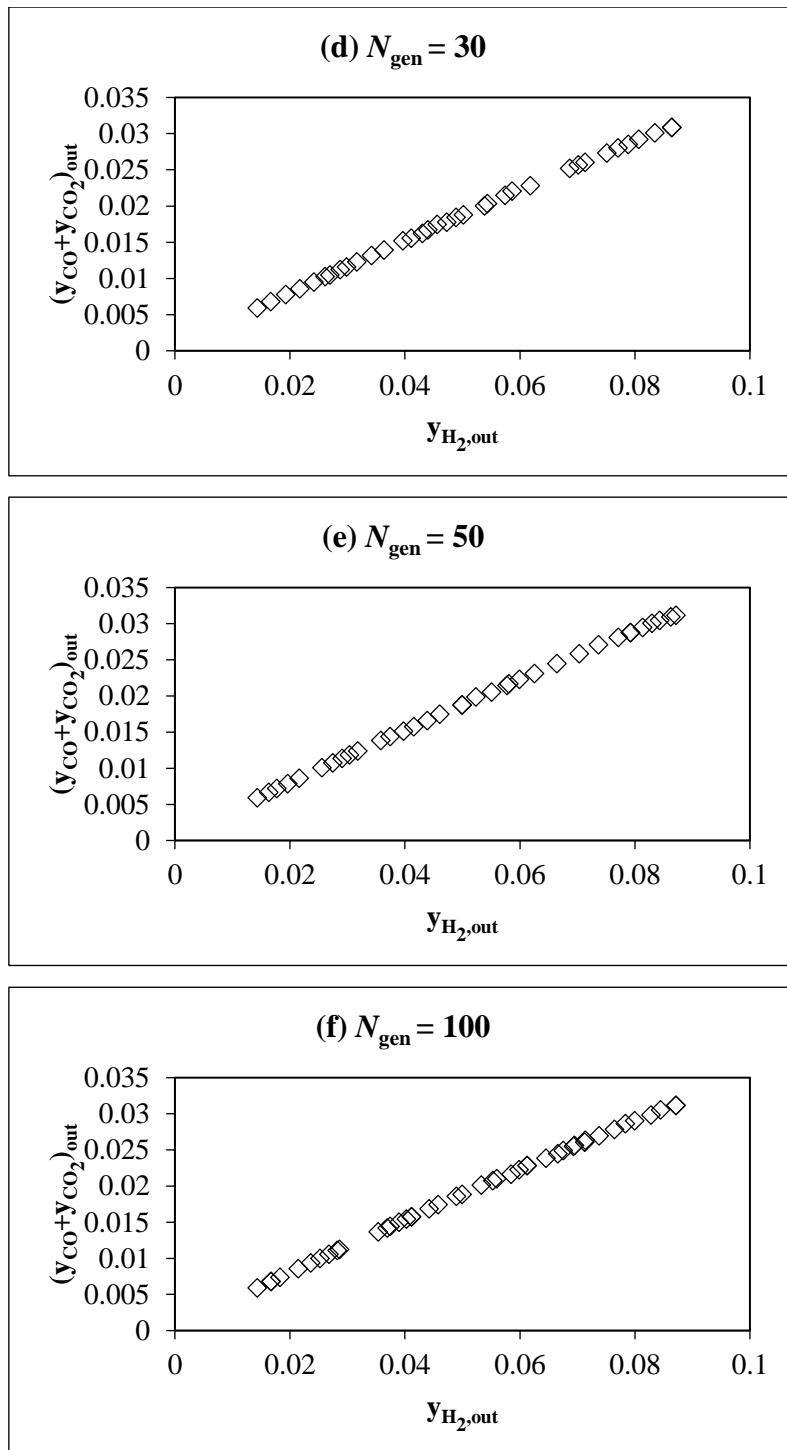
Fig. 4.12 Evolution of the Pareto set using NSGA-II-JG (P_{jump} = 0.5) with generation number (a) N_{gen} = 5, (b) N_{gen} = 10, (c) N_{gen} = 20, (d) N_{gen} = 30, (e) N_{gen} = 50 and (f) N_{gen} = 100
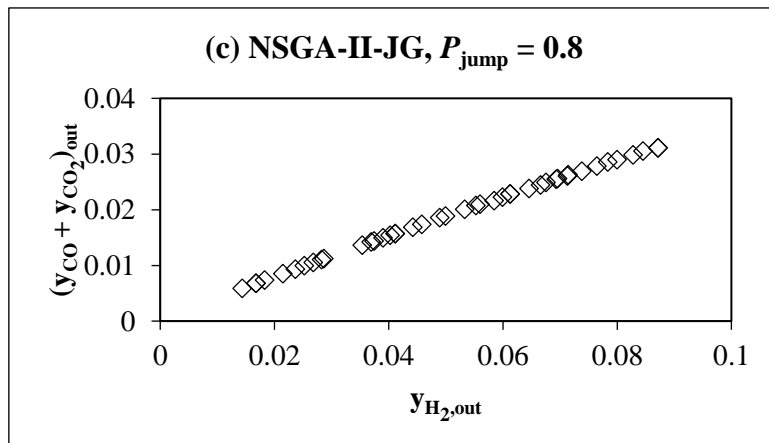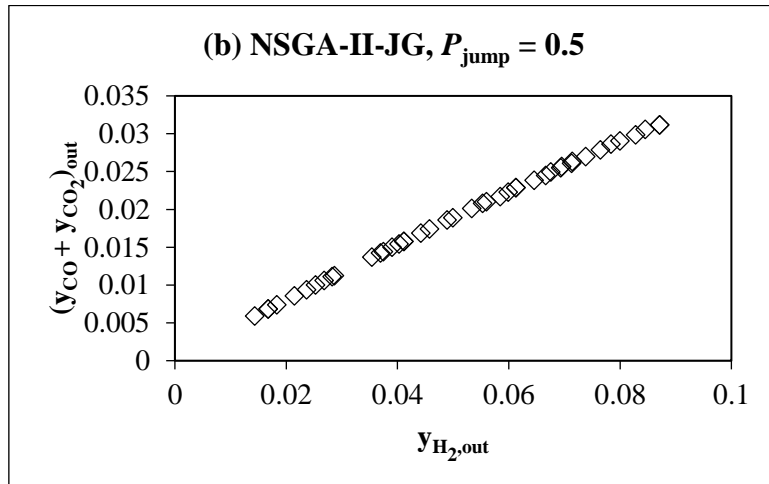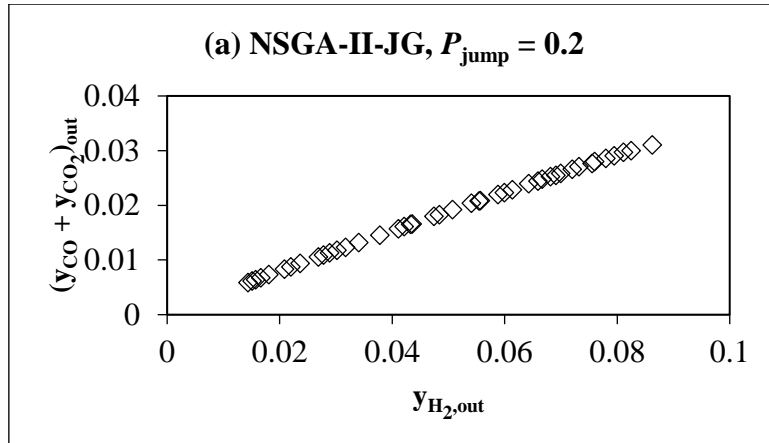
Fig. 4.13 Effect of jumping gene probability on the Pareto (a) $P_{jump} = 0.2$, (b) $P_{jump} = 0.5$ and (c) $P_{jump} = 0.8$

The Pareto sets for NSGA-II and NSGA-II-JG using $P_{jump} = 0.5$ for $N_{gen} = 50$ are shown in Fig. 4.14. The Pareto sets obtained for NSGA-II-JG is *slightly* smoother (continuous) than that obtained using NSGA-II without the JG adaptation. The computational time taken for obtaining the Pareto set using NSGA-II-JG for $N_{gen} = 50$ on a Core-i5-6400 CPU clocked at 2.70 GHz is 93 s (lower than about 290 s taken for NSGA-II). This shows that the computation time reduces threefold using NSGA-II-JG as compared to NSGA-II. It speeds up the optimization problem by improving the convergence characteristics and spread of the Pareto points. NSGA-II-JG increases the diversity through jumping gene operator, thus makes over the decrease in diversity associated with elitism.

Fig. 4.14 Pareto optimal fronts using NSGA-II and NSGA-II-JG using $P_{jump} = 0.5$ for $N_{gen} = 50$

A simple yet accurate model is developed to simulate, adequately, a fixed bed isothermal reactor for ESR using the kinetic model proposed by Mas et al [42]. The inconsistency in the results obtained by Mas et al. [42] and Rossetti et al. [44] for the proposed kinetic model of ESR is resolved by fitting a model predicted data with the experimental data [42] using the tuned kinetic parameters obtained by GA technique. The model B proposed by Mas et al. [42], which 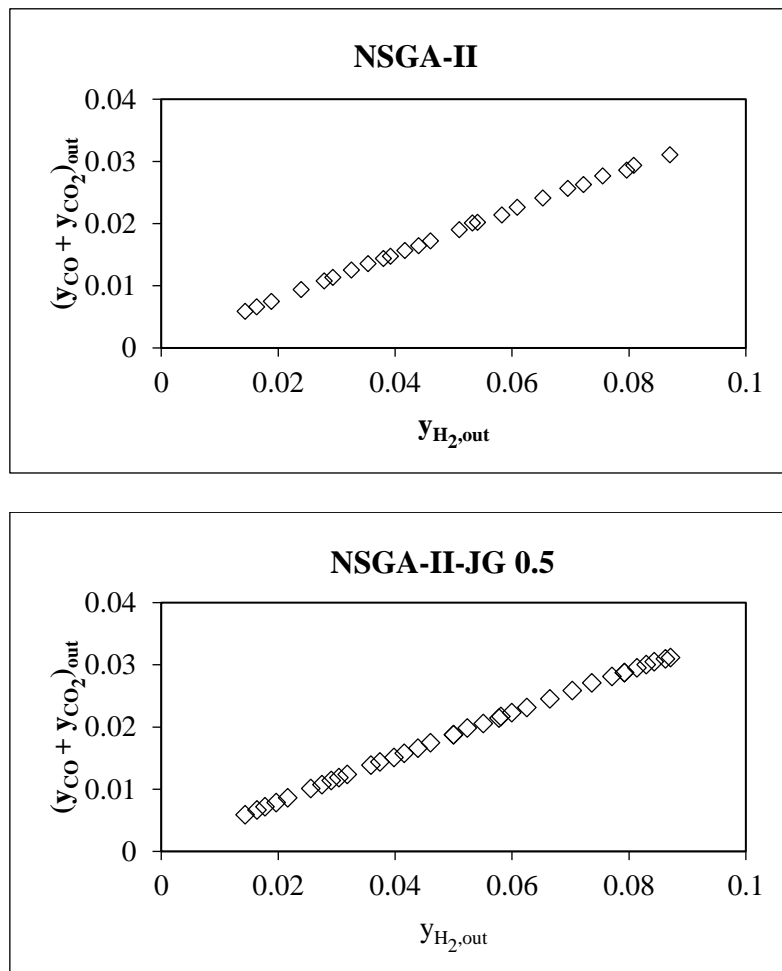considers reactions (Eqns. (3.1) - (3.4)) of ethanol decomposition, ethanol steam reforming and methane steam reforming, predicts correctly the conversion of ethanol and the composition of all the products at the reactor outlet. This model is valid for a wide range of reaction temperature and water to ethanol molar feed ratio at the reactor inlet. The GA technique is found to be effective and robust in estimating the kinetic parameters of the proposed rate model of ESR with an SSE value of about 10^{-4} over the SSE values of about 10^{-2} obtained for Mas et al. [42] and Rossetti et al. [44].

A MOO problem satisfactorily achieves the objectives of maximizing hydrogen mole fraction and minimizing the $CO + CO_2$ mole fractions simultaneously using NSGA-II. Hydrogen mole fraction is found to increase with increase in the reactor temperature (isothermal) and water to ethanol molar feed ratio at the reactor inlet. These results are in agreement with the experimental results [42]. A jumping gene adaptation of NSGA-II, NSGA-II-JG is used to obtain the solution of a MOO problem. It is observed that the computation time reduces threefold using NSGA-II-JG as compared to NSGA-II.

CHAPTER 5: CONCLUSIONS

An isothermal (and with no axial variation of the total pressure) ethanol steam reforming reactor has been studied. The 1-D, pseudo-homogeneous reactor model is simulated using the optimized kinetic (and a few other) parameters obtained by minimizing the sum-of-square errors between model predictions and experimental data of Mas et al. [42], using genetic algorithm (GA).

An SSE value of about 10^{-4} is obtained in the present study over the SSE values of about 10^{-2} obtained for Mas et al. [42] and Rossetti et al. [44]. The simulated results suggest that the present kinetic model proposed by Mas et al. [42] is reliable and valid for modeling a fixed-bed reactor to carry out ESR over Ni-based catalyst as it resolves the differences in the agreement of model predictions *vs*. experimental data by Rossetti et al. [44].

The GA optimized kinetic parameters have been used to solve a multi-objective optimization (MOO) problem (reported for the first time in the literature), using NSGA-II with one objective being to maximize the hydrogen mole fraction in the product and the other being to minimize the mole fractions of $CO + CO_2$ in the product. A Pareto optimal set of solutions is obtained.

The maximum theoretical mole fraction of hydrogen obtained is 0.088 (equivalent to hydrogen yield of 5.5) at 911.86 K *vs*. 0.080 (equivalent to hydrogen yield of 5.0) at 923 K as observed experimentally. The experimental [42] observations are verified theoretically by taking into account the effect of operating parameters on ESR. It is noted that the hydrogen mole fraction increases with an increase in the reaction temperature and the molar ratio of water/ethanol in the feed. The operating pressure of a fixed bed reactor also affects the desired values of hydrogen mole fraction due to the reversible reactions. The increase in mole fractions of CO and CO_2 supports the proven

reaction mechanism that the WGS reaction is not taking place over this Ni-based catalyst.

The use of the jumping gene adaptation of this technique, namely, NSGA-II-JG, gives only slightly improved Pareto solutions. NSGA-II-JG reduces the computation time three folds as compared to when NSGA-II is used.

FUTURE WORK

As stated in the introduction, hydrogen is used for electricity generation using the fuel cell technology. Of the different types of fuel cells, hydrogen fuel cells need a continuous supply of hydrogen for producing electrical and thermal energy. A study is planned to consider the integrated system of an ethanol steam reforming reactor (ESRR), a water gas shift reactor (WGSR) followed by a high temperature-polymer exchange membrane fuel cell (HT-PEMFC). The performance of this combination for electrical energy applications will be analyzed in the present study. Although studies are available on this combined system of ESRR, WGSR and HT-PEMFC, the ethanol steam reforming reactor is not modeled using a realistic kinetic mechanism. Rather, a simpler approach of modeling is used.

The feed to HT-PEMFC should contain low CO concentrations (<10%) and with no other contaminants. As the reliable mechanistic kinetic model [42] of ESR is evaluated using optimum conditions for ethanol conversion and product distribution, it can be used to obtain the desired feed composition at the inlet of HT-PEMFC. This integration will help to mitigate the climate changes as the emission of HT-PEMFC will be only water after energy application.

REFERENCES

1. Annual Energy Outlook (2019) Cost and performance characteristics of new generating technologies. US Energy Information Administration (https://www.eia.gov/outlooks/aeo/)

2. Panwar, N.L., Kaushik , S.C. and Kothari, S. (2011) Role of renewable energy sources in environmental protection: a review. Renewable and Sustainable Energy Reviews, Vol. 15, pp. 1513–1524.

3. Iulianelli, A., Ribeirinha, P., Mendes, A. and Basile, A. (2014) Methanol steam reforming for hydrogen generation via conventional and membrane reactors: A review. Renewable and Sustainable Energy Reviews, Vol. 29, pp. 355–368.

4. Haryanto, A., Fernando, S., Murali, N. and Adhikari, S. (2005) Current status of hydrogen production techniques by steam reforming of ethanol: a review. Energy and Fuels, Vol. 19. No. 5, pp. 2098-2106.

5. Martin, S., Kraaij, G., Ascher, T., Wails, D. and Worner, A. (2014) An experimental investigation of biodiesel steam reforming. International Journal of Hydrogen Energy, Vol. 40. No. 1, pp. 95–105.

6. Dou, B., Song, Y. Wang, C., Chen, H. and Xu, Y. (2014) Hydrogen production from catalytic steam reforming of biodiesel byproduct glycerol: Issues and challenges. Renewable and Sustainable Energy Reviews, Vol. 30, pp. 950–960.

7. Schadel, B.T., Duisberg, M. and Deutschmann, O. (2009) Steam reforming of methane, ethane, propane, butane, and natural gas over a rhodium-based catalyst. Catalysis Today, Vol. 142, pp. 42–51.

8. Bion, N., Eprona, F. and Dupreza, D. (2010) Bioethanol reforming for H_2 production. A comparison with hydrocarbon reforming. Catalysis, Vol. 22, pp. 1–55.

9. Sun, S., Yan, W., Sun, P. and Chen, J. (2012) Thermodynamic analysis of ethanol reforming for hydrogen production. Energy, Vol. 44, pp. 911-924.

10. Muktham, R., Bhargava, S.K., Bankupalli, S. and Ball A.S. (2016) A review on 1st and 2nd generation bioethanol production-recent progress. Journal of Sustainable Bioenergy Systems, Vol. 6, pp. 72-92

11. https://www.statista.com/statistics/281606/ethanol-production-in-selected-countries/

12. Conteras, J.L., Samones, J., et al. (2014) Catalysts for H_2 production using the ethanol steam reforming (a review). International Journal of Hydrogen Energy, Vol. 39, 18835-18853.

13. Wu, Y.J., Santos, J.C., Li, P., Yu, J.G., Cunha, A.F. and Rodrigues, A.E. (2014) Simplified kinetic model for steam reforming of ethanol on a Ni/Al_2O_3 catalyst. The Canadian Journal of Chemical Engineering, Vol. 92, pp. 116-130.

14. Wang, W. and Wang, Y.Q. (2008) Thermodynamic analysis of steam reforming of ethanol for hydrogen generation. International Journal of Energy Research, Vol. 32. No. 15, pp. 1432-1443.

15. Dehkordi, T.K., Hormozi, F. and Jahangiri, M. (2016) Using conical reactor to improve efficiency of ethanol steam reforming. International Journal of Hydrogen Energy, Vol. 41, pp. 17084-17092

16. Peela, N.R. and Kunzru, D. (2011) Steam reforming of ethanol in a microchannel reactor: Kinetic study and reactor simulation. Industrial and Engineering Chemistry Research, Vol. 50, pp.12881-12894.

17. Hou, T., Zhang, S., Chen, Y., Wang, D. and Cai, W. (2015) Hydrogen production from ethanol reforming: Catalyst and reaction mechanism. Renewable and Sustainable Energy Reviews, Vol. 44, pp. 132-148.

18. Vaidya, P.D. and Rodrigues, A.E. (2006) Insight into steam reforming of ethanol to produce hydrogen for fuel cells. Chemical Engineering Journal, Vol. 117, pp. 39-49.

19. Liguras, D.K., Kondarides, D.I. and Verykios, X.E. (2003) Production of hydrogen for fuel cells by steam reforming of ethanol over supported noble metal catalysts. Applied Catalysis: B, Vol. 43, pp. 345-354.

20. Bshish, A., Yaakob, Z., Narayanan, B., Ramakrishnan, R. and Ebshish, A. (2011) Steam reforming of ethanol for hydrogen production. Chemical Papers, Vol. 65. No. 3, pp. 251–266.

21. Cavallaro, S., Chiodo, V., Freni, S., Mondello, N. and Frusteri, F. (2003) Performance of Rh/Al_2O_3 catalyst in the steam reforming of ethanol: H_2 production for MCFC. Applied Catalysis-A, Vol. 249, pp. 119–128.

22. Sharma, P.K., Saxena, N., Roy, P.K. and Bhatt, A. (2016) Hydrogen generation by ethanol steam reforming over Rh/Al_2O_3 and $Rh/CeZrO_2$ catalysts: A comparative study. International Journal of Hydrogen Energy, Vol. 41. No. 14, pp. 6123-6133.

23. Aupretre, F., Descorme, C. and Duprez, D. (2002) Bio-ethanol catalytic steam reforming over supported metal oxide. Catalysis Communications Vol. 3. No. 6, pp. 263-267.

24. Diagne, C., Idriss, H. and Kiennemann, A. (2008) Hydrogen production by ethanol reforming over $Rh/CeO_2–ZrO_2$ catalysts. Catalysis Communications, Vol. 3. No. 12, pp. 565-571.

25. Frusteri, F., Freni, S., et al. (2004) H_2 production for MC fuel cell by steam reforming of ethanol over MgO supported Pd, Rh, Ni and Co catalysts. Catalysis Communications, Vol. 5. No. 10, pp. 611-615.

26. Bilal, M. and Jackson, S.D. (2013) Ethanol steam reforming over Rh and Pt catalysts: effect of temperature and catalyst deactivation. Catalysis Science and Technology, Vol. 3. No. 3, pp. 754-766.

27. Chiou, J.Y.Z., Siang, J.Y., Yang, S.Y., Ho, et al. (2012) Pathways of ethanol steam reforming over ceria-supported catalysts. International Journal of Hydrogen Energy, Vol. 37. No. 18, pp. 13667-73.

28. Scott, M., Goeffroy, M., Chiu, W., Blackford, M.A. and Idriss, H. (2008) Hydrogen production from ethanol over $Rh-Pd/CeO_2$ catalysts. Topics in Catalysis, Vol. 51. No. 1-4, pp. 13-21.

29. Wang, F., Cai, W., et al. (2011) Hydrogen production from ethanol steam reforming over Ir/CeO_2 catalysts: enhanced stability by PrOx Promotion. International Journal of Hydrogen Energy, Vol. 36. No. 21, pp.13566-74.

30. Freni, S., Cavallaro, S., Mondello, N., Spadaro, L. and Frusteri, F. (2003) Production of hydrogen for MC fuel cell by steam reforming of ethanol over MgO supported Ni and Co catalysts. Catalysis Communications, Vol. 4. No. 6, pp. 259-268.

31. Comas, J., Marino, F., Lamborde, M. and Amadeo, N. (2004) Bio-ethanol steam reforming on Ni/Al$_2$O$_3$ catalyst. Chemical Engineering Journal, Vol. 98, pp. 61-68.

32. Sun, J., Qiu, X.P., Wu, F. and Zhu, W.T. (2005) H$_2$ from steam reforming of ethanol at low temperature over Ni/Y$_2$O$_3$, Ni/La$_2$O$_3$ and Ni/Al$_2$O$_3$ catalysts for fuel-cell application. International Journal of Hydrogen Energy. Vol. 30, pp. 437-445.

33. Han, S.J., Bang ,Y., Seo, J.G., Yoo, J. and Song, I.K. (2013) Hydrogen production by steam reforming of ethanol over mesoporous Ni/Al$_2$O$_3$/ZrO$_2$ xerogel catalysts: effect of Zr/Al molar ratio. International Journal of Hydrogen Energy, Vol. 38. No. 3, pp. 1376-83.

34. Fatsikostas, A.N. and Verykios, X.E. (2004) Reaction network of steam reforming of ethanol over Ni-based catalysts. Journal of Catalysis, Vol. 225, pp. 439-452.

35. Haga, F., Nakajima, T., Miya, H. and Mishima, S. (1997) Catalytic properties of supported cobalt catalysts for steam reforming of ethanol. Catalysis Letters, Vol. 48. No. 3-4, pp. 223-227

36. Kaddouri, A. and Mazzocchia, C. (2004) A study of the influence of the synthesis conditions upon the catalytic properties of Co/SiO$_2$ or Co/Al$_2$O$_3$ catalysts used for ethanol steam reforming. Catalysis Communications, Vol. 5. No. 6, pp.339-345.

37. Cavallaro, S. and Freni, S. (1996) Ethanol steam reforming in a molten carbonate fuel cell. A preliminary kinetic investigation. International Journal of Hydrogen Energy, Vol. 21, pp. 465–469.

38. Freni, S., Mondello, N., Cavallaro, S., et al. (2000) Hydrogen production by steam reforming of ethanol: A two step process. Reaction Kinetics and Catalysis Letters, Vol. 71. No. 1, pp. 143-152.

39. Chang, F.W., Yang, H.C., Roselin, L. S. and Kuo, W.Y. (2006) Ethanol dehydrogenation over copper catalysts on rice husk ash prepared by ion exchange. Applied Catalysis A: General, Vol. 304, pp. 30–39.

40. Akande, A., Aboudheir, A., Idem, R. and Dalai, A. (2006) Kinetic modelling of hydrogen production by the catalytic reforming of crude ethanol over co-precipitated Ni-Al$_2$O$_3$ catalyst in a packed bed tubular reactor. International Journal of Hydrogen Energy, Vol. 31, pp.1707-1715.

41. Akpan, E., Akande, A., Aboudheir, A., Ibrahim, H. and Idem, R. (2007) Experimental, kinetic and 2-D reactor modelling for simulation of the production of hydrogen by the catalytic reforming of concentrated crude ethanol over a Ni-based commercial catalyst in a packed bed tubular reactor. Chemical Engineering Science, Vol. 62, pp. 3112–3126.

42. Mas, V., Bergamini, M.L., Baronetti, G., Amadeo, N. and Laborde, M. (2008) A kinetic study of ethanol steam reforming using a nickel based catalyst. Topics in Catalysis, Vol. 51, pp. 39-48.

43. Sahoo, D.R., Vajpai, S., Patel, S. and Pant, K.K. (2007) Kinetic modelling of steam reforming of ethanol for the production of hydrogen over Co/Al$_2$O$_3$ catalyst. Chemical Engineering Journal, Vol. 125, pp. 139-147.

44. Rossetti, I., Compagnoni, M. and Torli, M. (2015) Process simulation and optimization of H$_2$ production from ethanol steam reforming and its use in fuel cells 1. Thermodynamic and kinetic analysis. Chemical Engineering Journal, Vol. 281, pp. 1024-1035.

45. Graschinsky, C., Laborde, M., Amadeo, N. and Valant, A. (2010) Ethanol steam reforming over Rh(1%)MgAl$_2$O$_4$/Al$_2$O$_3$: A kinetic study. Industrial & Engineering Chemistry Research. Vol. 49, pp. 12383-12389.

46. Llera, I., Mas, V., Bergamini, M.L., Laborde, M. and Amadeo, N. (2012) Bio-ethanol steam reforming on Ni based catalyst. Kinetic study. Chemical Engineering Science, Vol. 71, pp. 356-366.

47. Gorke, O., Pfeifer P. and Schubert, P. (2009) Kinetic study of ethanol reforming in a microreactor. Applied Catalysis A: General, Vol. 360, pp. 232-241.

48. Gallucci, F., Falco, M.D., Tosti, S., Marrelli, L. and Basile, A. (2008) Ethanol steam reforming in a dense Pd–Ag membrane reactor: a modelling work. Comparison with the traditional system. International Journal of Hydrogen Energy, Vol. 33, pp. 644-651.

49. Falco, M.D. (2008) Pd-based membrane steam reformers: a simulation study of reactor performance. International Journal of Hydrogen Energy, Vol. 33, pp. 3036-3040.

50. Ma, R., Castro-Dominguez, B., Mardilovich, I.P., Dixon, A.G. and Ma, Y.H. (2016) Experimental and simulation studies of the production of renewable hydrogen through ethanol steam reforming in a large-scale catalytic membrane reactor. Chemical Engineering Journal, Vol. 303, pp. 302-313.

51. Ruocco, C., Meloni, E., Palma, V., Annaland, M.S., Spallina, V. and Gallucci, F. (2016) Pt–Ni based catalyst for ethanol reforming in a fluidized bed membrane reactor. International Journal of Hydrogen Energy. Vol. 41, pp. 20122-20136.

52. Montero, C., Remiro, A., Benito, L.P., Bibao, J. and Gayubo, A.G. (2018) Optimum operating conditions in ethanol steam reforming over a Ni/La_2O_3-αAl_2O_3 catalyst in a fluidized bed reactor. Fuel Processing Technology, Vol. 169, pp. 207-216.

53. Dehkordi, T.K.,Hormozi, F. and Jahangiri, M. (2016) Using conical reactor to improve efficiency of ethanol steam reforming. International Journal of Hydrogen Energy, Vol. 41, pp. 17084-17092.

54. Arteaga, L.E., Peralta, L.M., Casas, Y. and Castro, D. (2009) Optimal design, modeling and simulation of an ethanol steam reforming reactor. International Journal of Chemical Reactor Engineering, Vol. 7, pp. 1-15.

55. Dou B, Zhang H, Song Y, Zhao L, et al. (2019) Hydrogen production from thermochemical conversion of biomass: issues and challenges. Sustainable Energy & Fuels. Vol. 3, pp. 314-342.

56. Deb K. (1995) Optimization for Engineering Design: Algorithms and Examples. Prentice Hall, New Delhi, India, pp. 290-317.

57. Fatemi, S., Masoori, M. and Bozorgmehry, R. (2005) Application of genetic algorithm in kinetic modeling and reaction mechanism studies. Iranian Journal of Chemistry and Chemical Engineering, Vol. 24. No.4, pp. 37-46.

58. Wang. Q.J. (1997) Using genetic algorithms to optimise model parameters. Environmental Modelling & Software, Vol. 12. No. 1, pp. 27-34.

59. Tutkun, N. (2009) Parameter estimation in mathematical models using the real coded genetic algorithms. Expert Systems with Applications, Vol. 36, pp. 3342–3345.

60. Deb K. (2001) Multi-objective Optimization using Evolutionary Algorithms. Wiley, Chichester, UK.

61. Jaimes A.L., Coello Coello C.A., in Rangaiah G.P. (2009) Multi-objective Optimization: Techniques and Applications in Chemical Engineering. World Scientific, Singapore, pp. 61-90.

62. Rajesh, J.K., Gupta, S.K., Rangaiah, G.P. and Ray, A.K. (2000) Multiobjective optimization of steam reformer performance using genetic algorithm. Industrial & Engineering Chemistry Research. Vol. 39, pp. 706-717.

63. Kasat R.B., Gupta S.K. (2003) Multi-objective optimization of an industrial fluidized-bed catalytic cracking unit (FCCU) using genetic algorithm (GA) with the jumping genes operator. Computers and Chemical Engineering, Vol. 27. No. 12, pp. 1785-1800.

64. Fogler, H.S. (2006) Elements of Chemical Reaction Engineering. 4th Edition, Prentice-Hall Inc., New Jersey.

ANNEXURE I - RESUME

KUMARGAURAO DNYANESHWAR PUNASE
M. Tech Chemical Engineering, IIT Roorkee
(Computer Aided Process Plant Design)
E-mail ID: kumargaurav04@gmail.com
Phone No: +91 - 9917720952
Area(s) Of Interest: Process Modeling and Simulation, Heat Transfer and Equipment Design, Process Design and Flowsheeting, Engineering Economics.

EDUCATIONAL DETAILS

Educational Qualifications	Year	Board/Institution	CGPA/ Percentage
Ph. D Chemical Engg.	Pursuing	University of Petroleum Energy and Studies, Dehradun, India	Pursuing
M. Tech Chemical Engg.	2009	Indian Institute of Technology, Roorkee, India	8.29/10
B. Tech Chemical Engg.	2006	Laxminarayan Institute of Technology, RTM Nagpur University, India	68.31/100
Twelfth Class	2002	Amravati Board, India	86.00/100
Tenth Class	2000	Amravati Board, India	81.33/100

RESEARCH PUBLICATIONS

- Punase K.D., Rao N. and Vijay P. (2019) *A review on mechanistic kinetic models of ethanol steam reforming for hydrogen production using a fixed bed reactor.* Chemical Papers, Vol. 73. No. 5, 1027-1042. (ISI/JCR Impact Factor – 1.246)
- Punase K.D., Rao N., Vijay P. and Gupta S.K. (2019) *Simulation and multi-objective optimization of a fixed bed catalytic reactor to produce hydrogen using ethanol steam reforming.* International Journal of Energy Research, Vol. 43. No. 9, 4580-4591. (ISI/JCR Impact Factor – 3.343)
- Rao N., Punase K. D.; '*Evaluation of kinetic models of ethanol steam reforming for hydrogen production*' in CHEMCON – 2018 at NIT Jalandhar (December – 2018)

DECLARATION

I hereby declare that the above information is correct to my knowledge.

Date: (**Kumargaurao D. Punase)**